INFORMATION TO USERS

This manuscript has been reproduced from the microfilm master. UMI films the text directly from the original or copy submitted. Thus, some thesis and dissertation copies are in typewriter face, while others may be from any type of computer printer.

The quality of this reproduction is dependent upon the quality of the copy submitted. Broken or indistinct print, colored or poor quality illustrations and photographs, print bleedthrough, substandard margins, and improper alignment can adversely affect reproduction.

In the unlikely event that the author did not send UMI a complete manuscript and there are missing pages, these will be noted. Also, if unauthorized copyright material had to be removed, a note will indicate the deletion.

Oversize materials (e.g., maps, drawings, charts) are reproduced by sectioning the original, beginning at the upper left-hand corner and continuing from left to right in equal sections with small overlaps.

Photographs included in the original manuscript have been reproduced xerographically in this copy. Higher quality 6" x 9" black and white photographic prints are available for any photographs or illustrations appearing in this copy for an additional charge. Contact UMI directly to order.

ProQuest Information and Learning
300 North Zeeb Road, Ann Arbor, MI 48106-1346 USA
800-521-0600

NUMERICAL COMPUTATION OF MULTI-HULL SHIP RESISTANCE AND MOTION

by

Hongxuan Peng

Submitted
in partial fulfillment of the requirements
for the degree of

DOCTOR OF PHILOSOPHY

Major Subject: Naval Architecture

at

DALHOUSIE UNIVERSITY

Halifax, Nova Scotia

June 2001

Dalhousie University
Faculty of Engineering

The undersigned hereby certify that they have examined, and recommend to the Faculty of Graduate Studies for acceptance, the thesis entitled "Numerical Computation of Multi-Hull Resistance and Motion" by Hongxuan Peng in partial fulfillment of the requirements for the degree of Doctor of Philosophy.

Dated: June 20, 2001

Supervisor:

[redacted]

C.C. Hsiung

External Examiner:

[redacted]

S. Calisal
University of British Columbia
Canada

Examiners:

[redacted]

G. Fenton

[redacted]

J. Militzer

Dalhousie University
Faculty of Engineering

DATE: June 22, 2001

AUTHOR:	Hongxuan Peng
TITLE:	Numerical Computation of Multi-Hull Ship Resistance and Motion
MAJOR SUBJECT:	Mechanical Engineering/Naval Architecture
DEGREE:	DOCTOR OF PHILOSOPHY
CONVOCATION:	October 2001

Permission is herewith granted to Dalhousie University to circulate and to have copied for noncommercial purposes, at its discretion, the above thesis upon the request of individuals or institutions.

Signature of Author

TABLE OF CONTENTS

List of Tables

List of Figures

LIST OF SYMBOLS

$C(\xi_i, \zeta_i)$	camber surface function of the hull element
C_f	frictional resistance coefficient of a multi-hull ship
C_t	total resistance coefficient of a multi-hull ship
C_{cw}	wave resistance coefficient due to individual hull elements
C_{iw}	wave resistance coefficient due to the interaction between hull elements
C_w	total wave resistance coefficient of a multi-hull ship
$F_i^{MC}(t)$	miscellaneous forces which include propeller thrust, maneuvering forces, and rudder forces
$F_i^v(t)$	viscous forces
$F_i^{FK}(t)$	nonlinear Froude-Krylov forces
$F_i^{RS}(t)$	restoring forces
$H(\xi_i, \zeta_i)$	half thickness function of the hull element
$\bar{H}(t)$	Heaviside function
$K_{i7}^D(t)$	impulse response functions due to diffracted waves
$K_{ik}^R(t)$	impulse response functions due to radiated waves
k_0	wave number
lx_i	setback of the ith hull element
ly_i	hull spacing of the ith hull element

m_k	m-terms which are the gradients of the steady velocity in the normal direction
$\mathbf{n}=(n_x, n_y, n_z)$	normal vector directed outward from the hull surface
p	dynamic pressure
R_{cw}	wave resistance due to individual hull elements
R_f	frictional resistance of a multi-hull ship
R_{iw}	wave resistance due to the interaction between hull elements
R_w	wave resistance of a multi-hull ship
R_t	total resistance of a multi-hull ship
S	ship hull surface
S_0	mean wetted surface in time-domain
$S_B(t)$	body surface in time-domain
$S_F(t)$	free surface in time-domain
t	time
(u, v, w)	fluid velocity
$\vec{W}$	velocity vector of the steady flow
(X, Y, Z)	coordinates of a point in the space-fixed frame
(x_s, y_s, z_s)	coordinates of a point in the ship-fixed frame
$(\bar{x}, \bar{y}, \bar{z})$	coordinates of a point in the steady-moving frame
β	wave heading
ζ^*	wave elevation
ζ_f^*	free wave elevation
ζ_l^*	local wave elevation
$\eta_0(t)$	free surface elevation of the incident wave at the origin of the steady-moving coordinate system

μ_i	dipole density on the ith hull element
ρ_0	water density
σ_i	source density on the ith hull element
Φ	velocity potential
$\hat{\Phi}(\mathbf{x})$	potential of steady flow
$\phi_0(\mathbf{x}, t)$	potential of incident waves
$\phi_7(\mathbf{x}, t)$	diffracted wave potential
$\phi_k(\mathbf{x}, t)$	radiated wave potential due to the kth mode of motion
Ω	fluid domain

Acknowledgments

I would like to express my sincere gratitude to my supervisor, Professor C.C. Hsiung, who provided me with encouragement, guidance and direction throughout this research. He has continually given me valuable advices on my thesis work, and always kindly helped me to overcome difficulties. I take with me a small part of his knowledge as well as his philosophy in studying and dealing with problems.

I would also like to express my sincere gratitude to Professor Gordon Fenton, Professor Julio Militzer and Professor Sander M. Calisal, for serving as members on the Examining Committee and reviewing this thesis.

My thanks are due to the Natural Science and Engineering Research Council of Canada for their financial support to my studies. I thank the Department of Mechanical Engineering, Dalhousie University for their education support, and the financial support from Faculty Scholarship and Bruce and Dorothy Rosetti Engineering Research Scholarship.

I am grateful to the Martec Limited for the support of the last stage of the thesis work, especially to Dr. Michael Chernuka for encouragement and various helps during

my thesis writing.

Thanks are also to my parents, for their support and sacrifice during my studies, to my dear son, Christopher, for his cooperation, and my husband Wei, who is also my classmate, for his help and useful discussions throughout graduate studies and thesis research.

Abstract

In this thesis, the numerical computation methods for the resistance in calm water and for the seakeeping performance in waves of multi-hull ships have been developed. In the resistance computation, thin ship theory has been applied since this theory fits quite well to the nature of the slenderness and thinness of the hulls.

The problem is solved by the boundary element method in terms of the Green function. The symmetrical part uses the Havelock source distribution on the center plane of the hull whereas the asymmetrical part is achieved through the doublet distribution on the camber surface. By introducing the tent function, the hull form can be easily expressed by the hull offsets.

Employing the numerical methods developed in this thesis, various configurations of multi-hull ships have been analysed. The wave-making interference characteristics of multi-hull ships and the wave wake influence to the wave-making resistance have been discussed. The numerical results have shown significant influences of hull form, speed and arrangement of individual hulls on the resistance of the multi-hull ships. As one step further, the seakeeping performance of a catamaran has been studied. Motions of a catamaran in waves were computed in the time domain.

The external forces acting on hulls include the linearized radiation and diffraction forces, and nonlinear Froude-Krylov force. The linearized radiation and diffraction forces are obtained from the impulse response functions, which are solved by directly using the time-domain Green function. The nonlinear Froude-Krylov force is computed at the "instantaneous wetted surface" of hulls under the incident wave profile. Computed results have been validated with the published data. Then the computer program were used for general analysis.

Chapter 1

Introduction

1.1 Literature Review

In the past decade not only navy authorities but also commercial applications have shown a rapid growth of interest in the development of fast marine vehicles for various applications. A new vessel should be designed such that it will perform at the required speed with minimum power requirement. In the recent years, a great interest has turned to the development of multi-hull vessels. Primary design concerns is the minimization of the multi-hull ship resistance, particularly the wave-making resistance to take advantage of wave interference between hulls.

The multi-hull ships have the advantages of large internal volume, large deck area, good transverse stability, improved seakeeping quality, and a wide range of choices for reducing the wave-making resistance by exploiting arrangements of the hull elements

and varying hull forms. However, it is well known that, when the wave exciting frequency approaches its roll or pitch natural frequency for a multi-hull ship with large beam, simultaneous excitation of large coupled motion of roll and pitch that make crew and passenger seasick may occur. Large vertical motions due to pitch and heave may also cause cross-deck impact and produce heavy sea-loads on structures. The seakeeping study is indeed necessary for high-speed multi-hull vessels let along resistance study.

Advanced multi-hull ships pose many new technical challenges that are beyond the realm of conventional displacement ship design. These ships are characterized by more complex geometric configurations and operation at higher speed. Since a more limited base of experience exists for multi-hull ships, experimental or numerical modeling techniques are very important to a designer. One of the options available to the designers is to use full-scale data from an existing but similar vessel, but required data may not always be available, particularly for newest types of ships. Another involves using model tests for predicting full scale performance, but this requires experimental facilities and is also expensive. Therefore, a flexible, robust, and accurate numerical simulation of ship hydrodynamics is necessary for the performance and safety analysis of this new type of ships.

In the field of ship hydrodynamics, the first theoretical solution for the problem of wave resistance was given by Michell (1898) for a thin ship moving on the surface of an inviscid fluid. The solution is the well-known Michell Integral based on the double Fourier transformation of the velocity potential. Later on, Kelvin(1905) established the fundamental theory of ship waves. Since then many theoretical studies in ship hydrodynamics have been undertaken. But there were no advanced digital computers

available in the early years and the numerical computation, even based on first-order approximation, was still very difficult.

The fast growth of high performance computer has accelerated the development of ship hydrodynamics research. The three-dimensional panel method was developed to improve the solution of the wave-making problem. The Rankine source method was initiated by Gadd(1976) and Dawson(1977) and adopted by many researchers. In this method, the singularity have to be distributed on the water surface as well as the ship surface. On the other hand, the application of the Neumann-Kelvin theory, which is based on the Havelock moving source distribution on the hull surface, has been studied extensively in such works as those by Guevel *et al.*(1977), Noblesse(1983), Andrew and Zhang(1987), Doctors and Beck(1987), Cong and Hsiung(1991). Compared to the Rankine source method, the Havelock source needs only to be distributed on the ship surface since it has satisfied the free surface condition and far field conditions automatically. But the numerical solution of the Neumann-Kelvin problem is difficult due to the complicated kernel in the integral equation. The wave-making Green function, namely the Havelock moving source, contains a few complicated singularities and the function itself is highly oscillatory. This has been investigated by Wehausen and Laitone(1960), Havelock(1965) and Newman(1987).

With the modern Computational Fluid Dynamics technology, the resistance problem can be solved by the Reynolds Averaged Navier-Stokes (or RANS) method (see Larsson *et al.*(1998), Yang and Loehner(1998)). This relies on the numerical solution to the Reynolds-Averaged Navier-Stokes equations for the turbulent flow around the complex geometry of a surface ship. This method is still in the verification and validation stage and is very time consuming even with high speed computers. To be

usable in design and analysis, computational ship hydrodynamics must be accurate, generic and efficient. The slender nature of multi-hulls makes it possible to apply the linearized theory with acceptable accuracy during early stages of design.

As mentioned before, the multi-hull vessels have many advantages. By making its main hull very slender, the increase of wave resistance at high speeds can be within reasonable limits. The required stability can be provided by the outriggers, which can be relatively small and slender. A certain increase in the total wetted surface is inevitable, but this could be overcame by a suitable arrangement of the hull elements. In the development of multi-hull high speed vessels, it is important to pay attention not only to the fuel economy, but also to the detrimental effect of the wave wash on the environment. In a number of parts of the world, the fast-ferry operations have been already constrained in one way or another as a result of complaints of erosion, damage to fixed and floating structures, and danger to small boats, fisherman and swimmers (Kofoed-Hanson and Mikkelsen 1997, Stumbo *et al.* 1999). This boosts further interest in research on the interaction effect between hulls and the wave-making resistance.

Multi-hull ships can be catamarans, trimarans or even four body high speed ship called "SLICE" (Akers, 2000). Optimal forms of a catamaran for minimum resistance was studied by Hsiung and Xu (1988). Both analytical predictions and towing basin validation experiments for the Wave Cancellation Multihull (WCM) of a trimaran were carried out at the David Taylor Model Basin by Wilson *et al.*(1993). In Japan, optimization studies of trimaran configurations have been carried out at the Yokohama National University by Suzuki and Ikehata (1993). Development of trimaran has been reported from the University College London by Andrews and Zhang

(1995). In Sweden, numerical investigation of trimaran configurations was made by Larsson *et al.* (1997) using the SHIPFLOW software package. Computation of trimaran resistance by the tent function approach was carried out by Peng *et al.* (1999). Recent developments were reported at Fast Marine Transportation Conference which is a forum for researchers and operators interested in advanced high-speed marine vehicles and has been held every two years in various locations in the world.

The research on multi-hull seakeeping started later than the investigation of resistance. In early nineties, Kashiwagi (1993) computed the hydrodynamic forces on a Lewis-form catamaran advancing in waves based on Newman's unified slender-ship theory. Applying the strip theory, van't Veer and Siregar (1995) investigated the wave interaction effects of a Wigley catamaran model sailing in head waves in the frequency domain. The results showed that the strip theory became less satisfactory when the speed was increased and the three-dimension effect became more pronounced. Later, van't Veer (1997) used a three-dimensional panel method to compute motions of a catamaran in waves. The interaction effects are automatically included. The hydrodynamic forces of a catamaran with the Lewis form was computed by Ye and Hsiung(1999) in the time domain. When the forward speed is involved the time-domain Green's function is rather simple and requires less computational effort than the frequency-domain Green's function (Peng, *et al.* 2000).

The strip theory (Salvasen *et al.*,1970) and the three-dimensional panel method (Chang, 1977; Inglis and Price, 1981; Guevel and Bougis, 1982) have been widely used to predict ship motions in waves in the frequency domain. But these approaches have practical restrictions for application in multi-hull ships. The strip theory is hard to model interaction between multiple hulls and the three-dimensional Green function

with forward speed in the frequency domain is not easy to compute. For the monohull Green function with forward speed in the frequency domain, Wu and Eatock-Taylor (1987) were able to develop a formulation for computation with some success. On the contrary, the time-domain Green function is versatile in ship hydrodynamic force computation. Based on the methods introduced by Cummins(1962) and Wehausen (1967), the time-domain ship motion can be solved directly by using the time-domain Green function derived by Finklestein (1957). The advantages of the direct method are that it can be extended to solve the quasi-nonlinear hydrodynamic problem as shown by Lin and Yue (1990). More over, it is easier to compute the time-domain Green function numerically than to compute the frequency-domain Green function with a forward speed. Many works on computing motions in the time domain have been published, such as Liapis and Beck (1985), Beck and Liapis (1987), Beck and King (1989), Beck and Magee (1990), Lin and Yue (1994), Qiu, *et al.* (2000). This is quite important to compute motions in the time domain for the high speed multi-hull ships.

1.2 Main Objectives of the Thesis

In this thesis, computational methods for the resistance in calm water and for sea-keeping performance in waves of multi-hull ship are developed. In the resistance computation, thin ship theory is applied since the thin ship form is naturally suitable for the high speed multi-hull ships. By introducing the tent function (Hsiung, 1981), the hull form can be easily expressed by the hull offsets. The resistance coefficient can be expressed as a quadratic form in terms of ship geometry. This is

the first step in determining an optimized ship form. In the seakeeping analysis, the three-dimensional time-domain panel method has been developed to predicate the multi-hull ship motion in waves. The linear time-domain analysis was applied to compute the radiation and diffraction forces. The Froude-Krylov forces and restoring forces were computed on the instantaneous wetted surface under the incident wave profile. This captures some nonlinear phenomena of multi-hull ship motions.

The first objective of the thesis is to develop a numerical method to investigate the multi-hull ship resistance with arbitrary hull forms and arrangements. The problem can be solved in terms of the boundary element method based on the given steady motion Green function. The symmetrical part is based on the Havelock source distribution over the center plane of the hull and the asymmetrical part is achieved by a doublet distribution on the camber surface of the hull which is treated as an airfoil. The strength of the dipole can be found from the hyper-singular Fredholm integral equation of the first kind. By using the tent function, the resistance and wave profile can be easily expressed in terms of the offset of the ship and no effort is needed to panelize the hull surface. This is illustrated in Chapter 2. The present work is aimed at exploiting the wavemaking interference characteristics of multi hull ships and also the wake influence to the wave-making resistance.

The second objective of the thesis is to investigate the seakeeping characteristics of the multi-hull high speed ships. The problem of wave interaction becomes prominent and the time-domain three-dimensional panel method has been developed to predict the multi-hull ship motion in waves. The linearized radiation and diffraction forces were obtained from the impulse response functions, which were solved by using the time-domain Green function and applying the non-impulsive input to the multi-hull

ships. In this work, the discrete Fredholm integral equation of the first kind for the response was solved directly in the time domain at each instant. This method was found to be robust without much numerical difficulty. This aspect of the research is discussed in Chapter 3.

By applying the numerical methods developed for wave resistance computation, multi-hull ships of various configurations and arrangements have been analysed. The numerical results have shown significant influences of hull form, speed and arrangement of hulls on the resistance of multi-hull ships. Another numerical scheme has been developed for seakeeping analysis on a Wigley catamaran. Numerical results related to resistance and seakeeping studies are presented and discussed in Chapter 4. Finally in Chapter 5, conclusions of this thesis research are presented, and recommendations for further development are also proposed.

Chapter 2

Formulation of the Multi-hull Resistance Problem

In this chapter, a general formulation for the wave-making problem of a multi-hull ship with an arbitrary form of demi-hull will be discussed. The linearized wave resistance theory is outlined in section 2.1 and the numerical scheme of computing wave resistance are presented in section 2.2.

2.1 Theoretical Formulation of Wave Resistance

When a ship moves in calm water with a constant speed, it encounters resistance which is caused by the friction between the hull surface and water, and also due to the energy consumed in generating water waves. Froude(1955), as known as Froude's

Hypothesis, separated the total resistance into two components, namely frictional resistance and residuary resistance. The residuary resistance is, by definition, obtained by subtracting the total resistance with an equivalent plank frictional resistance for a plank of the same length and the same wetted surface area. It includes wave-making resistance and viscous form drag. When the ship moves through a viscous fluid which is otherwise at rest, a thin layer of fluid adheres to the body surface to form the boundary layer. Due to velocity gradient across the boundary layer, the fluid is in shear and the body experiences a resistance in the tangential direction which is termed the frictional resistance. The frictional resistance of a multi-hull ship is dependent upon the wetted surface area and Reynolds number, and is assumed to be the same frictional coefficient as an equivalent plank. The viscous form drag is evaluated from an associated form factor. Both the frictional resistance and viscous form drag are due to the viscous effect. By Froude's Hypothesis, viscous resistance and wave resistance are independent of each other. The wave-making resistance is the transfer of energy in the form of water waves, and manifests itself as a force opposing the forward motion. It is the main part of the residuary resistance and can be estimated through the potential flow theory. Conventionlly, the "wave-making" resistance has also been called "wave resistance". From now on, the term "wave resistance" will be used throughout in this thesis. In ship-model resistance tests, the original Froude's Law of Comparison states that if two geometrically similar forms are run at corresponding speeds (i.e. speeds proportional to the square root of their lengths), then their residuary resistances per unit of displacement are the same. Alternatively, the modern day Froude's Law of Fluid Similitude states that if two geometrically similar forms are run at the same Froude number their residuary resistance coefficients will be equal. This is the basis for model resistance tests. The experimentally obtained

residuary resistance coefficient can be corrected through a form factor on the equivalent plank frictional resistance coefficient to give the wave resistance coefficient. That is:

$$C_t = C_f + C_r = C_f(1 + k') + C_w \tag{2.1}$$

$$\text{then} \qquad C_w = C_t - C_f(1 + k') \quad \text{or} \quad C_w = C_r - k'C_f \tag{2.2}$$

where k' = form factor; C_w = wave resistance coefficient; C_r= residuary resistance coefficient; C_f = frictional resistance coefficient of an equivalent plank and C_t= total resistance coefficient. Then the numerical computation of wave resistance coefficient can be verified with the model test.

If all viscous effects are assumed to be limited to the boundary layer, the exterior fluid can be assumed to be inviscid, incompressible and the flow can be considered as irrotational. So the velocity field can be described by a velocity potential satisfying the Laplace equation in the whole fluid domain. At first, the steady potential flow caused by the multihull ship is considered. The multi-hull ship is moving with a constant speed U on an unbounded free surface of deep water. A right-hand Cartesian coordinate system $o - xyz$ moving with the ship has been assumed. The origin o has been taken in the undisturbed water surface at the midship section on the centre line with the oz-axis vertical upwards and the ox-axis parallel to the direction of motion.

The so-called demihulls are assumed having a general shape with an arbitrary camber. The projections of the wetted surfaces of each hulls on its centerplane are denoted by S_i. These projected domains are the planes on which the singularities are to be

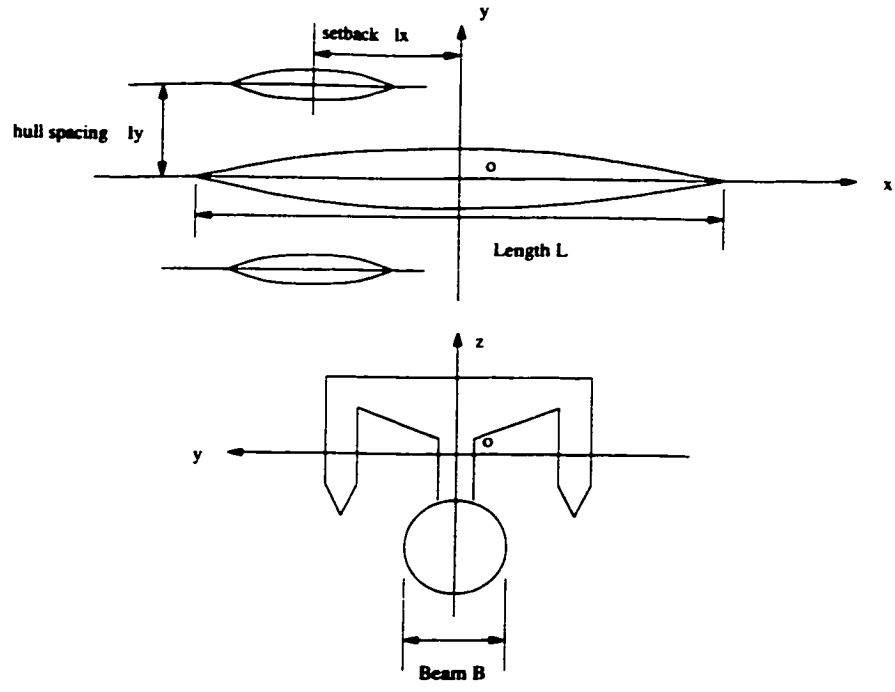

Figure 2.1: The coordinate system of a trimaran in steady forward speed

distributed.

For an irrotational flow, a velocity potential function Φ exists and components of the fluid velocity (u, v, w) can be determined by:

$$\begin{cases} u(x,y,z) = \frac{\partial \Phi}{\partial x}(x,y,z) \\ v(x,y,z) = \frac{\partial \Phi}{\partial y}(x,y,z) \\ w(x,y,z) = \frac{\partial \Phi}{\partial z}(x,y,z) \end{cases} \tag{2.3}$$

The wave-making problem is reduced to determine the potential function Φ, which is defined on the whole exterior domain of the ship as the following:

$$\Phi(x,y,z) = -Ux + \phi(x,y,z) \tag{2.4}$$

where the first term, $-Ux$, is a potential of the uniform flow determined by the steady motion of the ship, and the second term, $\phi(x, y, z)$, is a perturbation potential. Based on the continuity equation of fluid, the potential must satisfy the Laplace equation:

$$\nabla^2\Phi(x, y, z) = 0 \tag{2.5}$$

The unique solution of the governing equation depends on the boundary conditions.

The combined kinematic and dynamic condition on the free surface $z = \zeta(x, y)$ can be obtained as:

$$\frac{\partial^2\phi}{\partial x^2} + k_0\frac{\partial\phi}{\partial z} = k_0(\frac{\partial\phi}{\partial x}\frac{\partial\zeta}{\partial x} + \frac{\partial\phi}{\partial y}\frac{\partial\zeta}{\partial y}) + \frac{1}{2U}\frac{\partial}{\partial x}[(\nabla\phi)^2] \tag{2.6}$$

where k_0 is a wave number, defined as $k_0 = g/U^2$.

The boundary condition on ship hull surface S, which is the wetted surface under the free surface can be written as:

$$\frac{\partial\phi}{\partial n} = Un_x \qquad \text{on } S \tag{2.7}$$

The bottom condition for water of infinite depth is

$$\frac{\partial\phi}{\partial z} = 0 \qquad \text{as } z \to \infty \tag{2.8}$$

The radiation condition is

$$\phi = \left\{ \begin{array}{ll} O(1/\sqrt{x^2+y^2}) & \text{for } x > 0 \\ O(1) & \text{for } x < 0 \end{array} \right\} \quad as \quad R = \sqrt{x^2+y^2} \to \infty \qquad (2.9)$$

This condition guarantees that the wave can only be produced behind the moving disturbing source, but not in front of the source.

Integrating the x-component of dynamic pressure over the wetted hull, the wave resistance can be computed by

$$R_w = -\int\int_S p n_x ds \qquad (2.10)$$

where

S = wetted area of hull surface;

$\mathbf{n} = (n_x, n_y, n_z)$, is normal vector directed outward from the hull surface; and

p = dynamic pressure which is given by the Bernoulli equation as:

$$p = \rho_0 U \frac{\partial \phi}{\partial x} - \rho_0 g \zeta - \frac{1}{2}\rho_0 (\nabla \phi)^2 \qquad (2.11)$$

where ρ_0 = water density, and U = ship speed.

The boundary value problem mentioned above is the exact formulation for a steady wave-making problem. It is impossible to obtain an exact analytical solution of it. The principal difficulty is that the free surface condition is nonlinear and the shape of the free surface is unknown before solving the problem.

By a systematic perturbation expansion based on the thin ship assumption, we have

obtained the following boundary-value problem appropriate for the first-order approximation of the disturbance potential ϕ,

$$\frac{\partial^2\phi}{\partial x^2} + \frac{\partial^2\phi}{\partial y^2} + \frac{\partial^2\phi}{\partial z^2} = 0 \qquad for\ z < 0 \tag{2.12}$$

$$\frac{\partial^2\phi}{\partial x^2} + k_0\frac{\partial\phi}{\partial z} = 0 \quad at\ z = 0 \tag{2.13}$$

$$\phi = \left\{ \begin{array}{ll} O(1/\sqrt{x^2+y^2}) & \text{for } x > 0 \\ O(1) & \text{for } x < 0 \end{array} \right\} \quad as \quad x^2 + y^2 \to \infty \tag{2.14}$$

$$lim_{z\to-\infty}\frac{\partial\phi}{\partial z} = 0 \tag{2.15}$$

In addition, ϕ is required to satisfy the following kinematic conditions on the hull,

$$\frac{\partial\phi}{\partial y}(x, y_i^+, z) = -U\frac{\partial f_i^+}{\partial x} \tag{2.16}$$

$$\frac{\partial\phi}{\partial y}(x, y_i^-, z) = -U\frac{\partial f_i^-}{\partial x} \tag{2.17}$$

where f_i^+ is the port side of the ith hull function and f_i^- is the starboard side of the ith hull function.

The linearized wave elevation, ζ^*, is given by:

$$\zeta^*(x, y) = \frac{U}{g}\frac{\partial\phi(x, y, 0)}{\partial x} \tag{2.18}$$

One remarkable difference between the flow problem of a symmetric monohull and the current problem is the satisfaction of the linearized kinematic boundary conditions on the hull element plane. It requires distributions of both Havelock source and transverse doublets. This is due to the non-symmetric flow or cross-flow effect around the hull. This is from the existence of the other hull in the near field and/or the asymmetry of cambered hull element. The present problem may be decomposed into thickness and lifting problems, which can be treated individually. The results from the thickness problem are related to the strength of the source distribution explicitly to the demihull thickness. The lifting problem, on the other hand, provides an integral equation which is related to the strength of dipole distribution with the hull camber. This will be stated later on.

2.1.1 Wave Resistance for Multi-Hull Ships

The wave resistance for multi-hull ships can be expressed as an extension of the traditional wave resistance of Michell Integral for thin nonsymmetric ship hull forms by including, in addition to the centerplane sources σ_i, a camber surface dipole distribution, μ_i, where the strength of which is related to the asymmetry of the hull forms.

The potential function can be found by the Green function method:

$$\phi = \sum_{i=1}^{K} \phi_{i\sigma} + \sum_{i=1}^{K} \phi_{i\mu} \quad \text{for} \quad i = 1, 2, \cdots, K \tag{2.19}$$

where K = total number of hull elements

$$\phi_{i\sigma} = -\int\int \sigma_i \cdot G(x, y, z; \xi_i, \eta_i, \zeta_i) d\xi_i d\zeta_i \tag{2.20}$$

$$\phi_{i\mu} = \int\int \mu_i \cdot \frac{\partial}{\partial \eta_i} G(x, y, z; \xi_i, \eta_i, \zeta_i) d\xi_i d\zeta_i \tag{2.21}$$

where (x, y, z) is the field point and (ξ, η, ζ) is the source point. The Green function, $G(x, y, z; \xi, \eta, \zeta)$, can be expressed in terms of the Havelock moving source (Wehausen and Laitone, 1960),

$$\begin{aligned} G(x, y, z; \xi, \eta, \zeta) \quad &= -\frac{1}{r} + \frac{1}{r_1} \\ &+ \frac{4k_0}{\pi} \int_0^{\frac{1}{2}\pi} \sec^2\theta d\theta \oint_0^{\infty} dk e^{k(z+\zeta)} \frac{\cos[k(x-\xi)\cos\theta]\cos[k(y-\eta)\sin\theta]}{k - k_0 \sec^2\theta} \\ &+ 4k_0 \int_0^{\frac{1}{2}\pi} sec^2\theta e^{k_0 \sec^2\theta(z+\zeta)} \sin[k_0 \sec\theta(x-\xi)] \\ &\cos[k_0 \sec^2\theta(y-\eta)\sin\theta] d\theta \end{aligned} \tag{2.22}$$

where

$$\begin{aligned} \frac{1}{r} &= \frac{1}{\sqrt{(x-\xi)^2 + (y-\eta)^2 + (z-\zeta)^2}} \\ \frac{1}{r_1} &= \frac{1}{\sqrt{(x-\xi)^2 + (y-\eta)^2 + (z+\zeta)^2}} \end{aligned}$$

The source strength is

$$\sigma_i(x,z) = -\frac{U}{2\pi}\frac{\partial(f_i^+ - f_i^-)/2}{\partial x} \tag{2.23}$$

The dipole strength can be determined by the hyper-singular Fredholm integral equation of the first kind as given below:

$$\frac{1}{4\pi}\frac{\partial}{\partial y}\int\int_S \mu_i \frac{\partial(1/r)}{\partial \eta} d\xi d\zeta = U \cdot \frac{\partial(f_i^+ + f_i^-)/2}{\partial x} \tag{2.24}$$

Having determined the velocity potential in terms of the source and transverse-dipole strengths, we may find the force acting on the ship by Lagally's theorem (Lin 1970),

$$Rw = -16\pi\rho k_0^2 \int_0^{\pi/2} (P^2 + Q^2)\sec^3\theta d\theta \tag{2.25}$$

where

$$P = \sum_{i=1}^{K}(P_{i\sigma} - P_{i\mu}), \qquad Q = \sum_{i=1}^{K}(Q_{i\sigma} - Q_{i\mu}) \tag{2.26}$$

$$\left.\begin{matrix} P_{i\sigma} \\ Q_{i\sigma} \end{matrix}\right\} = \int\int_{S_i} \sigma_i \begin{matrix} \cos \\ \sin \end{matrix} [k_0((\xi_i - lx_i)\cos\theta + ly_i \sin\theta)\sec^2\theta] \exp(k_0\zeta_i \sec^2\theta) d\xi_i d\zeta_i \tag{2.27}$$

$$\left.\begin{matrix} P_{i\mu} \\ Q_{i\mu} \end{matrix}\right\} = k_0 \sec^2\theta \sin\theta \int\int_{S_i} \mu_i \begin{matrix} \sin \\ \cos \end{matrix} [k_0((\xi_i - lx_i)\cos\theta + ly_i \sin\theta)\sec^2\theta] \quad (2.28)$$
$$\exp(k_0\zeta_i \sec^2\theta) d\xi_i d\zeta_i$$

where $k_0 = g/U^2$, the domain S_i is the projected domain of ship hull on each hull centerplane, $\sigma_i(\xi_i, \zeta_i)$ is the source strength at (ξ_i, ζ_i), and $\mu_i(\xi_i, \zeta_i)$ is the dipole strength at (ξ_i, ζ_i).

Coordinates lx_i is the setback of the ith hull element, ly_i is the hull spacing of the ith hull element. The summation is carried out over all the hull elements. Wave resistance R_w contains components produced by the wave-making of each individual hull element (squared terms) $\sum P_i^2$ and $\sum Q_i^2$ and components produced by the wave-making interactions of different hull elements (cross-product terms) $2\sum P_i P_j$ and $2\sum Q_i Q_j$. The squared terms are positive, but the cross-product terms can be either positive or negative, depending on the hull arrangement. It is the negative cross-product terms that are responsible for the potential of a reduction in total wave resistance because of the favorable wave-making interactions for groups of ship hulls.

With the thin ship assumption, the source and dipole distributions are only on the center plane of each hull element. In spite of this, the actual numerical computation is still quite complicated. The numerical formulation should be tested and validated to ensure its applicability.

2.1.2 Wave Profile for Multi-hull Ships

In order to find the wave profile around the ship, the Green function for the thin ship theory can be written as the following form:

$$\begin{aligned} G(x,y,z;\xi,0,\zeta) &= -\frac{1}{r}+\frac{1}{r_1}-\frac{2k_0}{\pi}i\int_{-\frac{\pi}{2}}^{\frac{\pi}{2}} cos\theta e^{v_d}E_1(v_d)d\theta \\ &\quad -4k_0 i\bar{H}[-(x-\xi)]\int_{-\frac{\pi}{2}}^{\frac{\pi}{2}}\sec^2\theta e^{v_s}d\theta \end{aligned} \tag{2.29}$$

with

$$\begin{aligned} v_d &= k_0\cos\theta[-(z+\zeta)\cos\theta + y\sin\theta + i|x-\xi|] \\ v_s &= k_0\sec^2\theta\{-(z+\zeta)+i[(x-\xi)\cos\theta+|y|\sin\theta]\} \end{aligned}$$

the complex exponential integral is defined as

$$E_1(\zeta)=\int_{\zeta}^{\infty}\frac{e^{-\tau}}{\tau}d\tau, \qquad |arg(\zeta)|<\pi \tag{2.30}$$

and $\bar{H}(t)$ is the Heaviside function defined as:

$$\bar{H}(t)=\begin{cases} 0 & t<0 \\ 1 & t\geq 0 \end{cases} \tag{2.31}$$

The wave profile can be directly computed from the linearized dynamic free surface

boundary condition as

$$\zeta^*(x,y) = \frac{U}{g}\frac{\partial\phi(x,y,0)}{\partial x} \tag{2.32}$$

On calm water surface, waves induced by the double body term in the Green function canceled each other. The wave elevation can be computed from the last two terms of the Green function. One is called local wave elevation ζ_l^* and the other is called the free wave elevation ζ_f^* (Cong and Hsiung 1991),

$$\zeta^*(x,y) = \zeta_l^*(x,y) + \zeta_f^*(x,y) \tag{2.33}$$

$$\begin{aligned}
\zeta_l^*(x,y) &= -\frac{U}{4\pi g}\int\int\sum\sigma(\xi_i,\eta_i,\zeta_i)G_{lx}(x,y,0;\xi_i,\eta_i,\zeta_i)dS_i \\
\zeta_f^*(x,y) &= -\frac{U}{4\pi g}\int\int\sum\sigma(\xi_i,\eta_i,\zeta_i)G_{fx}(x,y,0;\xi_i,\eta_i,\zeta_i)dS_i
\end{aligned}$$

where

$$\begin{aligned}
G_{lx}(x,y,0;\xi_i,\eta_i,\zeta_i) &= -\frac{2k_0^2}{\pi}sig(x-\xi_i)\int_{-\frac{\pi}{2}}^{\frac{\pi}{2}}\cos^2\theta Re[e^{v_d}E_1(v_d) - \frac{1}{v_d}]d\theta \\
G_{fx}(x,y,0;\xi_i,\eta_i,\zeta_i) &= -4k_0^2\bar{H}[-(x-\xi_i)]\int_{-\frac{\pi}{2}}^{\frac{\pi}{2}}\sec^3\theta e^{v_s}d\theta
\end{aligned}$$

$sig(t)$ is a signal function defines as

$$sig(t) = \begin{cases} 1 & t > 0 \\ -1 & t < 0 \end{cases} \tag{2.34}$$

2.2 The Numerical Method for Multihull Ship Wave Resistance Computation

As discussed in the last section, the multihull wave resistance can be approximated by the following equation with the coordinate system shown in Figure 2.1:

$$R_w = -16\pi\rho k_0^2 \int_0^{\frac{\pi}{2}} [P^2 + Q^2] \sec^3\theta d\theta \tag{2.35}$$

with

$$P = \sum_{i=1}^{K} (P_{i\sigma} - P_{i\mu}), \qquad Q = \sum_{i=1}^{K} (Q_{i\sigma} - Q_{i\mu}) \tag{2.36}$$

$$\left.\begin{matrix} P_{i\sigma} \\ Q_{i\sigma} \end{matrix}\right\} = \int\int_{S_i} \sigma_i \begin{matrix} \cos \\ \sin \end{matrix} [k_0((\xi_i - lx_i)\cos\theta + ly_i \sin\theta)\sec^2\theta] \exp(k_0\zeta_i \sec^2\theta) d\xi_i d\zeta_i \tag{2.37}$$

$$\left.\begin{matrix} P_{i\mu} \\ Q_{i\mu} \end{matrix}\right\} = k_0 \sec^2\theta \sin\theta \int\int_{S_i} \mu_i \begin{matrix} \sin \\ \cos \end{matrix} [k_0((\xi_i - lx_i)cos\theta + ly_i \sin\theta)\sec^2\theta] \exp(k_0\zeta_i \sec^2\theta) d\xi_i d\zeta_i \tag{2.38}$$

where the wave number

$$k_0 = \frac{g}{U^2} \tag{2.39}$$

These equations are obtained with the thin ship assumption. As a result of the approximation, the strength of the source distribution is determined by the forward speed and the local longitudinal hull slopes:

$$\sigma_i(\xi_i, \zeta_i) = -\frac{U}{2\pi}\frac{\partial H}{\partial \xi_i}(\xi_i, \zeta_i) \tag{2.40}$$

where $H(\xi_i, \zeta_i) = (f_i^+ - f_i^-)/2$ is the half thickness function of the hull element. If the hull element is symmetrical, then $H(\xi_i, \zeta_i)$ coincides with the hull function.

The dipole strength can be found from the hyper-singular Fredholm integral equation of the first kind. It is also the function of the forward speed and the slope of the camber surface

$$\frac{1}{4\pi}\frac{\partial}{\partial y}\int\int \mu_i \frac{\partial(1/r)}{\partial \eta} d\xi_i d\zeta_i = U \cdot \frac{\partial(C(\xi_i, \zeta_i))}{\partial x} \tag{2.41}$$

where $C(\xi_i, \zeta_i) = (f_i^+ + f_i^-)/2$ is the camber surface function of the hull element. If the hull element is symmetrical to its own centerline, then the dipole strength, μ_i, will be zero.

Since there are singularities in the integrand of equation (2.35) at the upper limit of integral, the following transformation is introduced:

$$\sec\theta = \cosh u \tag{2.42}$$

for each θ over $[0, \pi/2]$, u corresponds to a single value within $[0, +\infty]$. Differentiating both sides of equation (2.42) yields:

$$d\theta = \frac{du \cdot \sinh u}{(\sinh u \cdot \cosh u)} = \frac{du}{\cosh u} \tag{2.43}$$

Substituting all these into equation (2.35) leads to

$$R_w = 16\pi\rho k_0^2 \int_0^\infty (P^2 + Q^2) \cosh^2 u du \tag{2.44}$$

$$\left.\begin{matrix} P_{i\sigma} \\ Q_{i\sigma} \end{matrix}\right\} = -\frac{U}{2\pi} \int\int_{S_i} H_{\xi_i}(\xi_i, \zeta_i) \begin{matrix} \cos \\ \sin \end{matrix} (k_0(\xi_i - lx_i) \cosh u + k_0 l y_i \cosh u \sinh u) \exp(k_0 \zeta_i \cosh^2 u) d\xi_i d\zeta_i \tag{2.45}$$

$$\left.\begin{matrix} P_{i\mu} \\ Q_{i\mu} \end{matrix}\right\} = \frac{g}{U^2} \cosh u \sinh u \int\int_{S_i} \mu(\xi_i, \zeta_i) \begin{matrix} \sin \\ \cos \end{matrix} (k_0(\xi_i - lx_i) \cosh u + k_0 l y_i \cosh u \sinh u) \exp(k_0 \zeta_i \cosh^2 u) d\xi_i d\zeta_i \tag{2.46}$$

The integration domain S_i is bounded by $\xi_i : [-\frac{L_i}{2}, \frac{L_i}{2}]$, $\zeta_i : [-T_i, 0]$.

For convenience, the coordinate system is transferred to a new coordinate system, $o' - \xi'\eta'\zeta'$, so the corresponding integral is evaluated within $\xi' : [0, L_i]$, $\zeta' : [0, T_i]$

The relationship between two coordinate systems are

$$\begin{aligned} \xi_i\prime &= \frac{L_i}{2} - \xi_i \\ \eta_i\prime &= -\eta_i \\ \zeta_i\prime &= T_i + \zeta_i \end{aligned} \tag{2.47}$$

with nondimensional forms of x, y and $x \in [0, 1]$

$$\begin{aligned} x_i &= \xi_i'/L_i \\ y_i &= \eta_i'/\frac{B_i}{2} \\ z_i &= \zeta_i'/T_i \end{aligned} \tag{2.48}$$

$$\begin{aligned} x_i &= (\frac{L_i}{2} - \xi_i)/L_i \\ y_i &= -\eta_i/\frac{B_i}{2} \\ z_i &= (T_i + \zeta_i)/T_i \end{aligned} \tag{2.49}$$

Then the integration domain becomes $x_i : [0, 1],\ z_i : [0, 1]$.

Furthermore,

$$\begin{aligned} d\xi_i &= -L_i dx_i \\ d\eta_i &= -\frac{B_i}{2} dy_i \\ d\zeta_i &= T_i dz_i \\ d\xi_i d\zeta_i &= -L_i T_i dx_i dy_i \\ k_0(\xi_i - lx_i) &= \frac{gL_i}{U^2}[\frac{1}{2} - x_i - \frac{lx_i}{L_i}] \\ k_0\zeta_i &= \frac{gL_i}{U^2}[z_i - 1.0]\frac{T_i}{L_i} \end{aligned} \tag{2.50}$$

As defined early, the half-thickness hull function is $H_i(\xi_i, \zeta_i)$, Let

$$h_i(x_i, z_i) = H_i(\xi_i, \zeta_i)/(B_i/2) \tag{2.51}$$

be the non-dimensionalized hull function, then the normalized slope function is:

$$h_{ix}(x_i, z_i) = -\frac{2L_i}{B_i} H_{i\xi}(\xi_i, \zeta_i) \tag{2.52}$$

or

$$H_{i\xi}(\xi_i, \zeta_i) = -\frac{B_i}{2L_i} h_{ix}(x_i, z_i) \tag{2.53}$$

Substituting all of these corresponding dimensionless forms into equation (2.44), the wave resistance formula becomes:

$$R_w = 16\pi\rho k_0^2 \int_0^\infty (P^2 + Q^2)\cosh^2 u du \tag{2.54}$$

$$\left.\begin{matrix} P_{i\sigma} \\ Q_{i\sigma} \end{matrix}\right\} = \frac{U}{2\pi}\frac{B_i T_i}{2}\int_0^1 dz_i \int_0^1 dx_i h_{ix}(x_i, z_i) \begin{matrix}\cos \\ \sin\end{matrix} [\gamma_0(\frac{1}{2} - x_i - \frac{lx_i}{L_i})\cosh u \qquad (2.55)$$
$$+\gamma_0 \frac{ly_i}{L_i}\cosh u \sinh u] \exp[\gamma_0(z_i - 1)\frac{T_i}{L_i}\cosh^2 u]$$

$$\left.\begin{matrix} P_{i\mu} \\ Q_{i\mu} \end{matrix}\right\} = -\frac{gL_i T_i}{U^2}\cosh u \sinh u \int_0^1 dz_i \int_0^1 dx_i \mu_i \begin{matrix}\sin \\ \cos\end{matrix} [\gamma_0(\frac{1}{2} - x_i - \frac{lx_i}{L_i})\cosh u \quad (2.56)$$
$$+\gamma_0 \frac{ly_i}{L_i}\cosh u \sinh u] \exp[\gamma_0(z_i - 1)\frac{T_i}{L_i}\cosh^2 u]$$

where

$$\gamma_0 = \frac{gL_i}{U^2} \qquad (2.57)$$

It can be seen that the hull function now appears in the wave resistance formula explicitly. Thus, in order to carry out the numerical computations, the hull forms must be described analytically. This may cause some difficulties since the hull form usually is given in terms of hull offsets.

By applying the tent function introduced by Hsiung (1981), the hull form can be expressed by the linear shape functions in terms of hull offsets. A unit tent function associated with a grid point in the centerplane, (x_m, z_n), is defined as:

$$h^{m,n}(x,z) = \begin{cases} (1-\frac{x_m-x}{x_m-x_{m-1}})(1-\frac{z_n-z}{z_n-z_{n-1}}) & x_{m-1} \le x \le x_m, z_{n-1} \le z \le z_n \\ (1-\frac{x_m-x}{x_m-x_{m-1}})(1-\frac{z_n-z}{z_n-z_{n+1}}) & x_{m-1} \le x \le x_m, z_n \le z \le z_{n+1} \\ (1-\frac{x_m-x}{x_m-x_{m+1}})(1-\frac{z_n-z}{z_n-z_{n-1}}) & x_m \le x \le x_{m+1}, z_{n-1} \le z \le z_n \\ (1-\frac{x_m-x}{x_m-x_{m+1}})(1-\frac{z_n-z}{z_n-z_{n+1}}) & x_m \le x \le x_{m+1}, z_n \le z \le z_{n+1} \\ 0 \ \textit{elsewhere} \end{cases} \tag{2.58}$$

and

$$h_x^{m,n}(x,z) = \begin{cases} (\frac{1}{x_m-x_{m-1}})(1-\frac{z_n-z}{z_n-z_{n-1}}) & x_{m-1} \le x \le x_m, z_{n-1} \le z \le z_n \\ (\frac{1}{x_m-x_{m-1}})(1-\frac{z_n-z}{z_n-z_{n+1}}) & x_{m-1} \le x \le x_m, z_n \le z \le z_{n+1} \\ (\frac{1}{x_m-x_{m+1}})(1-\frac{z_n-z}{z_n-z_{n-1}}) & x_m \le x \le x_{m+1}, z_{n-1} \le z \le z_n \\ (\frac{1}{x_m-x_{m+1}})(1-\frac{z_n-z}{z_n-z_{n+1}}) & x_m \le x \le x_{m+1}, z_n \le z \le z_{n+1} \\ 0 \ \textit{elsewhere} \end{cases} \tag{2.59}$$

Note that although $h^{(m,n)}(x,z)$ is not a linear function, it is linear in x for z fixed and in z for x fixed in each quadrant of its rectangular element. Figure (2.2) shows a unit tent function.

To construct the hull surface function $h(x,z)$, a family of tent functions will be used. If y_{mn} is the hull offset at (x_m, y_n), we obtain the approximation hull function as:

$$h(x,z) = \sum_{m=1}^{M} \sum_{n=1}^{N} y_{mn} h^{(m,n)}(x,z) \tag{2.60}$$

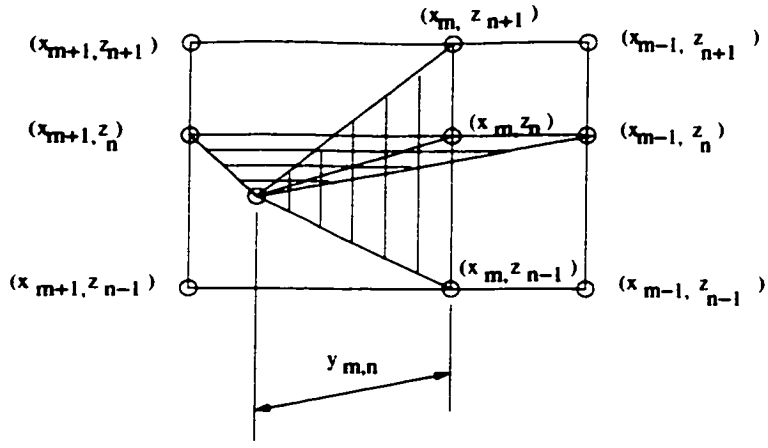

Figure 2.2: A unit tent function

$$h_x(x,z) = \sum_{m=1}^{M}\sum_{n=1}^{N} y_{mn} h_x^{(m,n)}(x,z) \tag{2.61}$$

where $M+1$ is the total number of stations and $N+1$ is the total number of waterlines.

It is clear that in this approximation, the hull function retains exact values at each grid point. In between the adjacent grid points, waterlines and section lines are approximated by straight lines. Figure (2.3) illustrates how a family tent functions can be used to construct a portion of hull. The numerical computation for wave resistance coefficient would be significantly simplified by introducing this approximation.

With the application of the tent function,

$$P_i(u) = \frac{B_i T_i}{2} \sum_{m=1}^{M}\sum_{n=1}^{N} y_{mn} E_n(u,\gamma_0,\frac{T_i}{L_i}) C_m(u,\gamma_0,\frac{ly_i}{L_i})) \tag{2.62}$$

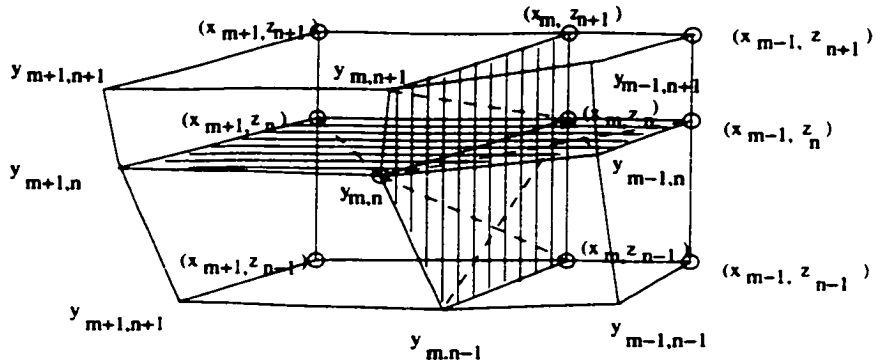

Figure 2.3: A family of tent functions

$$Q_i(u) = \frac{B_i T_i}{2} \sum_{m=1}^{M} \sum_{n=1}^{N} y_{mn} E_n(u, \gamma_0, \frac{T_i}{L_i}) S_m(u, \gamma_0, \frac{ly_i}{L_i}))$$

$$C_m(u, \gamma_0, \frac{B_i ly_i}{2L_i}) = \frac{1}{x_m - x_{m-1}} \tag{2.63}$$
$$\int_{x_{m-1}}^{x_m} \cos[\gamma(\frac{1}{2} - x - \frac{lx_i}{L_i}) \cosh u - \gamma_0 \frac{ly_i}{L_i} \cosh u \sinh u] dx$$
$$+ \frac{1}{x_m - x_{m+1}} \int_{x_m}^{x_{m+1}} \cos[\gamma(\frac{1}{2} - x - \frac{lx_i}{L_i}) \cosh u - \gamma_0 \frac{ly_i}{L_i} \cosh u \sinh u] dx$$
$$= \frac{1}{\gamma_0 \cosh u} \{ \frac{1}{x_m - x_{m-1}} [\sin(\gamma_0 (x_m - \frac{1}{2} + \frac{lx_i}{L_i} \cosh u + \gamma_0 \frac{ly_i}{L_i} \cosh u \sinh u)$$
$$- \sin(\gamma_0 (x_m - \frac{1}{2} + \frac{lx_i}{L_i} \cosh u + \gamma_0 \frac{ly_i}{L_i} \cosh u \sinh u)]$$
$$- \frac{1}{x_{m+1} - x_m} [\sin(\gamma_0 (x_{m+1} - \frac{1}{2} + \frac{lx_i}{L_i} \cosh u + \gamma_0 \frac{ly_i}{L_i} \cosh u \sinh u)$$
$$- \sin(\gamma_0 (x_m - \frac{1}{2} + \frac{lx_i}{L_i} \cosh u + \gamma_0 \frac{ly_i}{L_i} \cosh u \sinh u)] \}$$

where lx_i is the setback of the ith hull element and ly_i is the spacing of the ith hull element.

$$E_n(u,\gamma_0,\frac{T_i}{L_i}) = -\frac{1}{\gamma_0^2(\frac{T_i}{L_i})^2\ cosh^4 u} \tag{2.64}$$
$$\{\frac{1}{z_n - z_{n-1}}[exp(\gamma_0(z_n-1)\frac{T_i}{L_i}\cosh^2 u) - exp(\gamma_0(z_{n-1}-1)\frac{T_i}{L_i}\cosh^2 u)]$$
$$-\frac{1}{z_{n+1}-z_n}[exp(\gamma_0(z_{n+1}-1)\frac{T_i}{L_i}\cosh^2 u) - exp(\gamma_0(z_n-1)\frac{T_i}{L_i}\cosh^2 u)]\}$$

$$S_m(u,\gamma_0,\frac{B_i l y_i}{2L_i}) = \tag{2.65}$$
$$\frac{1}{x_m - x_{m-1}}\int_{x_{m-1}}^{x_m}\sin[\gamma(\frac{1}{2} - x - \frac{lx_i}{L_i})\cosh u - \gamma_0\frac{ly_i}{L_i}\cosh u\sinh u]dx$$
$$+\frac{1}{x_m - x_{m+1}}\int_{x_m}^{x_{m+1}}\sin[\gamma(\frac{1}{2} - x - \frac{lx_i}{L_i})\cosh u - \gamma_0\frac{ly_i}{L_i}\cosh u\sinh u]dx$$
$$= \frac{1}{\gamma_0\cosh u}\{\frac{1}{x_m - x_{m-1}}[\cos(\gamma_0(x_m - \frac{1}{2} + \frac{lx_i}{L_i}\cosh u + \gamma_0\frac{ly_i}{L_i}\cosh u\sinh u)$$
$$-\cos(\gamma_0(x_m - \frac{1}{2} + \frac{lx_i}{L_i}\cosh u + \gamma_0\frac{ly_i}{L_i}\cosh u\sinh u)]$$
$$-\frac{1}{x_{m+1}-x_m}[\cos(\gamma_0(x_{m+1} - \frac{1}{2} + \frac{lx_i}{L_i}\cosh u + \gamma_0\frac{ly_i}{L_i}\cosh u\sinh u)$$
$$-\cos(\gamma_0(x_m - \frac{1}{2} + \frac{lx_i}{L_i}\cosh u + \gamma_0\frac{ly_i}{L_i}\cosh u\sinh u)]\}$$

$$P_{i\mu} = -\frac{U^2\sinh u}{g\cosh^2 U}\sum_{m=1}^{M}\sum_{n=1}^{N}\mu_{(mn)}A_m B_n \tag{2.66}$$

$$Q_{i\mu} = -\frac{U^2\sinh u}{g\cosh^2 U}\sum_{m=1}^{M}\sum_{n=1}^{N}\mu_{(mn)}D_m B_n \tag{2.67}$$

$$
\begin{aligned}
A_m &= \int_{x_{m-1}}^{x_m} \sin(\gamma_0(\frac{1}{2} - x - \frac{l_{xi}}{L_i})\cosh u + \gamma_0(\frac{l_{yi}}{L_i}\cosh u \sinh u)dx \qquad (2.68)\\
&= \frac{1}{\gamma_0 \cosh u}\left[\cos(\gamma_0(x_m - \frac{1}{2} + \frac{l_{xi}}{L_i})\cosh u - \gamma_0(\frac{l_{yi}}{L_i}\cosh u \sinh u))\right]\\
&- \frac{1}{\gamma_0 \cosh u}\left[\cos(\gamma_0(x_m - \frac{1}{2} + \frac{l_{xi}}{L_i})\cosh u - \gamma_0(\frac{l_{yi}}{L_i}\cosh u \sinh u))\right]
\end{aligned}
$$

$$
\begin{aligned}
B_n &= \int_{z_{n-1}}^{z_n} exp[\gamma_0(z-1)\frac{T_i}{L_i}\cosh^2 u]dz \qquad (2.69)\\
&= \frac{1}{\gamma_0}\frac{T_i}{L_i}\cosh^2 u\{exp[\gamma_0(z_n - 1)\frac{T_i}{L_i}\cosh^2 u]\\
&\quad -exp[\gamma_0(z_{n-1} - 1)\frac{T_i}{L_i}\cosh^2 u]\}
\end{aligned}
$$

$$
\begin{aligned}
D_m &= \int_{x_{m-1}}^{x_m} \cos(\gamma_0(\frac{1}{2} - x - \frac{l_{xi}}{L_i})\cosh u + \gamma_0(\frac{l_{yi}}{L_i}\cosh u \sinh u))dx \qquad (2.70)\\
&= \frac{1}{\gamma_0 \cosh u}\left[\sin(\gamma_0(x_m - \frac{1}{2} + \frac{l_{xi}}{L_i})\cosh u - \gamma_0(\frac{l_{yi}}{L_i}\cosh u \sinh u))\right]\\
&- \frac{1}{\gamma_0 \cosh u}\left[\sin(\gamma_0(x_{m-1} - \frac{1}{2} + \frac{l_{xi}}{L_i})\cosh u - \gamma_0(\frac{l_{yi}}{L_i}\cosh u \sinh u))\right]
\end{aligned}
$$

For the purpose of wave resistance coefficient computation, the above integral can be computed numerically.

Here, the total wave resistance has two main components: the resistance of individual hull elements and the resistance due to the interactions between hull elements.

$$R_w = R_{cw} + R_{iw} \tag{2.71}$$

where R_{cw}= wave resistance due to individual hull elements and R_{iw}= wave resistance due to the interaction between hull elements.

Then, the wave-making resistance coefficient of a multi-hull ship can be expressed as:

$$C_w = \frac{R_w}{\frac{1}{2}\rho U^2 S} = C_{cw} + C_{iw} \tag{2.72}$$

where S is the total wetted surface of all hull elements; C_{cw} is wave resistance coefficient due to individual hull elements; and C_{iw} is wave resistance coefficient due to the interaction between hull elements.

2.2.1 Derivation of the Dipole Strength

The potential function of the dipole is

$$\phi_\mu(P) = -\frac{1}{4\pi}\int_{S+S_{wake}} \mu(Q)\frac{\partial}{\partial n}\frac{1}{r(P,Q)}ds \tag{2.73}$$

where μ is the strength of the dipole, S is the camber surface and S_{wake} is the free vortex surface shed from the camber surface.

The camber surface and wake can be discretized into panels according to the base of the tent function. If the strength of the dipole in each panel is constant, then

$$\phi_\mu(P) = -\frac{1}{4\pi}\sum_{j=1}^{N}\mu_j\int_{S_j}\frac{\partial}{\partial n}\frac{1}{r(P,Q)}ds \tag{2.74}$$

where N is the total number of panels.

According to the law of Biot-Savart, the velocity induced from the jth panel of dipole is equal to the velocity generated by the vortex line around that panel, that is

$$\begin{aligned} V_j(P) &= \nabla\phi_j \\ &= \nabla\frac{-\mu_j}{4\pi}\int_{S_j}\frac{\partial}{\partial n}\frac{1}{r(P,Q)}ds \\ &= \frac{-\mu_j}{4\pi}\oint\frac{\mathbf{r}}{r^3}\times d\vec{\ell} \end{aligned} \tag{2.75}$$

where $\mathbf{r} = \mathbf{P}(x,y,z) - \mathbf{Q}(\xi,\eta,\zeta)$, $r = |\mathbf{r}|$ and $\vec{\ell}$ is the direction vector along the vortex line.

The velocity at the control point P will be

$$\begin{aligned} V(P) &= -\sum_j\frac{-\mu_j}{4\pi}\oint\frac{\mathbf{r}}{r^3}\times d\vec{\ell} \\ &= \sum_{j=1}^{N}\mu_j C_j(P) \end{aligned} \tag{2.76}$$

where

$$C_j(P) = \frac{-1}{4\pi} \oint \frac{\mathbf{r}}{r^3} \times d\vec{\ell} \tag{2.77}$$

According to the boundary condition on the camber surface for each control point P_i, we can write

$$n_i \cdot \sum_{j=1}^{N} \mu_j C_j(P_i) = -U \cdot n_i, \qquad i = 1, 2 \cdots N \tag{2.78}$$

Solving the linear system of equations, the dipole strength can be obtained. If the panel points and the field point are known, see Figure 2.4, the $C_j(P)$ will be obtained (Zhang *et al.* (1994)).

$$C_j(P) = C_{12} + C_{23} + C_{34} + C_{41} \tag{2.79}$$

$$C_{mn} = \frac{1}{4\pi} \frac{\mathbf{r}_m \times \mathbf{r}_n}{|\mathbf{r}_m \times \mathbf{r}_n|^2} (\mathbf{r}_{mn} \cdot (\frac{\mathbf{r}_m}{r_m} - \frac{\mathbf{r}_n}{r_n})] \tag{2.80}$$

where $m = 1, 2, 3, 4$, and $n = 2, 3, 4, 1$.

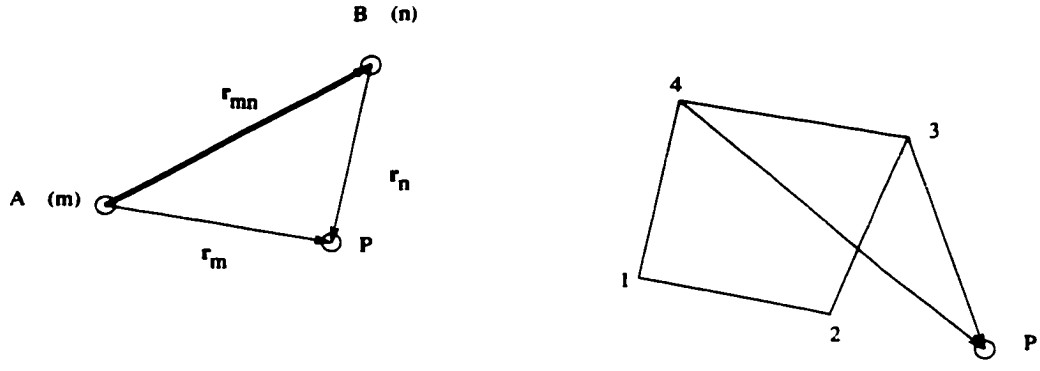

Figure 2.4: Vortex line and panel element

2.2.2 Numerical Formula for Wave Elevation

The wave elevation can be computed by equation (2.33). The local wave can be numerically computed by:

$$\zeta_l^*(x,y) = \frac{Uk_0^2}{2\pi^2 g}\sum_{i=1}^{K}\sum_{m=1}^{M}\sum_{n=1}^{N}\int\int_{\nabla S_{mn}} d\xi_i d\zeta_i \sigma(\xi_i,\eta_i,\zeta_i) sig(-(x-\xi_m)) \quad (2.81)$$
$$\cdot\int_{-\pi/2}^{\pi/2} d\theta \cos^2\theta Re[e^{v_d}E_1(v_d) - \frac{1}{v_d}]$$

where K=the number of hulls, $M+1$ = total number of stations on the centre plane, $N+1$ = total number of waterlines on the centre plane and

$$v_d = k_0 cos\theta[-\zeta_i \cos\theta + y\sin\theta + i|x-\xi_i|] \quad (2.82)$$

Equation (2.81) can not be further reduced by analytical integration because of the existence of the complex exponential integral function E_1. In this case, numerical integration on each element becomes inevitable. The inner integral can be computed

in terms of the Chebyshev expansion (Cong and Hsiung, 1991). Since the effect of the local wave decays quickly with the increase of distance between the field and source points, numerical integration on each panel usually does not produce significant error in the final result on the total wave, particularly in the far field. However, the free wave is a dominant component in the total wave system and is very sensitive to the relative position between the field and source points. Thus analytical integration on each panel is necessary. The free wave due to a quadrilateral panel can be derived as follows:

$$
\begin{aligned}
\zeta^*_{f_{mn}}(x,y) \;=\; & -\frac{4U^2}{\pi g}\int_0^\infty \frac{du}{1+u^2}[\bar{H}(-(x-x_{m+1}+l_{xi})) \\
& \sin[k_0\sqrt{1+u^2}(x-x_{m+1}+l_{xi})]\cos(k_0|y-l_{yi}|u\sqrt{1+u^2}) \\
& -\bar{H}(-(x-\xi_m+l_{xi}))\sin[k_0\sqrt{1+u^2}(x-x_m+l_{xi})]cos(k_0|y-l_{yi}|u\sqrt{1+u^2})] \\
& \cdot\{[e^{-k_0z_{n+1}(1+u^2)}-e^{-k_0z_n(1+u^2)}]\sum_{k=0}^{1}\sum_{l=0}^{1}\frac{y_{m+k,n+l}}{\nabla x_k}[1-\frac{z_{n+l}}{\nabla z_l}+\frac{1}{k_0(1+u^2)\nabla z_l}] \\
& +[z_{n+1}e^{-k_0z_{n+1}(1+u^2)}-z_ne^{-k_0z_n(1+u^2)}]\sum_{k=0}^{1}\sum_{l=0}^{1}\frac{y_{m+k,n+l}}{\nabla x_k}\frac{1}{\nabla z_l}\}
\end{aligned}
\tag{2.83}
$$

Finally, the non-dimensional wave elevation is defined as:

$$
\bar{\zeta} = \frac{\zeta^*}{2k_0} \tag{2.84}
$$

2.2.3 Total Resistance for Multihull Ship

After the wave resistance of multi-hull ships is obtained, the frictional resistance will be calculated. As discussed before, the frictional resistance coefficient is simply taken to be that of the equivalent plank, which has the same length and wetted surface as those of the multi-hull ships, moving with the same forward speed in the direction of its own length. The ITTC (International Towing Tank Conference) 1957 formula is adopted in the current work,

$$C_f = \frac{0.075}{(log_{10}R_n - 2)^2} \tag{2.85}$$

where the C_f is the frictional resistance coefficient and R_n is the Reynolds number in terms of ship length.

Because the individual hull of a multihull ship may have different lengths, even though the speed is the same the Reynolds numbers of the individual hull may be different. Let ρ be the water density and S_i be the wetted surface area of the individual hull, the total frictional resistance of a multi-hull ship can be computed as:

$$R_f = \sum_{i=1}^{K}(\frac{1}{2}\rho U^2 S_i C_{fi}) \tag{2.86}$$

where K is the total number of individual hull; C_{fi} is frictional resistance coefficient of individual hull; U is ship speed.

The total resistance of a multi-hull ship is:

$$R_t = R_w + R_f \tag{2.87}$$

The total resistance coefficient of a multi-hull ship is:

$$C_t = \frac{R_t}{\frac{1}{2}\rho U^2 S} \tag{2.88}$$

where S is the total wetted surface area of a multi-hull ship.

Chapter 3

Time-Domain Analysis of Multi-Hull Motion

3.1 Mathematical Formulation and Assumptions

After the resistance of a multi-hull ship in calm water has been studied, then the motion of a multi-hull ship in waves is now considered. It is assumed that the fluid is inviscid and incompressible. and the flow is irrotational. The multihull ship, assumed to be a rigid body, oscillates in six degrees of freedom with a forward speed in waves. A right-hand Cartesian coordinate system $o - xyz$ moving with the ship has been assumed. The origin o has been taken on the undisturbed water surface intersecting with midship section on the center line with the z-axis vertical upwards and the x-axis parallel to the direction of motion. The flow problem can be described by an initial-boundary value problem which is governed by the Laplace equation subject to

the free surface boundary condition, body boundary condition, bottom condition, far field condition and initial condition. Based on the continuity equation of fluid, the velocity potential Φ satisfies the Laplace equation:

$$\nabla^2\Phi = 0, \quad \text{in the fluid domain} \quad \Omega \tag{3.1}$$

On the body surface $S_B(t)$,

$$\frac{\partial\Phi}{\partial\mathbf{n}} = -V_n, \quad \text{on} \quad S_B \tag{3.2}$$

where t is the time and $\mathbf{n}$ is the unit normal vector pointing into the hull surface from the fluid, and V_n is the velocity normal to the hull surface. On the free surface $S_F(t)$, the dynamic and kinematic boundary conditions have to be satisfied. In the dynamic condition, the pressure on the water surface is equal to the atmospheric pressure. The kinematic condition assures the water particles stay on the free surface. Combining both free surface conditions leads to a nonlinear free surface condition,

$$\Phi_{tt} + 2\nabla\Phi\cdot\nabla\Phi_t + \frac{1}{2}\nabla\Phi\cdot\nabla(\nabla\Phi\cdot\nabla\Phi) + g\Phi_z = 0, \quad \text{on} \quad z = \eta(\mathbf{x},t) \tag{3.3}$$

where $\mathbf{x}(x,y,z)$ represents a point on the free surface and g is the gravitational acceleration. In the far-field, S_∞, $\nabla\Phi \to 0$. On the bottom S_{BT}, $\partial\Phi/\partial n = 0$. The initial conditions are $\Phi(t) = 0$ and $\partial\Phi(t)/\partial t = 0$, for $t = 0$. The initial-boundary value problem mentioned above is highly nonlinear and difficult to solve directly.

With the assumptions that the flow disturbance by a ship is relatively small and the wave is also sufficiently small, a linearized theory can be applied.

The total potential can be written as a summation of four components after linearization:

$$\Phi(\mathbf{x},t) = \hat{\Phi}(\mathbf{x}) + \sum_{k=1}^{6} \phi_k(\mathbf{x},t) + \phi_7(\mathbf{x},t) + \phi_0(\mathbf{x},t) \tag{3.4}$$

where $\hat{\Phi}(\mathbf{x})$ represents the potential of steady flow; $\phi_k(\mathbf{x},t)$ is the radiated wave potential due to the kth mode of motion, $\phi_7(\mathbf{x},t)$ is the diffracted wave potential and $\phi_0(\mathbf{x},t)$ is the potential of incident waves.

The free surface can be linearized on the equilibrium position $z = 0$ for the radiation or diffraction problem as

$$(\frac{\partial}{\partial t} - U\frac{\partial}{\partial z})^2\phi + g\frac{\partial \phi}{\partial z} = 0, \quad \text{on } z = 0 \tag{3.5}$$

where ϕ can be ϕ_k or ϕ_7. The body boundary conditions can be linearized about the mean wetted surface S_0 as

$$\mathbf{n} \cdot \nabla\Phi = 0 \tag{3.6}$$

For the radiation problem, the body boundary condition can be derived according to Timman and Newman (1962) and given by

$$\frac{\partial \phi_k}{\partial n} = U n_k + m_k, \quad \text{on} \quad S_0 \quad \text{for} \quad k = 1, 2, ..., 6 \tag{3.7}$$

where U is the ship forward speed and m_k is the m-term (Newman, 1978), defined by:

$$\begin{aligned} (m_1, m_2, m_3) &= -(\mathbf{n} \cdot \nabla)\vec{W} \\ (m_4, m_5, m_6) &= -(\mathbf{n} \cdot \nabla)(\mathbf{r} \times \vec{W}) \end{aligned}$$

where $\vec{W} = (U, 0, 0)$.

For the diffraction problem, the boundary body condition is given by

$$\frac{\partial \phi_7}{\partial n} = -\frac{\partial \phi_0}{\partial n} \quad \text{on} \quad S_0 \tag{3.8}$$

The Bernoulli equation can be linearized as follows:

$$p(\mathbf{x}, t) = -\rho \frac{\partial \phi}{\partial t} - \rho \vec{W} \cdot \nabla \phi \tag{3.9}$$

where $\vec{W}$ is the velocity vector of the steady flow; ϕ can be either ϕ_k or ϕ_7. Forces acting on the hull then can be computed by integrating the pressure as

$$F(\mathbf{x}, t) = \int_{S_0} p(\mathbf{x}, t) \mathbf{n} dS \tag{3.10}$$

3.2 Equations of Ship Motion

In the multi-hull ship motion analysis, three right-handed coordinate systems (Figure 3.1) are employed. The space-fixed coordinate system, $OXY'Z$, has the OXY' plane coinciding with the undisturbed water surface and the Z-axis pointing vertically upward. The steady moving coordinate system, $\bar{o}\bar{x}\bar{y}$, moves at a steady forward speed, U, with respect to the $OXY'Z$ system in the OX direction, and the $\bar{o}\bar{x}$-axis is in the same direction as the OX-axis; the $\bar{o}\bar{x}\bar{y}$ plane coincides with the calm water surface and the $\bar{o}\bar{z}$-axis is positive upward. In the ship-fixed coordinate system, $o_s x_s y_s z_s$, the origin, o_s, is at the midship section intersecting with the longitudinal plane of symmetry on the calm water surface; the $o_s x_s y_s$ plane coincides with the undisturbed water surface when the ship is at rest; and the positive x_s-axis points toward the bow and the y_s-axis to the port side.

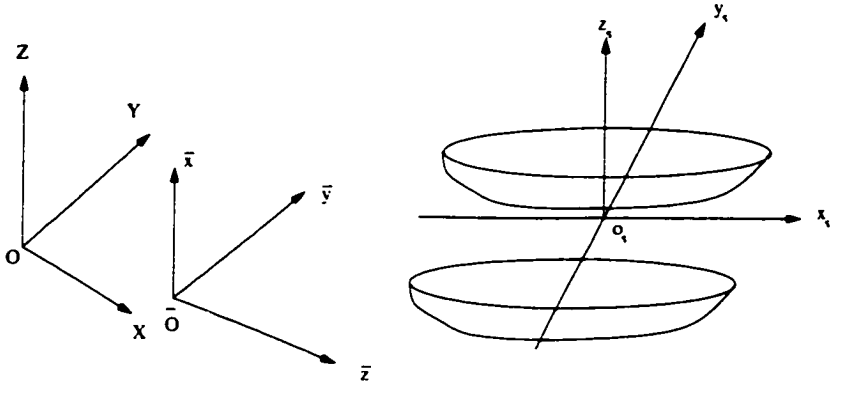

Figure 3.1: The coordinate systems of a catamaran moving in waves

Ship motions are represented by $\boldsymbol{\xi} = \{\xi_1, \xi_2, \xi_3, \xi_4, \xi_5, \xi_6\}$ in the $\bar{o}\bar{x}\bar{y}\bar{z}$ system, where $\{\xi_1, \xi_2, \xi_3\}$ are the displacements of the center of gravity CG, and $\{\xi_4, \xi_5, \xi_6\}$ are the Eulerian angles of the ship. The Eulerian angles are the measurements of the ship's

angular displacements about the axes which pass through the CG. The instantaneous translational velocities of ship motion in the directions of $o_s x_s$, $o_s y_s$ and $o_s z_s$ are $\{\dot{x}_1, \dot{x}_2, \dot{x}_3\}$, and the angular velocities about axes parallel to $o_s x_s$, $o_s y_s$ and $o_s z_s$ and passing through CG are $\{\dot{x}_4, \dot{x}_5, \dot{x}_6\}$. The equations of motion for a multi-hull ship are

$$(M_{ij} + \Delta m_{ij})\ddot{X}_j + B_{ij}\dot{X}_j + C_{ij}X_j + S_i = F_i, \quad i = 1, 2, ..., 6 \tag{3.11}$$

where $\ddot{\mathbf{X}} = \{\ddot{x}_1, \ddot{x}_2, \ddot{x}_3, \ddot{x}_4, \ddot{x}_5, \ddot{x}_6\}$; Δm_{ij}, B_{ij} and C_{ij} are the added-mass, the damping coefficient and the restoring force coefficient in the time domain, respectively. Details on the computation of these coefficients are given by Liapias (1986). The mass and inertia matrices are

$$\mathbf{M} = \begin{bmatrix} m & 0 & 0 & 0 & 0 & 0 \\ 0 & m & 0 & 0 & 0 & 0 \\ 0 & 0 & m & 0 & 0 & 0 \\ 0 & 0 & 0 & I_{11} & 0 & -I_{13} \\ 0 & 0 & 0 & 0 & I_{22} & 0 \\ 0 & 0 & 0 & -I_{13} & 0 & I_{33} \end{bmatrix} \tag{3.12}$$

$$\mathbf{S} = \begin{Bmatrix} m(\dot{x}_5\dot{x}_3 - \dot{x}_6\dot{x}_2) \\ m(\dot{x}_6\dot{x}_1 - \dot{x}_4\dot{x}_3) \\ m(\dot{x}_4\dot{x}_2 - \dot{x}_5\dot{x}_1) \\ \dot{x}_5\dot{x}_6(I_{33} - I_{22}) - I_{13}\dot{x}_4\dot{x}_5 \\ \dot{x}_4\dot{x}_6(I_{11} - I_{33}) - I_{13}(\dot{x}_6^2 - \dot{x}_4^2) \\ \dot{x}_4\dot{x}_5(I_{22} - I_{11}) + I_{13}\dot{x}_5\dot{x}_6 \end{Bmatrix} \tag{3.13}$$

where m is the ship mass and I_{ij} is the moment of inertia.

The external force vector, $\mathbf{F}$, acting on the ship is

$$\begin{aligned} F_i(t) &= \sum_{k=1}^{6} \int_0^t K_{ik}^R(t-\tau)\dot{x}_k(\tau)d\tau + \int_{-\infty}^{\infty} K_{i7}^D(t-\tau)\eta_0(\tau)d\tau \\ &+ F_i^{FK}(t) + F_i^{RS}(t) + F_i^{SLAM}(t) + F_i^{\nu}(t) + F_i^{MC}(t), \quad \text{for} \quad i = 1, 2, ..., 6 \end{aligned} \tag{3.14}$$

where $K_{ik}^R(t)$ and $K_{i7}^D(t)$ are the impulse response functions due to radiated and diffracted waves, which are computed by employing non-impulsive input, details are given by King (1987), Cong, *et al.* (1998) and Qiu *et al.* (2001); $\eta_0(t)$ is the free surface elevation of the incident wave at the origin of the steady-moving coordinate system; $F_i^{FK}(t)$ is the nonlinear Froude-Krylov force vector; $F_i^{RS}(t)$ is the restoring force vector; $F_i^{\nu}(t)$ is the viscous force vector; $F_i^{SLAM}(t)$ is the bow flare slamming forces; and $F_i^{MC}(t)$ is the vector of miscellaneous forces which include the propeller thrust, maneuvering forces, and rudder forces. These forces were computed based on

the work by Huang and Hsiung (1996).

The velocities of motion in the $\bar{o}\bar{x}\bar{y}\bar{z}$ system are related to those in the $o_s x_s y_s z_s$ system as follows:

$$\dot{\xi}_i = R_{ij}\dot{X}_j, \quad i = 1, 2, ..., 6 \tag{3.15}$$

where $\dot{\boldsymbol{\xi}}$ represents the vector of ship perturbation velocities in the steady-moving coordinate system. The transformation matrix $\mathbf{R}$ is

$$\mathbf{R} = \begin{bmatrix} \mathbf{R_C} & \mathbf{0} \\ \mathbf{0} & \mathbf{R_D} \end{bmatrix} \tag{3.16}$$

where

$$\mathbf{R_C} = \begin{bmatrix} c_2c_3 & s_1s_2c_3 - c_1s_3 & c_1s_2c_3 + s_1s_3 \\ c_2s_3 & s_1s_2s_3 + c_1c_3 & c_1s_2s_3 - s_1c_3 \\ -s_2 & s_1c_2 & c_1c_2 \end{bmatrix} \tag{3.17}$$

and

$$\mathbf{R_D} = \begin{bmatrix} 1 & s_1t_2 & c_1t_2 \\ 0 & c_1 & -s_1 \\ 0 & s_1/c_2 & c_1/c_2 \end{bmatrix} \tag{3.18}$$

where $c_i = \cos(x_i)$, $s_i = \sin(x_i)$ and $t_i = \tan(x_i)$ for i=4, 5 and 6.

Ship motions in the steady-moving coordinate system can be solved from equations

(3.11) and (3.15) by the Runge-Kutta scheme.

3.2.1 Radiation and Diffraction Forces

By employing the time-dependent Green function (Wehausen and Laitone, 1960), the boundary integral equation of linearized radiation and diffraction problems can be solved from the integral equations in terms of source strength distribution. A panel method has been developed to solve the integral equations for the radiation and diffraction problems in the time domain. The impulse response function method is used to describe the radiation forces on the ship hull. One way to obtain the impulse response function is by introducing a non-impulsive input motion and solving the integral equation directly in the time domain (Cong, et al. 1998).

3.2.2 Time-Domain Green Function

The Green function is given by

$$G(P,Q,t-\tau) = G_0(P,Q)\delta(t-\tau) + \bar{H}(t-\tau)G_F(P,Q,t-\tau) \qquad (3.19)$$

with

$$G_0(P,Q) = \frac{1}{r} - \frac{1}{r'} \qquad (3.20)$$

the Dirac delta function:

$$\delta(t-\tau) = \begin{cases} 0, & t \neq \tau \\ \infty, & t = \tau \end{cases} \tag{3.21}$$

and $\bar{H}(t-\tau)$ is the Heaviside unit step function expressed before as equation (2.31)

$$\bar{H}(t-\tau) = \begin{cases} 0 & t < \tau \\ 1 & t \geq \tau \end{cases} \tag{3.22}$$

$$G_F(P,Q,t-\tau) = 2\int_0^\infty \sqrt{gk}\sin[\sqrt{gk}(t-\tau)]e^{k(z+z')}J_0(kR)dk \tag{3.23}$$

where

$$r = \sqrt{(x-x')^2+(y-y')^2+(z-z')^2}, \tag{3.24}$$

$$r' = \sqrt{(x-x')^2+(y-y')^2+(z+z')^2}, \tag{3.25}$$

$$R = \sqrt{(x-x')^2+(y-y')^2}, \tag{3.26}$$

and J_0 is the first kind Bessel function of the zeroth order.

3.2.3 Solving for the Source Strength

In a radiation problem, the source strength can be solved from the boundary integral equation as follows (Qiu, et al. 2001):

$$\begin{aligned} V_n(P,t) = & -\frac{1}{2}\sigma(P,t) - \frac{1}{4\pi}\int_0^t d\tau \int\int_{S_0} \frac{\partial G(P,Q,t-\tau)}{\partial n}\sigma(Q,\tau)dS \\ & - \frac{U^2}{4\pi g}\int_0^t d\tau \oint_\Gamma n_1 \frac{\partial G(P,Q,t-\tau)}{\partial n}\sigma(Q,\tau)dl \end{aligned} \tag{3.27}$$

where $V_n(P,t)$ is the normal velocity of a point P on hull surface at time t in ship fixed coordinate system. For simplicity, we assume the mean wetted surfaces of demihulls of a catamaran are represented by S_a and S_b ($S_0 = S_a + S_b$), respectively. The waterlines on demihulls are represented by Γ_a and Γ_b ($\Gamma = \Gamma_a + \Gamma_b$). The number of panels on demihulls are n_a for S_a and n_b for S_b, respectively; and the number of segments on Γ_a and Γ_b are m_a and m_b, respectively.

By defining

$$\begin{aligned} G_{n_{ij}}^{aa}(t) &= -\frac{1}{4\pi}\int_0^t d\tau \int\int_{S_a^j} \frac{\partial G(P_a^i, Q_a^j, t-\tau)}{\partial n}\sigma(Q_a^j,\tau)dS \\ G_{n_{ij}}^{ab}(t) &= -\frac{1}{4\pi}\int_0^t d\tau \int\int_{S_b^j} \frac{\partial G(P_a^i, Q_b^j, t-\tau)}{\partial n}\sigma(Q_b^j,\tau)dS \\ G_{n_{ij}}^{ba}(t) &= -\frac{1}{4\pi}\int_0^t d\tau \int\int_{S_a^j} \frac{\partial G(P_b^i, Q_a^j, t-\tau)}{\partial n}\sigma(Q_a^j,\tau)dS \end{aligned} \tag{3.28}$$

$$G_{n_{ij}}^{bb}(t) = -\frac{1}{4\pi}\int_0^t d\tau \int\int_{S_b^j} \frac{\partial G(P_b^i, Q_b^j, t-\tau)}{\partial n}\sigma(Q_b^j,\tau)dS$$

$$\begin{aligned}
L_{n_{ij}}^{aa}(t) &= -\frac{U^2}{4\pi g}\int_0^t d\tau \oint_{\Gamma_a^j} {}^a n_1^j \frac{\partial G(P_a^i, Q_a^j, t-\tau)}{\partial n}\sigma(Q_a^j,\tau)dl \qquad (3.29)\\
L_{n_{ij}}^{ab}(t) &= -\frac{U^2}{4\pi g}\int_0^t d\tau \oint_{\Gamma_b^j} {}^b n_1^j \frac{\partial G(P_a^i, Q_b^j, t-\tau)}{\partial n}\sigma(Q_b^j,\tau)dl\\
L_{n_{ij}}^{ba}(t) &= -\frac{U^2}{4\pi g}\int_0^t d\tau \oint_{\Gamma_a^j} {}^a n_1^j \frac{\partial G(P_b^i, Q_a^j, t-\tau)}{\partial n}\sigma(Q_a^j,\tau)dl\\
L_{n_{ij}}^{bb}(t) &= -\frac{U^2}{4\pi g}\int_0^t d\tau \oint_{\Gamma_a^j} {}^b n_1^j \frac{\partial G(P_b^i, Q_b^j, t-\tau)}{\partial n}\sigma(Q_b^j,\tau)dl
\end{aligned}$$

where i and j denote the ith and jth panels. Equation (3.27) can be written as

$$\begin{aligned}
V_n(P_i^a, t) &= -\frac{1}{2}\sigma(P_i^a, t) + \sum_{j=1}^{n_a} G_{n_{ij}}^{aa}(t) + \sum_{j=1}^{n_b} G_{n_{ij}}^{ab}(t) \qquad (3.30)\\
&+ \sum_{j=1}^{m_a} L_{n_{ij}}^{aa}(t) + \sum_{j=1}^{m_b} L_{n_{ij}}^{ab}(t)
\end{aligned}$$

$$V_n(P_i^b, t) = -\frac{1}{2}\sigma(P_i^b, t) + \sum_{j=1}^{n_a} G_{n_{ij}}^{ba}(t) + \sum_{j=1}^{n_b} G_{n_{ij}}^{bb}(t) \qquad (3.31)$$

$$+ \sum_{j=1}^{m_a} L_{n_{ij}}^{ba}(t) + \sum_{j=1}^{m_b} L_{n_{ij}}^{bb}(t)$$

where P_i^a and P_i^b represent the ith panel on S_a and S_b. respectively. Substituting the Green function into equation (3.28) leads to

$$\begin{aligned}
{}^{aa}I_{ij}^0 &= -\frac{1}{4\pi}\int\int_{S_a^j} \frac{\partial G_0(P_a^i, Q_a^j)}{\partial n} dS \\
{}^{ab}I_{ij}^0 &= -\frac{1}{4\pi}\int\int_{S_b^j} \frac{\partial G_0(P_a^i, Q_b^j)}{\partial n} dS \\
{}^{ba}I_{ij}^0 &= -\frac{1}{4\pi}\int\int_{S_a^j} \frac{\partial G_0(P_b^i, Q_a^j)}{\partial n} dS \\
{}^{bb}I_{ij}^0 &= -\frac{1}{4\pi}\int\int_{S_b^j} \frac{\partial G_0(P_b^i, Q_b^j)}{\partial n} dS
\end{aligned} \tag{3.32}$$

$$\begin{aligned}
{}^{aa}I_{F_{ij}}^{k_t-k} &= -\frac{1}{4\pi}\int\int_{S_a^j} \frac{\partial G_F(P_a^i, Q_a^j, t-t_k)}{\partial n} dS \\
{}^{ab}I_{F_{ij}}^{k_t-k} &= -\frac{1}{4\pi}\int\int_{S_b^j} \frac{\partial G_F(P_a^i, Q_b^j, t-t_k)}{\partial n} dS \\
{}^{ba}I_{F_{ij}}^{k_t-k} &= -\frac{1}{4\pi}\int\int_{S_a^j} \frac{\partial G_F(P_b^i, Q_a^j, t-t_k)}{\partial n} dS \\
{}^{bb}I_{F_{ij}}^{k_t-k} &= -\frac{1}{4\pi}\int\int_{S_b^j} \frac{\partial G_F(P_b^i, Q_b^j, t-t_k)}{\partial n} dS
\end{aligned} \tag{3.33}$$

$${}^{aa}L_{F_{ij}}^{k_t-k} = -\frac{U^2}{4\pi g}\int\int_{\Gamma_a^j} {}^{a}n_1{}^{j} \frac{\partial G_F(P_a^i, Q_a^j, t-t_k)}{\partial n} dl \tag{3.34}$$

$$
\begin{aligned}
{}^{ab}L_{F_{ij}}^{k_t-k} &= -\frac{U^2}{4\pi g}\int\int_{\Gamma_b^j} {}^{b}n_1{}^{j}\frac{\partial G_F(P_a^i, Q_b^j, t-t_k)}{\partial n}dl \\
{}^{ba}L_{F_{ij}}^{k_t-k} &= -\frac{U^2}{4\pi g}\int\int_{\Gamma_a^j} {}^{a}n_1{}^{j}\frac{\partial G_F(P_b^i, Q_a^j, t-t_k)}{\partial n}dl \\
{}^{bb}L_{F_{ij}}^{k_t-k} &= -\frac{U^2}{4\pi g}\int\int_{\Gamma_b^j} {}^{b}n_1{}^{j}\frac{\partial G_F(P_b^i, Q_b^j, t-t_k)}{\partial n}dl
\end{aligned}
$$

Assuming that the source strength is constant over a panel and using the trapezoidal integration method for the time integration, equation (3.27) can be discretized as follows:

$$
\mathbf{V}_{ni}^{k_t} = -\frac{1}{2}\boldsymbol{\sigma}_i^{k_t} + \mathbf{I}_i^0\boldsymbol{\sigma}_i^{k_t} + \Delta t\left(\frac{1}{2}\boldsymbol{\phi}_i^0 + \sum_{k=1}^{k_t-1}\boldsymbol{\phi}_i^k\right) + \Delta t\left(\frac{1}{2}\boldsymbol{\phi}_{\boldsymbol{L}_i}{}^0 + \sum_{k=1}^{k_t-1}\boldsymbol{\phi}_{\boldsymbol{L}_i}{}^k\right) \tag{3.35}
$$

where

$$
\mathbf{V}_{ni}^{k_t} = \begin{pmatrix} {}^{a}\mathbf{V}_{ni}^{k_t} \\ {}^{b}\mathbf{V}_{ni}^{k_t} \end{pmatrix} \qquad \boldsymbol{\sigma}_i^{k_t} = \begin{pmatrix} {}^{a}\sigma_i^{k_t} \\ {}^{b}\sigma_i^{k_t} \end{pmatrix} \tag{3.36}
$$

$$
\mathbf{I}_i^0 = \begin{bmatrix} \sum_{j=1}^{n_a} {}^{aa}I_{ij}^0 & \sum_{j=1}^{n_b} {}^{ab}I_{ij}^0 \\ \sum_{j=1}^{n_a} {}^{ba}I_{ij}^0 & \sum_{j=1}^{n_b} {}^{bb}I_{ij}^0 \end{bmatrix} \tag{3.37}
$$

$$\boldsymbol{\phi}_i^0 = \begin{pmatrix} \sum_{j=1}^{n_a} {}^{aa}I_{F_{ij}}^{k_t a}\sigma_j^0 + \sum_{j=1}^{n_b} {}^{ab}I_{F_{ij}}^{k_t b}\sigma_j^0 \\ \sum_{j=1}^{n_a} {}^{ba}I_{F_{ij}}^{k_t a}\sigma_j^0 + \sum_{j=1}^{n_b} {}^{bb}I_{F_{ij}}^{k_t b}\sigma_j^0 \end{pmatrix} \tag{3.38}$$

$$\boldsymbol{\phi}_i^k = \begin{pmatrix} \sum_{j=1}^{n_a} {}^{aa}I_{F_{ij}}^{k_t-k a}\sigma_j^k + \sum_{j=1}^{n_b} {}^{ab}I_{F_{ij}}^{k_t-k b}\sigma_j^k \\ \sum_{j=1}^{n_a} {}^{ba}I_{F_{ij}}^{k_t-k a}\sigma_j^k + \sum_{j=1}^{n_b} {}^{bb}I_{F_{ij}}^{k_t-k b}\sigma_j^k \end{pmatrix} \tag{3.39}$$

$$\boldsymbol{\phi}_{\boldsymbol{L}_i}^0 = \begin{pmatrix} \sum_{j=1}^{n_a} {}^{aa}L_{F_{ij}}^{k_t a}\sigma_{L_j}^0 + \sum_{j=1}^{n_b} {}^{ab}L_{F_{ij}}^{k_t b}\sigma_{L_j}^0 \\ \sum_{j=1}^{n_a} {}^{ba}L_{F_{ij}}^{k_t a}\sigma_{L_j}^0 + \sum_{j=1}^{n_b} {}^{bb}L_{F_{ij}}^{k_t b}\sigma_{L_j}^0 \end{pmatrix} \tag{3.40}$$

$$\boldsymbol{\phi}_{\boldsymbol{L}_i}^k = \begin{pmatrix} \sum_{j=1}^{n_a} {}^{aa}L_{F_{ij}}^{k_t-k a}\sigma_{L_j}^k + \sum_{j=1}^{n_b} {}^{ab}L_{F_{ij}}^{k_t-k b}\sigma_j^k \\ \sum_{j=1}^{n_a} {}^{ba}L_{F_{ij}}^{k_t-k a}\sigma_{L_j}^k + \sum_{j=1}^{n_b} {}^{bb}L_{F_{ij}}^{k_t-k b}\sigma_j^k \end{pmatrix} \tag{3.41}$$

where Δt is the time step; ${}^a\sigma_i^{k_t}$ and ${}^b\sigma_i^{k_t}$ are the source strengths in six modes of motion for the ith panel on S_a and S_b at the time $t = k_t\Delta t$, respectively; ${}^aV_{ni}^{k_t}$ ${}^bV_{ni}^{k_t}$ are the corresponding normal velocities in six modes; $\tau = t_k = k\Delta t$; ${}^a\sigma_{L_i}^{k_t}$ and ${}^b\sigma_{L_i}^{k_t}$ denote the source strength on the ith waterline segment on Γ_a and Γ_b, respectively,

at time step t;

With these definitions, we obtain a system of linear equations which are solved for $\boldsymbol{\sigma}^{k_t}$.

$$\mathbf{A}^{k_t}\boldsymbol{\sigma}^{k_t} = \mathbf{B}^{k_t} \tag{3.42}$$

where

$$\mathbf{A}_i^{k_t} = -\frac{1}{2}\mathbf{I} + \mathbf{I}_i^0 \tag{3.43}$$

where $\mathbf{I}$ is the unit matrix.

$$\mathbf{B}_i^{k_t} = (\mathbf{V}_{ni})^{k_t} - \Delta t\left(\frac{1}{2}\boldsymbol{\phi}^0 + \sum_{k=1}^{k_t-1}\boldsymbol{\phi}_i^k\right) - \Delta t\left(\frac{1}{2}(\boldsymbol{\sigma}_{\boldsymbol{L}_i}^0 + \sum_{k=1}^{k_t-1}\boldsymbol{\sigma}_{\boldsymbol{L}_i}^k\right) \tag{3.44}$$

3.2.4 Computation of the Velocity Potential

After the source strength is solved from equation (3.27), the velocity potential $\phi(P,t)$ can be obtained from:

$$\begin{aligned}\phi(P,t) &= -\frac{1}{4\pi}\int_0^t d\tau \int\int_{S_0} G(P,Q,t-\tau)\sigma(Q,\tau)dS \\ &- \frac{U^2}{4\pi g}\int_0^t d\tau \oint_\Gamma n_1 G(P,Q,t-\tau)\sigma(Q,\tau)dl\end{aligned} \tag{3.45}$$

The above equation can be discretized in a similar way to equation (3.27). Introducing

$$
\begin{aligned}
G_{ij}^{aa}(t) &= -\frac{1}{4\pi}\int_0^t d\tau \int\int_{S_a^j} G(P_a^i, Q_a^j, t-\tau)\sigma(Q_a^j,\tau)dS \\
G_{ij}^{ab}(t) &= -\frac{1}{4\pi}\int_0^t d\tau \int\int_{S_b^j} G(P_a^i, Q_b^j, t-\tau)\sigma(Q_b^j,\tau)dS \\
G_{ij}^{ba}(t) &= -\frac{1}{4\pi}\int_0^t d\tau \int\int_{S_a^j} G(P_b^i, Q_a^j, t-\tau)\sigma(Q_a^j,\tau)dS \\
G_{ij}^{bb}(t) &= -\frac{1}{4\pi}\int_0^t d\tau \int\int_{S_b^j} G(P_b^i, Q_b^j, t-\tau)\sigma(Q_b^j,\tau)dS
\end{aligned}
\tag{3.46}
$$

$$
\begin{aligned}
L_{ij}^{aa}(t) &= -\frac{U^2}{4\pi g}\int_0^t d\tau \oint_{\Gamma_a^j} {}^a n_1^j G(P_a^i, Q_a^j, t-\tau)\sigma(Q_a^j,\tau)dl \\
L_{ij}^{ab}(t) &= -\frac{U^2}{4\pi g}\int_0^t d\tau \oint_{\Gamma_b^j} {}^b n_1^j G(P_a^i, Q_b^j, t-\tau)\sigma(Q_b^j,\tau)dl \\
L_{ij}^{ba}(t) &= -\frac{U^2}{4\pi g}\int_0^t d\tau \oint_{\Gamma_a^j} {}^a n_1^j G(P_b^i, Q_a^j, t-\tau)\sigma(Q_a^j,\tau)dl \\
L_{ij}^{bb}(t) &= -\frac{U^2}{4\pi g}\int_0^t d\tau \oint_{\Gamma_a^j} {}^b n_1^j G(P_b^i, Q_b^j, t-\tau)\sigma(Q_b^j,\tau)dl
\end{aligned}
\tag{3.47}
$$

then the velocity potential ${}^a\phi_i^{k_t}$ and ${}^b\phi_i^{k_t}$ at the ith panel of S_a and S_b can be computed from

$$
{}^a\phi_i^{k_t} = \sum_{j=1}^{n_a} G_{ij}^{aaa}\sigma_j^{k_t} + \sum_{j=1}^{n_b} G_{ij}^{abb}\sigma_j^{k_t} \tag{3.48}
$$

$$+ \sum_{j=1}^{m_a} L_{ij}^{aaa} \sigma_{L_j}^{k_t} + \sum_{j=1}^{m_b} L_{ij}^{abb} \sigma_{L_j}^{k_t} \quad i = 1, \ldots n_a$$

$$\begin{aligned} {}^{b}\phi_i^{k_t} &= \sum_{j=1}^{n_a} G_{ij}^{baa} \sigma_j^{k_t} + \sum_{j=1}^{n_b} G_{ij}^{bbb} \sigma_j^{k_t} \\ &+ \sum_{j=1}^{m_a} L_{ij}^{baa} \sigma_{L_j}^{k_t} + \sum_{j=1}^{m_b} L_{ij}^{bbb} \sigma_{L_j}^{k_t} \quad i = 1, \ldots n_b \end{aligned} \tag{3.49}$$

In the diffraction problem, the source strength and velocity potential can be solved by employing the same method as discussed above.

3.2.5 Nonlinear Incident Wave Forces

The Froude-Krylov forces and restoring forces were computed on the instantaneous wetted surface of the multihull ship under the incident wave profile.

At each time step the instantaneous position of any point on the surface of the hull can be computed in the steady-moving coordinate system as follows:

$$\begin{pmatrix} \bar{x} \\ \bar{y} \\ \bar{z} \end{pmatrix} = \begin{pmatrix} d_1 + x_g \\ d_2 + y_g \\ d_3 + z_g \end{pmatrix} + [R_{ij}] \begin{pmatrix} x_s - x_g \\ y_s - y_g \\ z_s - z_g \end{pmatrix}, \quad i, j = 1, 2, 3 \tag{3.50}$$

where $(\bar{x}, \bar{y}, \bar{z})$ are the coordinates of a point in the steady-moving coordinate system;

(x_g, y_g, z_g) are coordinates of the center of gravity in the ship-fixed coordinate system; (d_1, d_2, d_3) are translational displacements in the steady-moving coordinate system; and (x_s, y_s, z_s) are the coordinates of a point in the ship-fixed coordinate system. $[R_{ij}]$ is the transformation matrix, as in equation (3.16), between the ship-fixed coordinate system and the steady-moving coordinate system. The corresponding point in the space-fixed system, (X, Y, Z), can be expressed as

$$\begin{pmatrix} X \\ Y \\ Z \end{pmatrix} = \begin{pmatrix} Ut + \bar{x} \\ \bar{y} \\ \bar{z} \end{pmatrix} \tag{3.51}$$

At each time step, the instantaneous position of the hull in the space-fixed system can be obtained from equation (3.50) and (3.51). Pressures are computed on panels up to the bulwark.

When computing the hydrodynamic pressure due to incident waves, it is assumed that the pressure is bilinearly distributed over a panel. The hull up to the bulwark is discretized by quadrilateral panels. A quadrilateral panel and its mapping relationship to the local reference coordinate system is shown in Figure 3.2.

The pressure at any point on a panel due to the incident wave is given as

$$\bar{p}_0(X, Y, Z; t) = \sum_{i=1}^{4} N_i(X, Y, Z) p_{0_i}(X, Y, Z, t) \tag{3.52}$$

where p_{0_i} is the pressure at node i. The shape function $N_i(r, s)$ in the local reference

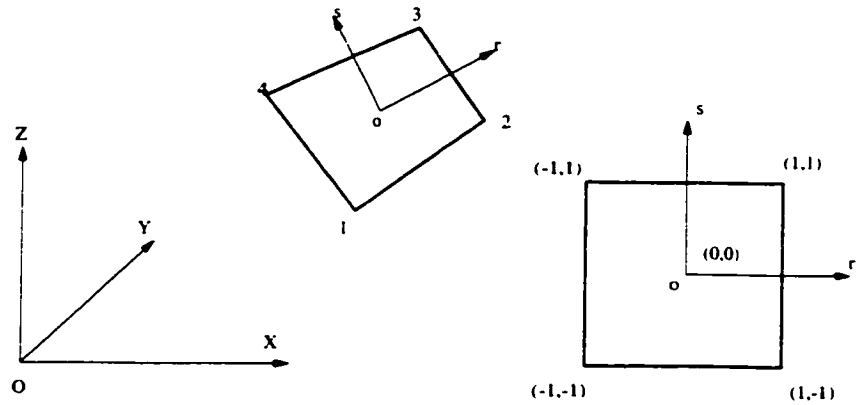

Figure 3.2: A quadrilateral panel and the local reference coordinate system

frame can be expressed in terms of the local coordinates (r, s):

$$\begin{aligned} N_1 &= \frac{1}{4}(1-r)(1-s) \\ N_2 &= \frac{1}{4}(1+r)(1-s) \\ N_3 &= \frac{1}{4}(1+r)(1+s) \\ N_4 &= \frac{1}{4}(1-r)(1+s) \end{aligned}$$

and $r, s \in [-1, 1]$. The pressure at a local coordinate system (r, s), is then written as

$$\bar{p}_0(r, s; t) = \sum_{i=1}^{4} N_i(r, s) p_{0_i}(r, s, t) \tag{3.53}$$

By employing Gaussian quadrature, the Froude-Krylov force can be obtained as

$$F_k^{FK}(t) = -\sum_{i=1}^{m}\sum_{j=1}^{n} w_i w_j \bar{p}_0^d(r_i, s_j, t) n_k(r_i, s_j) |J(r_i, s_j)| \tag{3.54}$$

where w_i and w_j are the weighting factors at (r_i, s_j), and $|J(r_i, s_j)|$ is the Jacobian given by:

$$|J(r_i, s_j)| = \begin{vmatrix} i & j & k \\ \frac{\partial X}{\partial r} & \frac{\partial Y}{\partial r} & \frac{\partial Z}{\partial r} \\ \frac{\partial X}{\partial s} & \frac{\partial Y}{\partial s} & \frac{\partial Z}{\partial s} \end{vmatrix} \tag{3.55}$$

m and n are the number of Gaussian points along r and s direction, respectively, and n_k is the kth component of the normal.

The restoring forces are given by

$$F_k^{RS}(t) = -\sum_{i=1}^{m}\sum_{j=1}^{n} w_i w_j \bar{p}_0^s(r_i, s_j, t) n_k(r_i, s_j) |J(r_i, s_j)| \tag{3.56}$$

where, in equation (3.54) and (3.56), $\bar{p}_0^s$ and $\bar{p}_0^d$ are the static and dynamic pressure of a point on a panel induced by the incident waves.

Chapter 4

Computation of Multihull Resistance and Motion

To understand the resistance and motion characteristics of the multihull and the interaction between individual hulls is one of the major objectives of this thesis. The numerical computation was made it possible to analyze the details of relationship between the resistance and the hull form or the hull arrangement. In this chapter, different types of multihull ships with symmetric and asymmetric demihulls were selected to test the computer programs which have been developed on the basis of the formulation in Chapter 2 and Chapter 3. The computational results and their comparisons with the experimental data are presented.

4.1 Computation of Multihull Resistance

Although some theoretical and experimental investigations on the resistance of catamaran vessels have been conducted in the past (Hsiung and Xu, 1988), there are still hydrodynamic phenomena needed to be studied. As we have known, the ship designers have relied on their experience to reduce the interaction effects for demihull with inward flattened side walls. In order to improve the understanding of the calm water wave resistance of asymmetric demihull with high speed catamarans, the method for numerical computation of the wave resistance of a multi-hull vessel with arbitrary demihull has been applied to catamaran next.

4.1.1 Catamaran Wave Resistance

The steady motion of a twin-hull ship on an unbounded free surface of deep water is considered. A right-hand Cartesian coordinated system moving with the catamaran has been assumed. The origin o has been taken on the undisturbed water surface of one of the hulls at the intersection of midship section and the center plane, with the oz-axis upwards and the ox-axis pointing to the direction of motion. The two demihulls are assumed to have a general shape with an arbitrary camber. They are always mirror images of each other. The coordinate system is shown in Figure 4.1.

The catamaran wave resistance based on thin ship theory with the coordinate system shown in Figure 4.1 is from the basic solution given by equation (2.25):

$$R_w = -16\pi\rho k_0^2 \int_0^{\frac{\pi}{2}} [P^2 + Q^2] \sec^3(\theta) d\theta \tag{4.1}$$

with $i = 1, 2$ for catamarans,

$$P = \sum_{i=1}^{2} (P_{i\sigma} - P_{i\mu}), \qquad Q = \sum_{i=1}^{2} (Q_{i\sigma} - Q_{i\mu}) \tag{4.2}$$

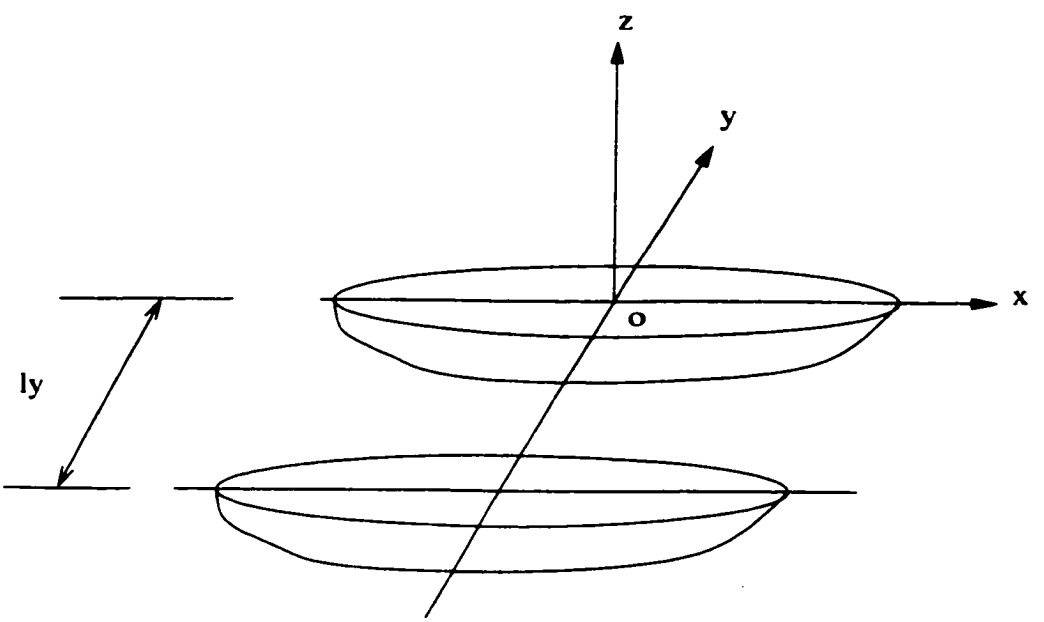

Figure 4.1: The coordinate system of a catamaran

That is

$$R_w = -16\pi\rho k_0^2 \int_0^{\frac{\pi}{2}} [(P_1^2 + Q_1^2) + (P_2^2 + Q_2^2) + 2P_1P_2 + 2Q_1Q_2] \sec^3(\theta) d\theta \tag{4.3}$$

It is found that the wave resistance of demihull 1 by itself is:

$$R_{1w} = -16\pi\rho k_0^2 \int_0^{\frac{\pi}{2}} [(P_1^2 + Q_1^2)] \sec^3(\theta) d\theta \tag{4.4}$$

The wave resistance of demihull 2 is:

$$R_{2w} = -16\pi\rho k_0^2 \int_0^{\frac{\pi}{2}} [(P_2^2 + Q_2^2)] \sec^3(\theta) d\theta \tag{4.5}$$

In equation (4.3), the wave resistance component due to the interaction between two demihulls is:

$$R_{iw} = -16\pi\rho k_0^2 \int_0^{\frac{\pi}{2}} [2P_1P_2 + 2Q_1Q_2] \sec^3(\theta) d\theta \tag{4.6}$$

Defining

$$C_w = R_w/(\frac{1}{2}\rho U^2 S) = C_{w1} + C_{w2} + C_{iw} \tag{4.7}$$

where C_w is the total wave resistance coefficient; C_{w1} is the wave resistance coefficient of demihull 1; C_{w2} is the wave resistance coefficient of demihull 2; C_{iw} is the wave resistance coefficient due to the interaction between demihull 1 and demihull 2.

4.1.2 Numerical Results

In order to validate the program developed based on the theory discussed on Chapter 2, the Wigley hull catamaran with symmetrical demihulls was first investigated. The mathematical Wigley hull is described by the following formula:

$$y = \frac{B}{2}(1 - \xi^2)(1 - \zeta^2) \tag{4.8}$$

where

$$\xi = \frac{x}{L/2} \in [-1, 1] \tag{4.9}$$

and

$$\zeta = \frac{z}{T} \in [-1, 0] \tag{4.10}$$

The body plan of Wigley hull is shown in Figure 4.2.

In Figure 4.3, a comparison between theoretical predictions and model test (Papanikolaou, *et al.* 1996) for the wave resistance coefficient (for ship dimensions with $L/B = 10.0$, $B/T = 1.6$, $l_y/L = 0.6$) is shown. The agreement of numerical results and experimental data is very good, except at lower Froude numbers the numerical results show highly oscillatory.

In order to study the camber and spacing effects on the wave resistance for a catmaran, symmetric and asymmetric demihulls have been applied to the halved Wigley demihulls with dimensions: $L/B = 10.0$, $B/T = 1.6$, $l_{y1}/L = 0.6$, $l_{y2}/L = 0.4$. We define $l_{y1}/L = 0.6$ as Case 1 and $l_{y2}/L = 0.4$ as Case 2 as shown in Figure 4.4. The wave resistance coefficients were computed and compared with the corresponding symmetrical Wigley demihulls, see Figure 4.5. It is found that the camber of the Wigley hull would reduce the wave resistance for $F_n = 0.35$ to 0.6. For $F_n \geq 0.6$, it increases the wave resistance. As for the spacing effect, for $F_n = 0.35$ to 0.6, $l_y/L = 0.6$ gives lower wave resistance. But for $F_n \geq 0.6$, $l_y/L = 0.4$ is better.

For more information on the wave resistance and also to know how the wave systems generated by individual hulls and interacting to each other, the wave patterns generated by the multihull ships have been computed and analyzed. In order to validate the program developed, the Wigley hull was chosen as the basic model. The dimension of the monohull is the same as the Wigley demihull mentioned before. The wave generated by Wigley monohull at two Froude numbers ($F_n = 0.348$ and $F_n = 0.452$) are shown in Figure 4.6 through Figure 4.11. The comparison between numerical results and experimental data shows that the thin ship theory gives reasonably good results, except for the regions near the bow and the stern where the assumption of the linear wave theory may be too far away from the realistic situation. In Figures 4.10 and 4.11, the nondimensional wave height is $\zeta^*/(U^2/g)$, where ζ^* is the wave amplitude, U is the ship velocity. Nondimensional distance is $2x/L$ with -1.0 corresponding to the bow and 1.0 corresponding to the stern of the ship. In Figures 4.12 and 4.13, the wave field generated by a Wigley catmaran are shown. The contours generated by the Wigley catamaran are shown in Figure 4.14 for $l_y/L = 0.6$ and Figure 4.15 for $l_y/L = 0.4$. With different spacings of two hulls, the wave patterns are different. That is the reason why the different hull spacings cause different wave resistance. The ship that generates higher waves will expend more energy and hence has greater resistance. The Froude number for wave computation is 0.40. The maximum wave elevation range is [-0.334, 0.345] for $l_y/L = 0.4$ and [-0.279, 0.333] for $l_y/L = 0.6$. Obviously, the wave height with $l_y/L = 0.6$ is smaller than that with $l_y/L = 0.4$. It means the wave resistance with $l_y/L = 0.6$ is lower than that with $l_y/L = 0.4$ at $F_n = 0.4$.

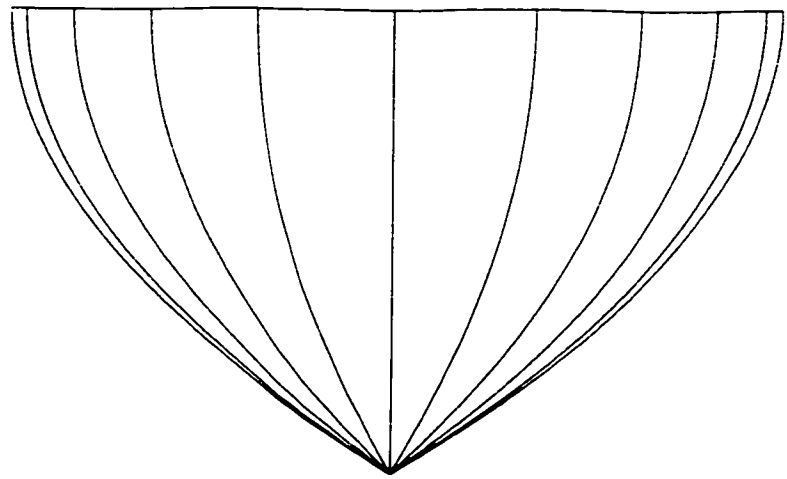

Figure 4.2: Wigley hull body plan

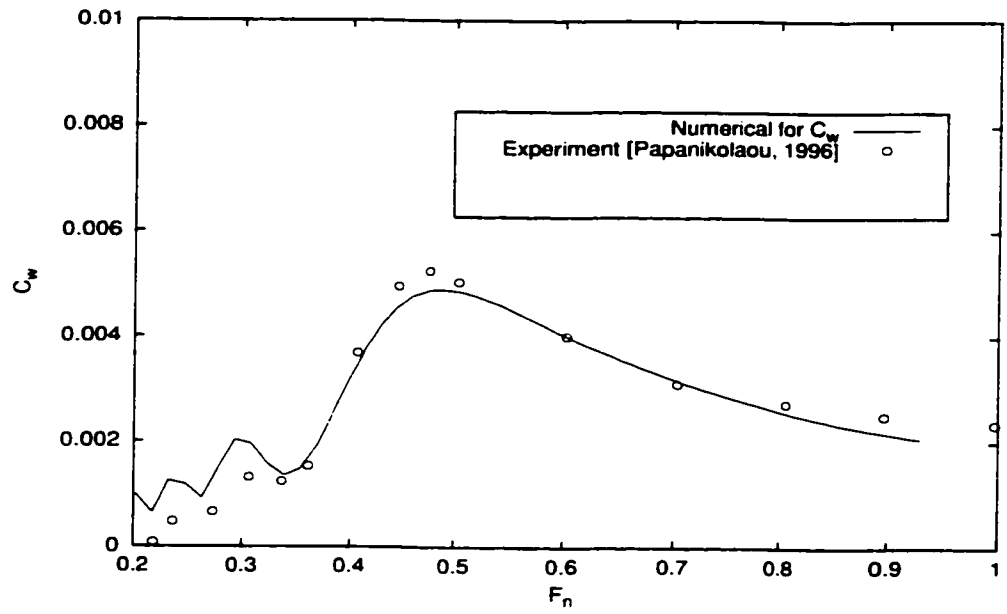

Figure 4.3: Comparison of the wave resistance coefficients for a catamaran with Wigley demihulls.

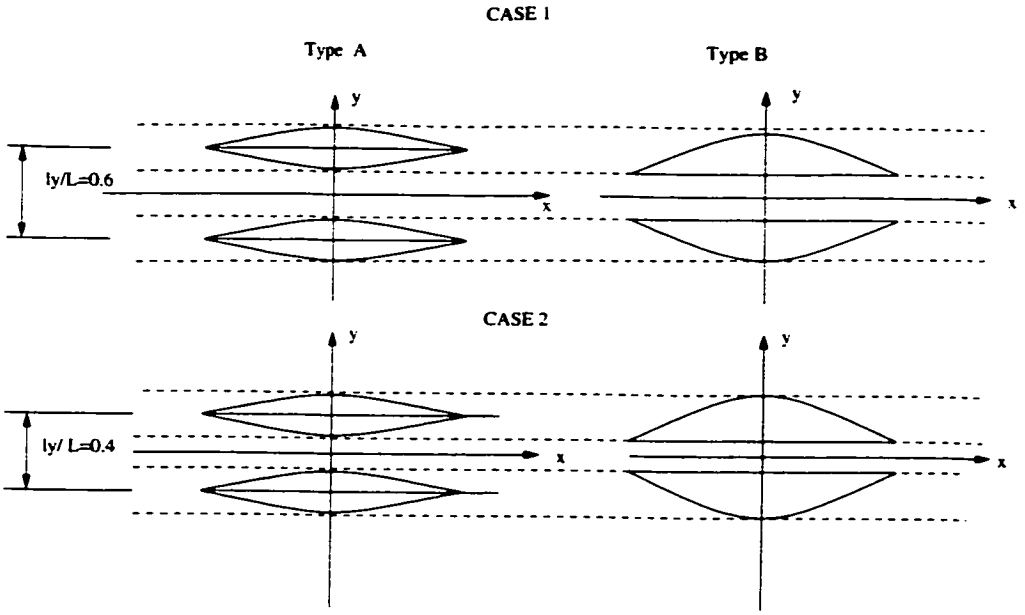

Figure 4.4: Two types of Wigley demihulls.

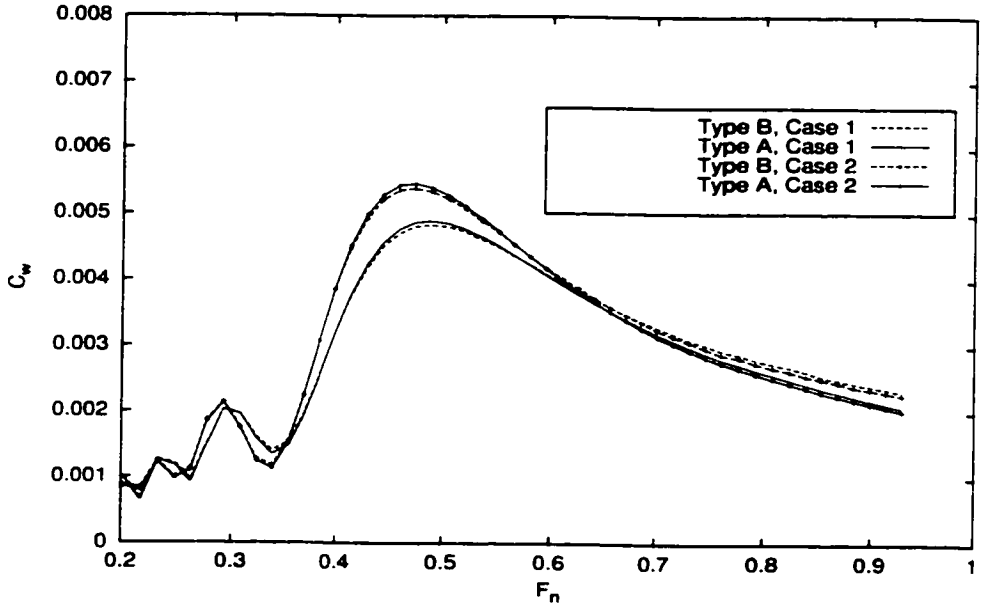

Figure 4.5: Comparison of the wave resistance coefficients for catamarans with Wigley demihulls.

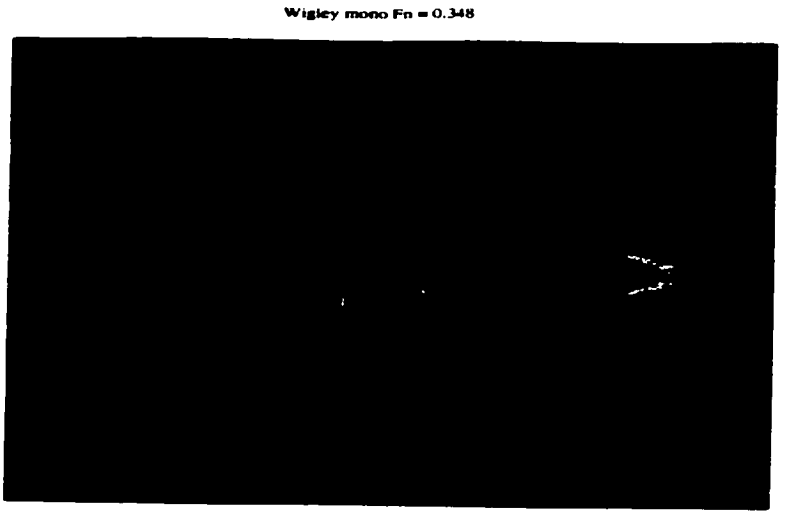

Figure 4.6: Wave pattern generated by a Wigley monohull for $F_n = 0.348$

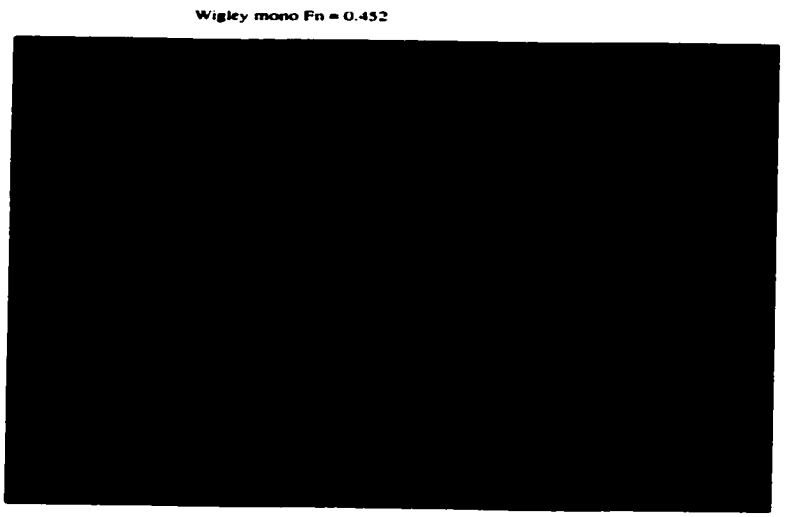

Figure 4.7: Wave pattern generated by a Wigley monohull for $F_n = 0.452$

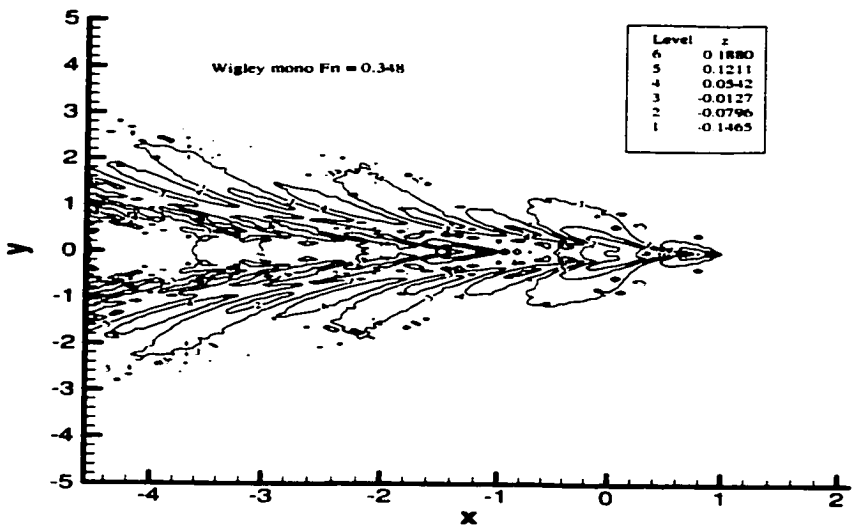

Figure 4.8: Wave contours generated by a Wigley monohull for $F_n = 0.348$

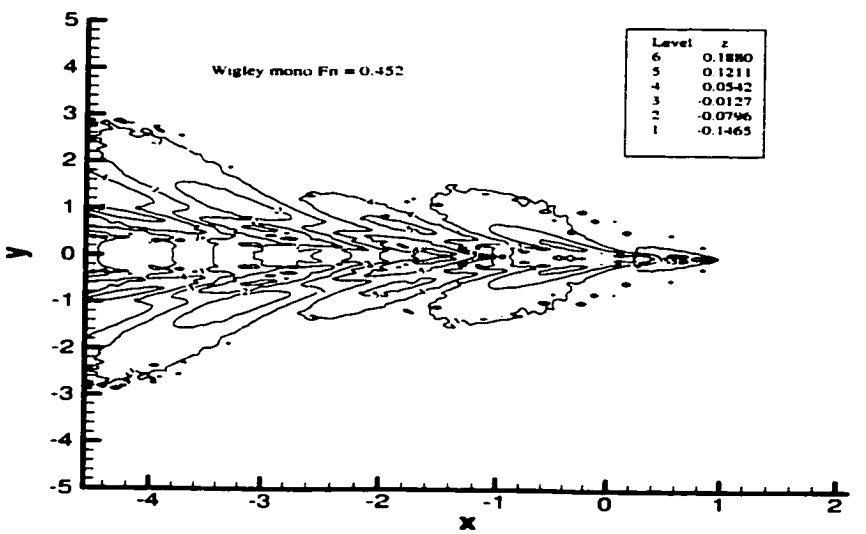

Figure 4.9: Wave contours generated by a Wigley monohull for $F_n = 0.452$

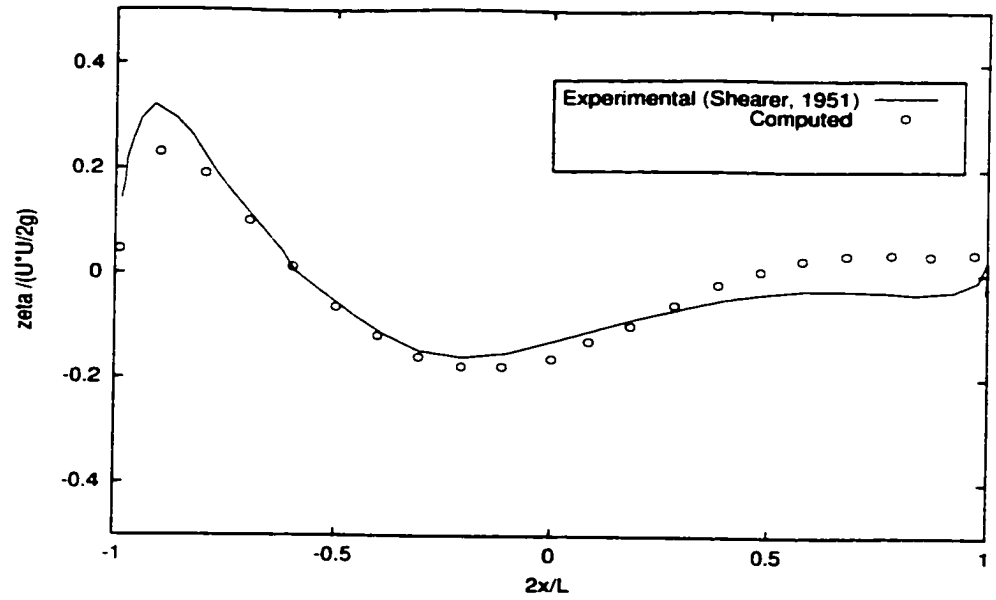

Figure 4.10: Wave profile along a Wigley monohull for $F_n = 0.348$

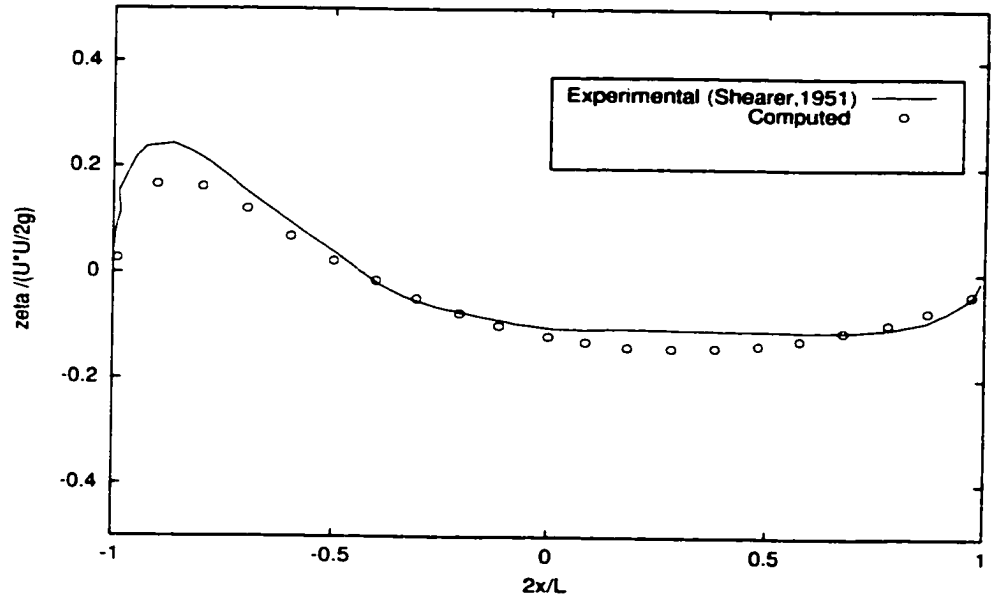

Figure 4.11: Wave profile along a Wigley monohull for $F_n = 0.452$

Figure 4.12: Wave pattern generated by a Wigley catamaran for $F_n = 0.4$ and $l_y/L = 0.6$

Figure 4.13: Wave pattern generated by a Wigley catamaran for $F_n = 0.4$ and $l_y/L = 0.4$

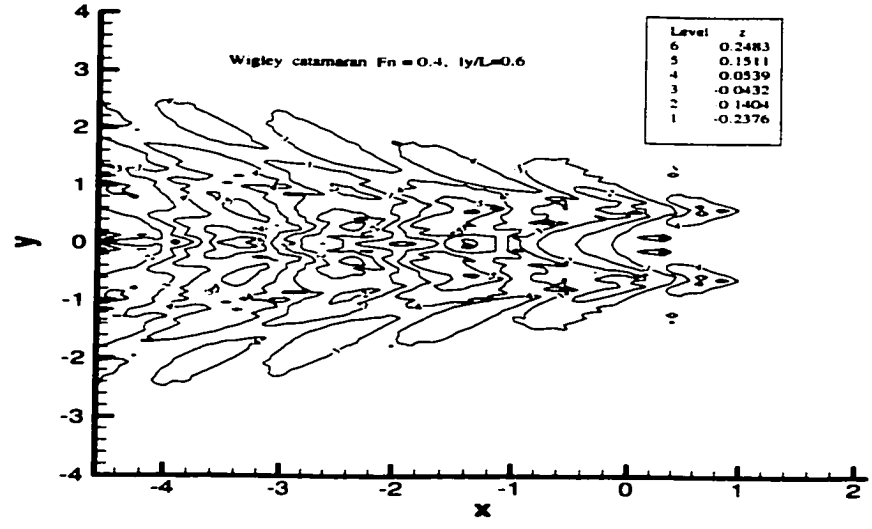

Figure 4.14: Wave contours generated by a Wigley catamaran for $F_n = 0.4$ and $l_y/L = 0.6$

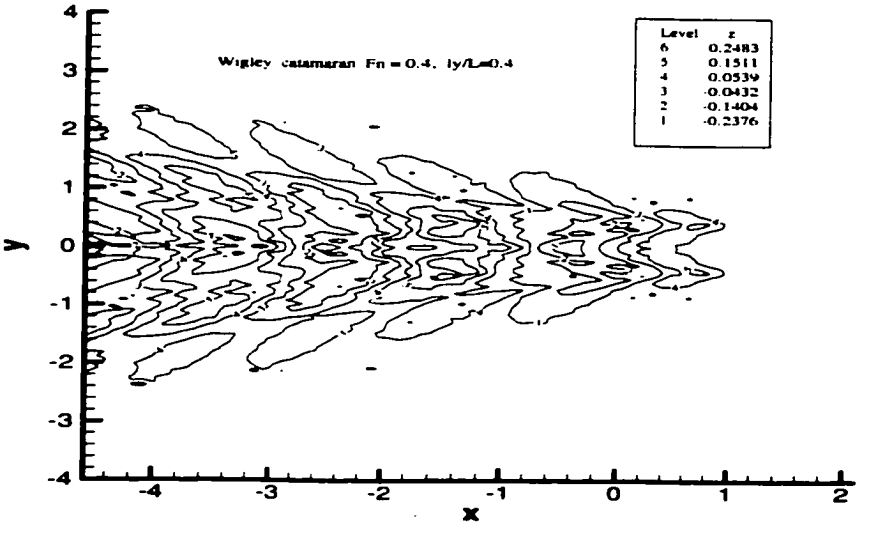

Figure 4.15: Wave contours generated by a Wigley catamaran for $F_n = 0.4$ and $l_y/L = 0.4$

As for a realistic catamaran, CAT2, from an experimental research carried out by Brizzolara *et al.* (1998) at the University of Trieste, was chosen for computation. The computed wave resistance coefficient and wave profile of catamaran inside were compared with experimental results, as shown in Figure 4.17 and Figure 4.20. Examining these figures, it can be seen that the agreement between theoretical and experimental values is quite well. In Figure 4.20, the nondimensional wave elevation was ζ/L where the L is the ship length, and $x/L = 0$ corresponding to the bow, and $x/L = 1.0$ corresponding to the stern. The wave pattern were also computed for $F_n = 0.5$. The wave pattern and wave contours are illustrated in Figure 4.18 to Figure 4.19. The maximum wave elevation range is [-0.323, 0.341]. The contour elevations are $z = -0.0150$ to $z = 0.0127$.

The principals of the demihull of the CAT2 are as follows: Length, L, is 2.5m; Beam, B, is 0.2m; Draft, T, is 0.177m, and spacing ratio l_y/L is 0.225. The body plan of the demihull is shown in Figure 4.16.

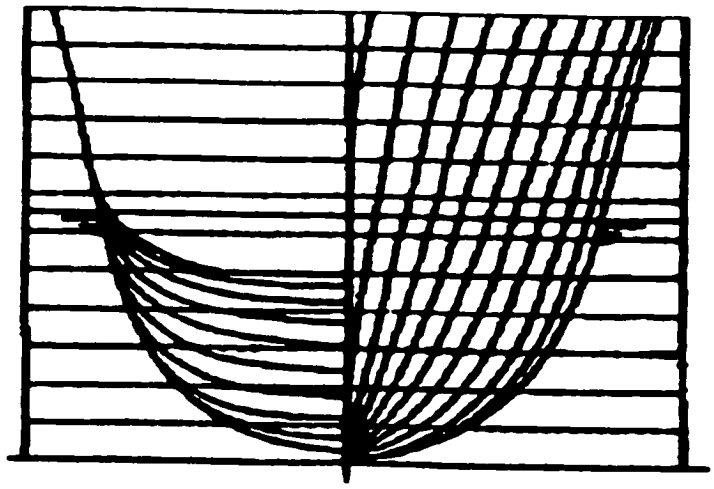

Figure 4.16: CAT2 body plan

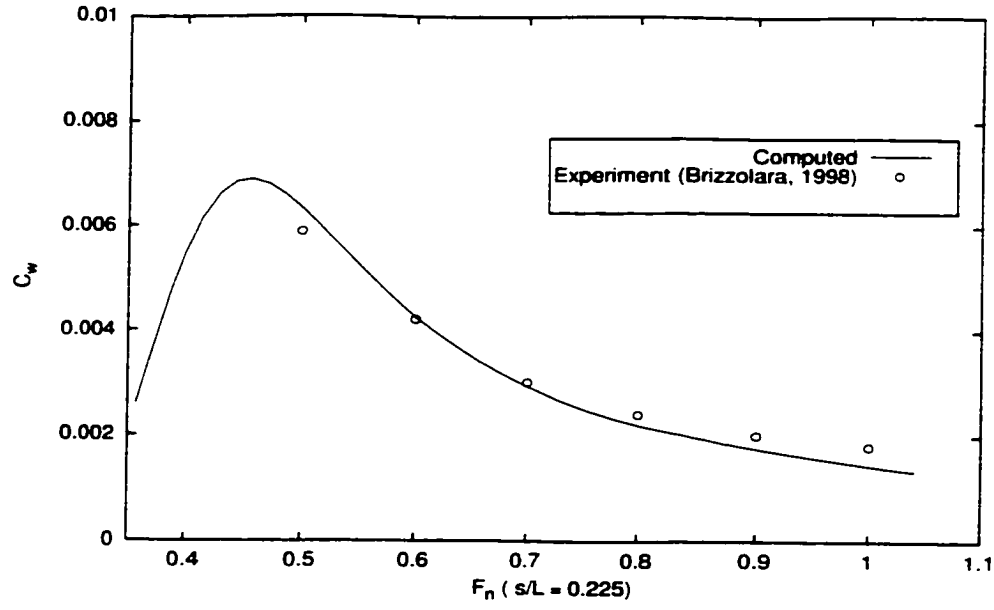

Figure 4.17: Comparison of the wave resistance coefficients for CAT2.

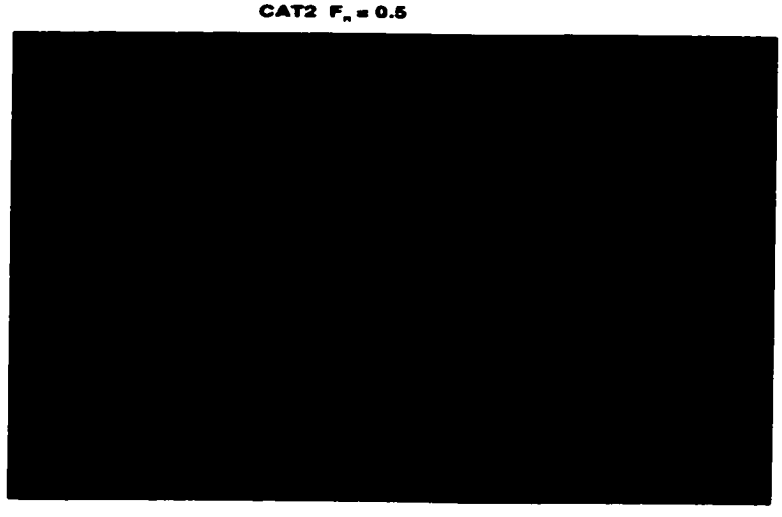

Figure 4.18: Wave pattern generated by CAT2 for $F_n = 0.5$

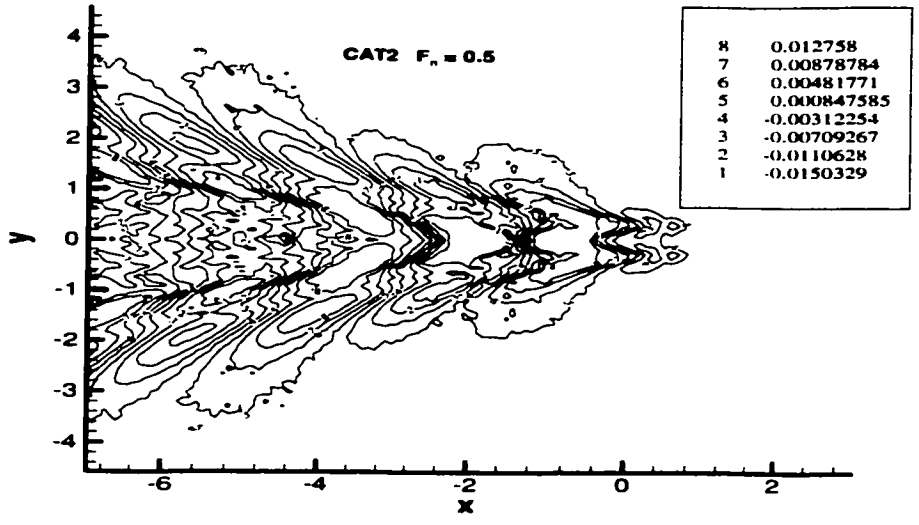

Figure 4.19: Wave contours generated by CAT2 for $F_n = 0.5$

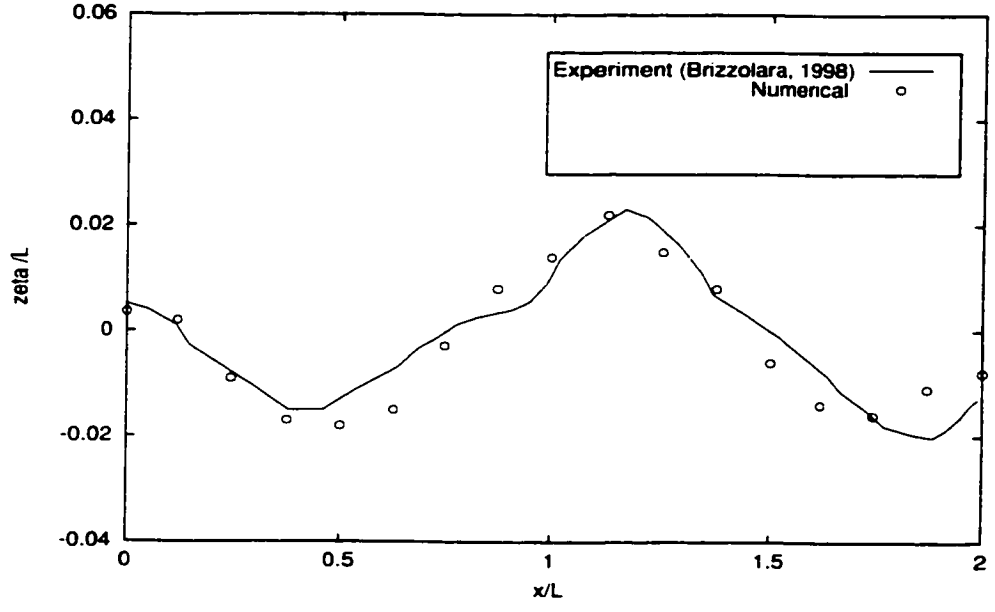

Figure 4.20: Wave profile along CAT2 for $F_n = 0.5$

4.1.3 Trimaran Resistance

In the case of wave resistance computation, the steady motion of a trimaran on an unbounded free surface of deep water is considered. A right-hand Cartesian coordinate system moving with the trimaran has been used. The origin o has been taken in the undisturbed water surface, at the midships section of the main hull intersecting with the centerplane, with the oz-axis upwards and the ox-axis pointing to the direction of motion. The hull elements are assumed having a general shape with an arbitrary camber. The coordinate system is shown in Figure 4.21.

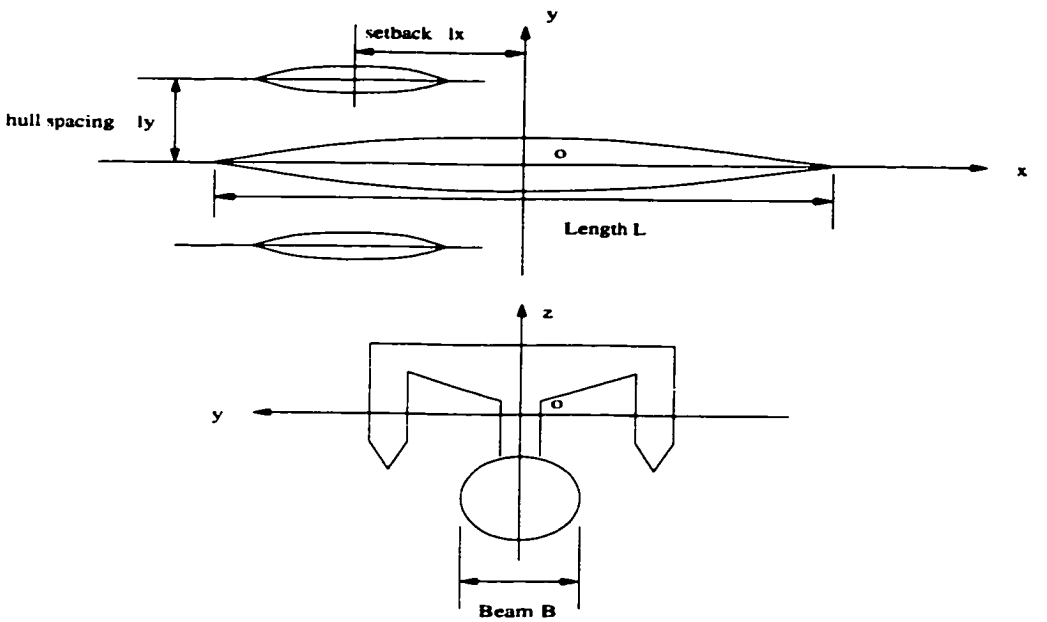

Figure 4.21: The coordinate system of a trimaran

The trimaran wave resistance based on thin ship theory with the coordinate system shown above is from the basic solution given by equation (2.25):

$$R_w = -16\pi\rho k_0^2 \int_0^{\frac{\pi}{2}} [P^2 + Q^2] \sec^3(\theta) d\theta \tag{4.11}$$

with $i = 1, 2, 3$ for a trimaran:

$$P = \sum_{i=1}^{3} (P_{i\sigma} - P_{i\mu}), \qquad Q = \sum_{i=1}^{3} (Q_{i\sigma} - Q_{i\mu}) \tag{4.12}$$

$$\left.\begin{matrix} P_{i\sigma} \\ Q_{i\sigma} \end{matrix}\right\} = \int\int_{S_i} \sigma_i \begin{matrix} \cos \\ \sin \end{matrix} [k_0(\xi_i \cos\theta + ly_i \sin\theta) \sec^2\theta] exp(k_0 \zeta_i \sec^2\theta) d\xi_i d\zeta_i \tag{4.13}$$

$$\left.\begin{matrix} P_{i\mu} \\ Q_{i\mu} \end{matrix}\right\} = k_0 \sec^2\theta \sin\theta \int\int_{S_i} \mu_i \begin{matrix} \sin \\ \cos \end{matrix} [k_0(\xi cos\theta + ly_i \sin\theta) \sec^2\theta] exp(k_0 \zeta_i \sec^2\theta) d\xi_i d\zeta_i \tag{4.14}$$

That is

$$\begin{aligned} R_w \;=\; & -16\pi\rho k_0^2 \int_0^{\frac{\pi}{2}} [(P_1^2 + Q_1^2) + (P_2^2 + Q_2^2) + (P_3^2 + Q_3^2) \\ & + 2P_1P_2 + 2P_2P_3 + 2P_1P_3 + 2Q_1Q_2 + 2Q_2Q_3 + 2Q_1Q_3] \sec^3(\theta) d\theta \end{aligned} \tag{4.15}$$

The wave resistance of hull element 1 alone is:

$$R_{1w} = -16\pi\rho k_0^2 \int_0^{\frac{\pi}{2}} [(P_1^2 + Q_1^2)] \sec^3(\theta) d\theta. \tag{4.16}$$

The wave resistance of hull element 2 alone is:

$$R_{2w} = -16\pi\rho k_0^2 \int_0^{\frac{\pi}{2}} [(P_2^2 + Q_2^2)] \sec^3(\theta) d\theta. \tag{4.17}$$

The wave resistance of hull element 3 alone is:

$$R_{3w} = -16\pi\rho k_0^2 \int_0^{\frac{\pi}{2}} [(P_3^2 + Q_3^2)] \sec^3(\theta) d\theta. \tag{4.18}$$

In equation (4.15), the wave resistance component due to the interaction between the hull elements is:

$$R_{iw} = -16\pi\rho k_0^2 \int_0^{\frac{\pi}{2}} [2P_1P_2 + 2P_2P_3 + 2P_1P_3 + 2Q_1Q_2 + 2Q_2Q_3 + 2Q_1Q_3] \sec^3(\theta) d\theta \tag{4.19}$$

We define:

$$C_w = R_w/(\frac{1}{2}\rho U^2 S) = C_{w1} + C_{w2} + C_{w3} + C_{iw} \tag{4.20}$$

where C_w is the total wave resistance coefficient; C_{w1} is the wave resistance coefficient of hull element 1; C_{w2} is the wave resistance coefficient of hull element 2; C_{w3} is the wave resistance coefficient of hull element 3 and C_{iw} is the wave resistance coefficient due to the interaction between the center hull and outriggers.

The total resistance of a trimaran is:

$$R_t = R_w + R_f \tag{4.21}$$

where R_f is the frictional resistance of trimaran found from equation (2.86).

The total resistance coefficient of a trimaran is:

$$C_t = R_t/(\frac{1}{2}\rho U^2 S) \tag{4.22}$$

where S is the total wetted surface area of the trimaran.

4.1.4 Numerical Results

A trimaran of the mathematical Wigley form with the central hull two times longer than the outriggers was first investigated (Battistin, *et al.* 2000) . They all have dimensions of $L/B = 10$ and $B/T = 1.6$. The setback l_x is defined as the longitudinal distance between midsection of the central main hull and the outriggers, positive for outriggers towards the stern. The spacing l_y is defined as the lateral distance between the centerplane of the main hull and that of the outriggers. These two parameters were systematically varied: l_y took values of 0.2L, 0.3L; and l_x took values of -0.25 L, 0.0L, 0.125L and 0.25L where L is the length of the main hull. (for l_x = 0.25L and l_x = -0.25L, the FP's and AP's of the main hull and the outriggers are aligned each other, respectively). A total of eight validation cases were considered as shown

in Tables 4.1:

Table 4.1: Validation Conditions for the Wigley Trimaran

	$l_x/L = -0.25$	$l_x/L = 0.0$	$l_x/L = 0.125$	$l_x/L = 0.25$
$l_y/L = 0.2$	CASE 1	CASE 3	CASE 5	CASE 7
$l_y/L = 0.3$	CASE 2	CASE 4	CASE 6	CASE 8

The computed wave resistance coefficients were compared with the experimental results by Battistin, *et al.* (2000), as shown in Figure 4.23 to Figure 4.30. Examining these figures, it can be seen that the agreement between the theoretical and the experimental data is good. The computed curves showing a big second hump around $F_n = 0.3$ in most cases is the typical phenomenon for thin ship theory.

The wave patterns were also computed for CASE 5 and CASE 7. The Froude number for wave pattern computation is 0.35. The wave patterns and wave contours are illustrated in Figure 4.31 to Figure 4.34. The maximum wave elevation range is [-0.334, 0.344] for CASE 5 and [-0.266, 0.239] for CASE 7. The contours of wave elevation are $z = -0.2461$ to $z = 0.2141$ with an increment of 0.092.

The hull arrangement is shown in Figure 4.22. In order to investigate the relationship of the wave interaction effect for various positions of outriggers, a computation table was set up for Wigley trimaran as shown in Table 4.2.

At first, the longitudinal position of outriggers was fixed. The spacing effect on wave resistance and the wave interaction was studied. The comparisons of computed results are shown in Figure 4.35 to Figure 4.42 with l_x/L = -0.25, 0.0, 0.125, 0.25,

Table 4.2: Investigation Conditions for the Wigley Trimaran

	$l_x/L = -0.25$	$l_x/L = 0.00$	$l_x/L = 0.125$	$l_x/L = 0.25$
$l_y/L = 0.15$	condition 1	condition 4	condition 7	condition 10
$l_y/L = 0.20$	condition 2	condition 5	condition 8	condition 11
$l_y/L = 0.25$	condition 3	condition 6	condition 9	condition 12

respectively. Then, the lateral position of the outriggers was fixed. The setback effect on wave resistance and the wave interaction were studied. The comparisons of computed results are shown in Figure 4.43 to Figure 4.48 for l_y/L=0.15, 0.2, 0.25, respectively.

In general, the negative wave interference speed range is for $F_n = 0.25$ to 0.45, which is the most favorable condition for low wave resistance in operation, and we have find that the wave resistance coefficient is not very sensitive to the spacing. For F_n = 0.3 to 0.4, $l_y/L = 0.15$ gives lower resistance. When F_n is between 0.4 to 0.5, the maximum wave resistance occurs. Comparing the wave resistance for three spacings, the hull configuration with $l_y/L = 0.25$ has the lowest resistance. It means that for the high design speeds the outrigger should move out from the main hull. Certainly on very high speed ($F_n \geq 0.6$), the wave interaction between the hull elements, C_{iw}, approaches to zero. To study the setback effect on the wave resistance and the wave interaction values, comparisons of computed results are given in Figure 4.43 to Figure 4.48 with l_y/L=0.15, 0.2, 0.25. From these figures, the wave resistance coefficients of trimaran are very sensitive to the longitudinal position of the outriggers. For F_n= [0.25 to 0.35], $l_x/L = 0.0$ is the best position to cause lowest wave resistance among three setbacks. For $F_n = 0.35$ to 0.55, $l_x/L = 0.25$ is the best choice. It means that for the high design speed the outrigger should move back. From Figure 4.43, we find

that if the design speed is $F_n = 0.43$ the optimum position of $l_x/L = 0.25$ reduces the wave resistance to about one-half of that for the worst position of $l_x/L = 0.0$.

In Figure 4.43 to Figure 4.48, it is interesting to find that the computed wave resistance coefficient of the hull configuration with $lx/L = 0.25$ is exactly the same as that of with $lx/L = -0.25$, for Conditions 1, 2, 3 versus Conditions 10, 11, 12, respectively. This is because these two positions are symetrical with respect to the midship and centerplane. By potential theory, the interaction between the front left side outrigger with the main hull is the same as the back right side outrigger with the main hull, vise versa. This pheonomenon is verified by experiments, as shown by CASE 1 (Figure 4.23) verse CASE 7 (Figure 4.29) for Condition 2 versus Condition 11, as well as shown by Case 2 (Figure 4.24) versus CASE 8 (Figure 4.30).

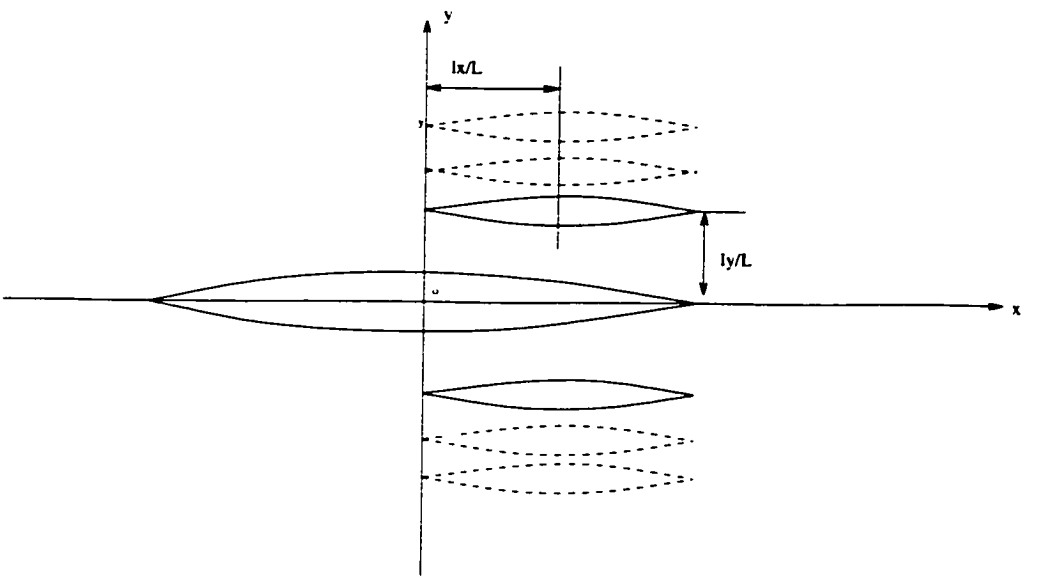

Figure 4.22: Hull arrangement

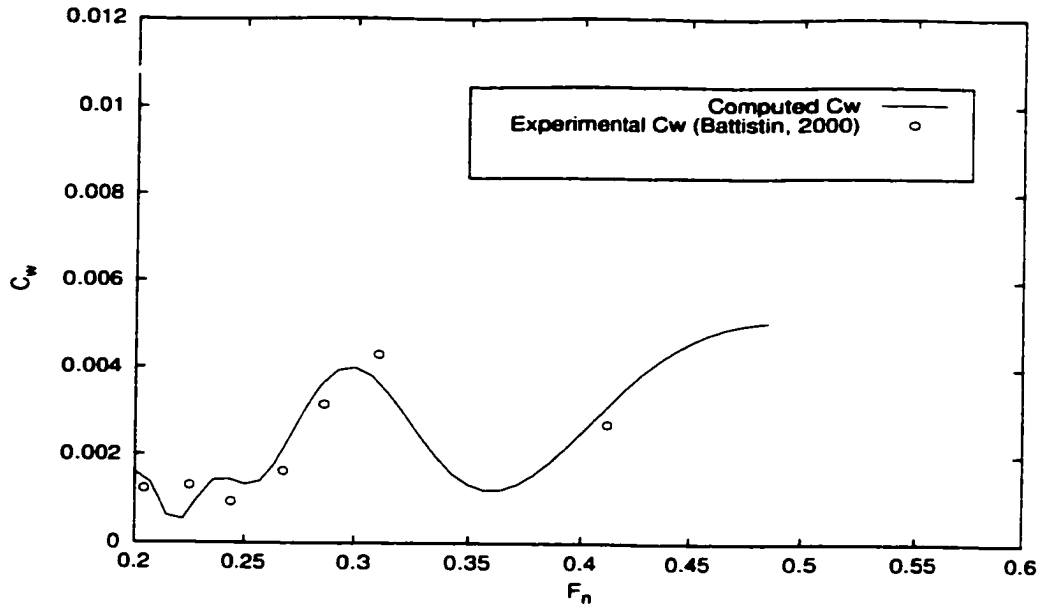

Figure 4.23: Comparison of computed and experimental results for C_w of the Wigley trimaran, CASE 1

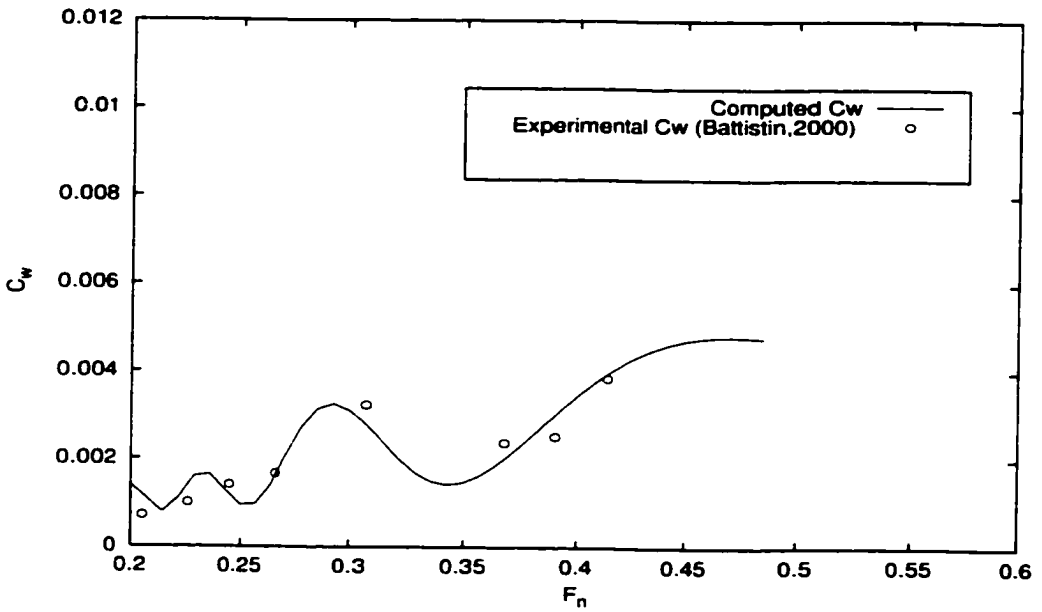

Figure 4.24: Comparison of computed and experimental results for C_w of the Wigley trimaran, CASE 2

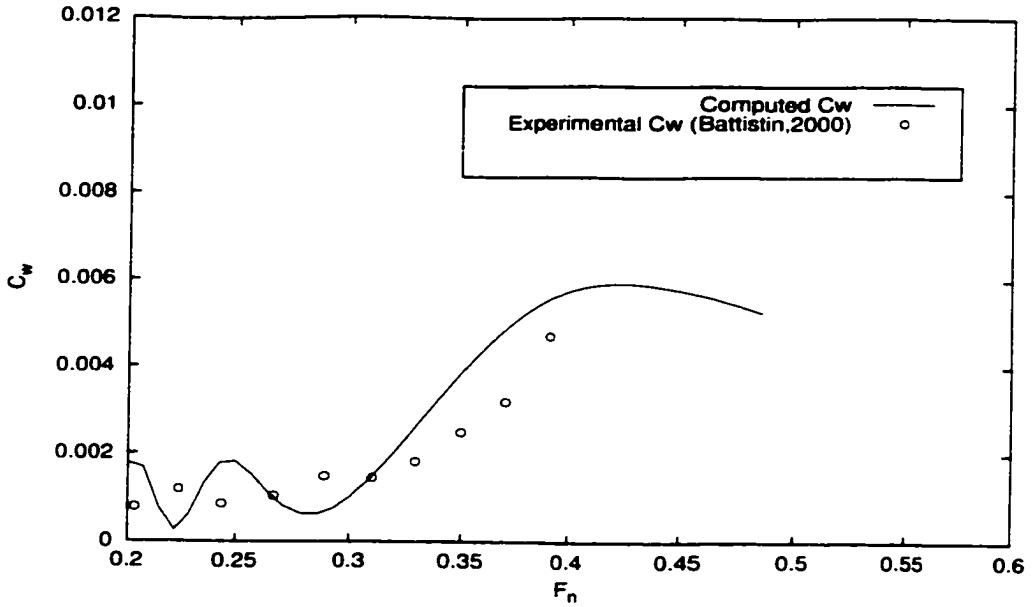

Figure 4.25: Comparison of computed and experimental results for C_w of the Wigley trimaran, CASE 3

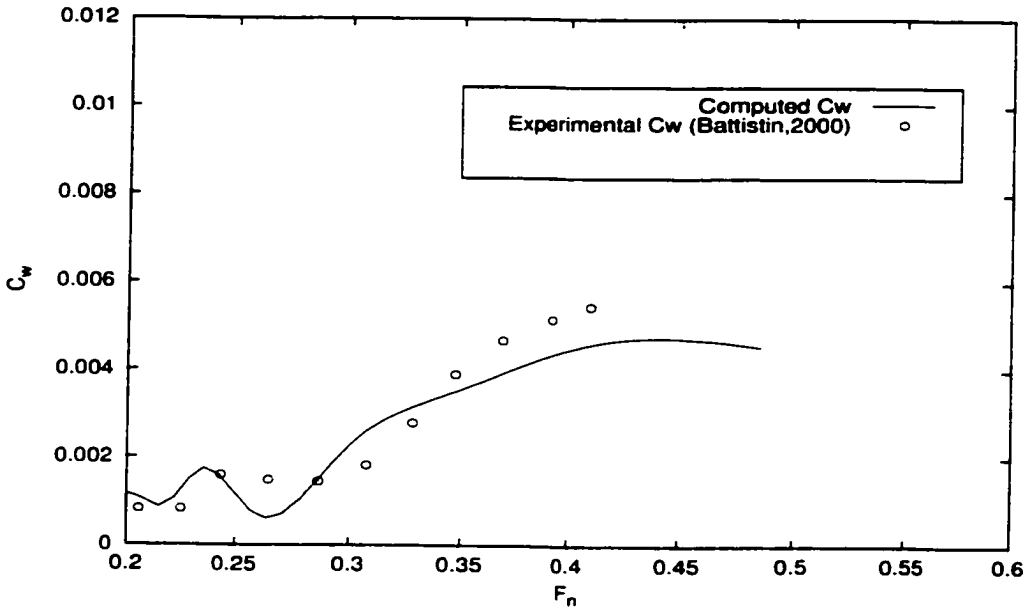

Figure 4.26: Comparison of computed and experimental results for C_w of the Wigley trimaran, CASE 4

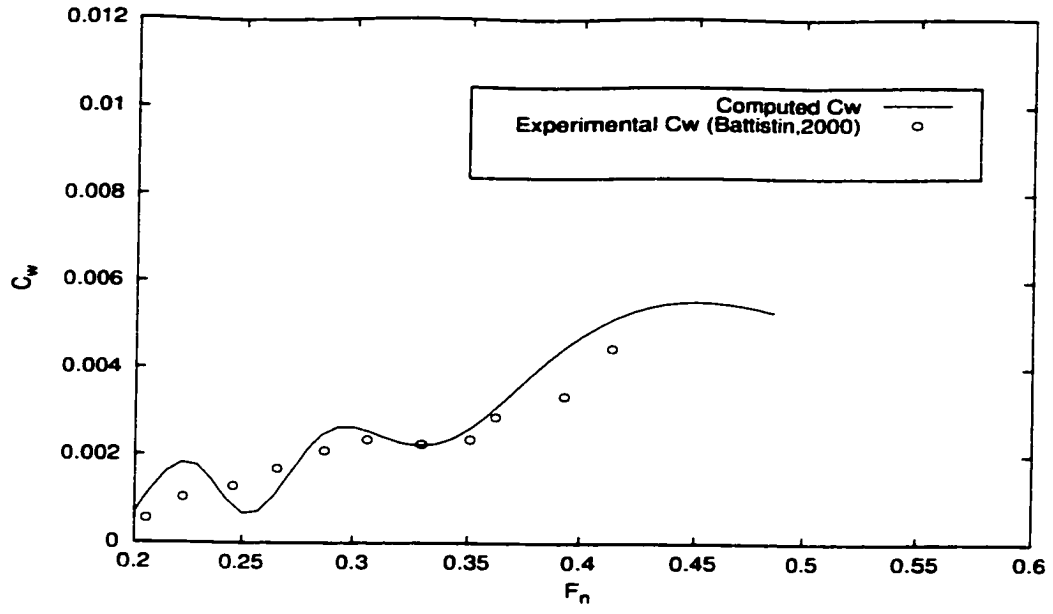

Figure 4.27: Comparison of computed and experimental results for C_w of the Wigley trimaran, CASE 5

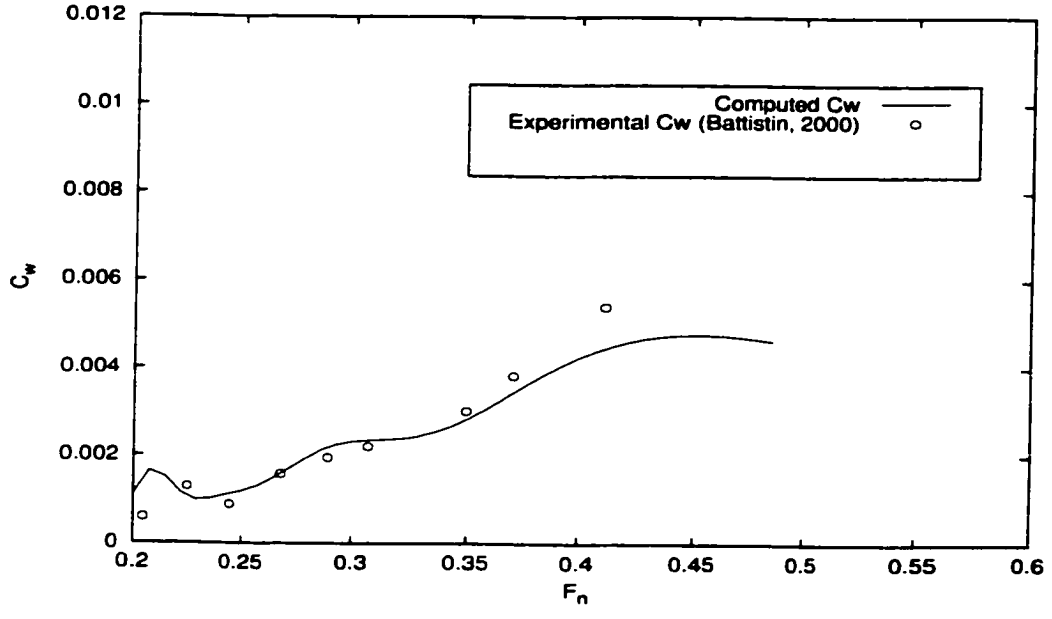

Figure 4.28: Comparison of computed and experimental results for C_w of the Wigley trimaran, CASE 6

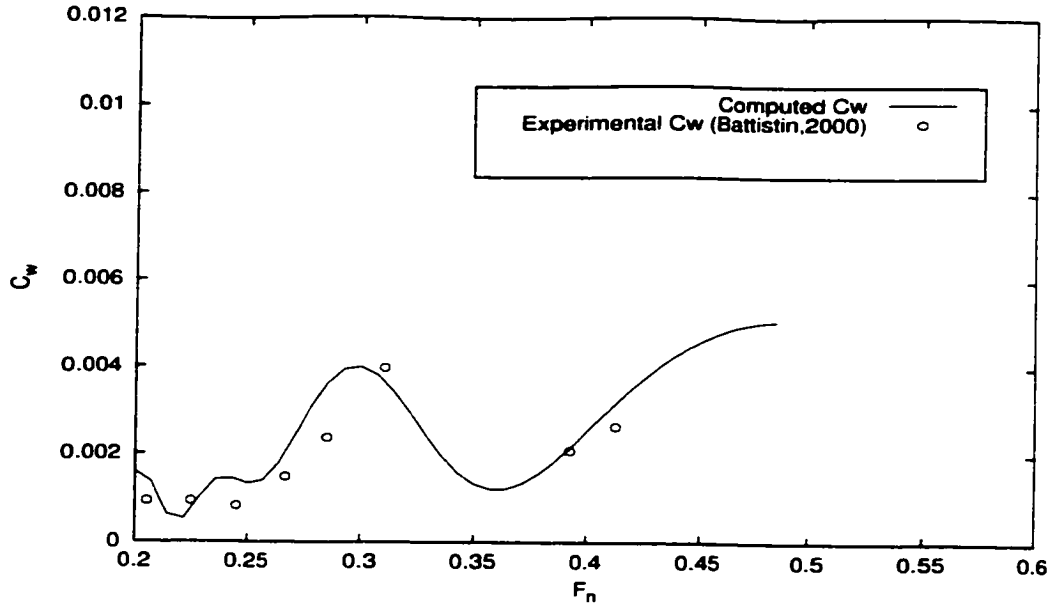

Figure 4.29: Comparison of computed and experimental results for C_w of the Wigley trimaran, CASE 7

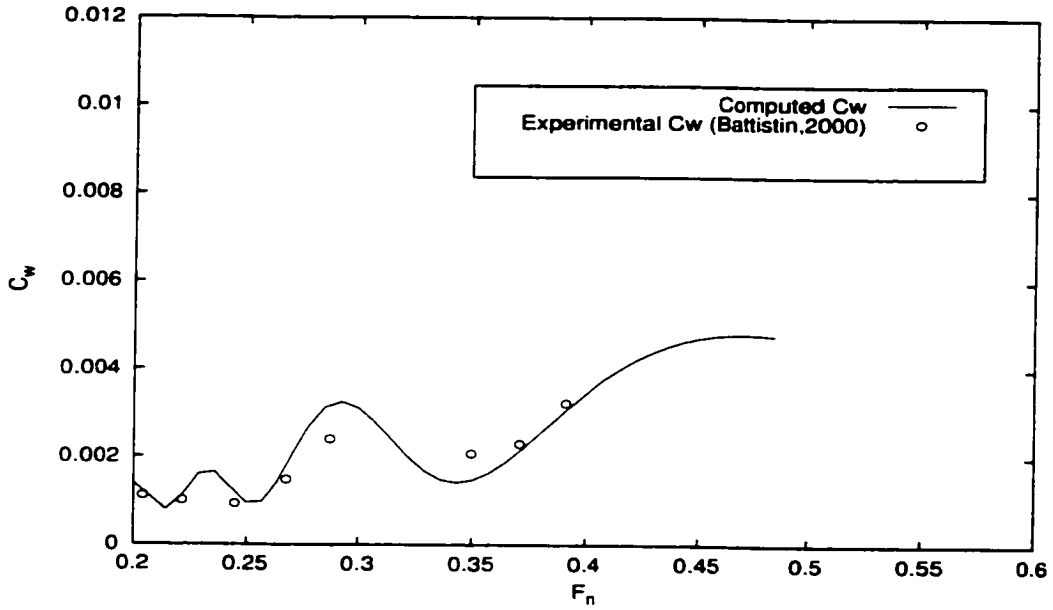

Figure 4.30: Comparison of computed and experimental results for C_w of the Wigley trimaran, CASE 8

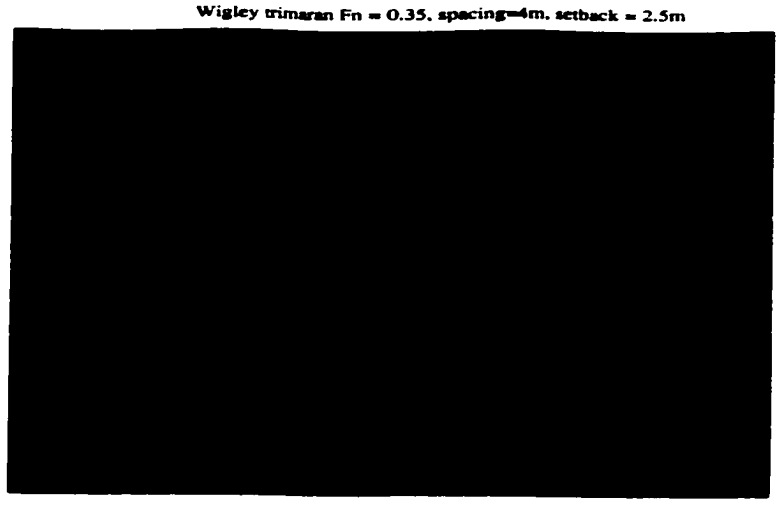

Figure 4.31: Wave pattern generated by Wigley trimaran for $F_n = 0.35$, CASE 5

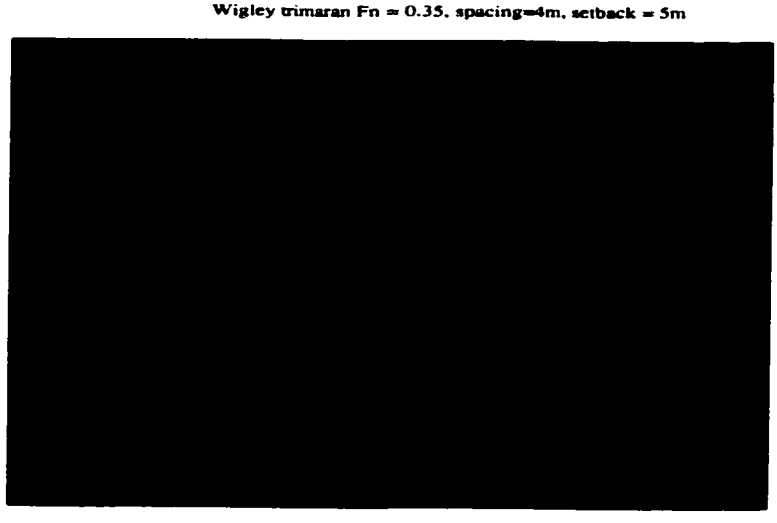

Figure 4.32: Wave pattern generated by Wigley trimaran for $F_n = 0.35$, CASE 7

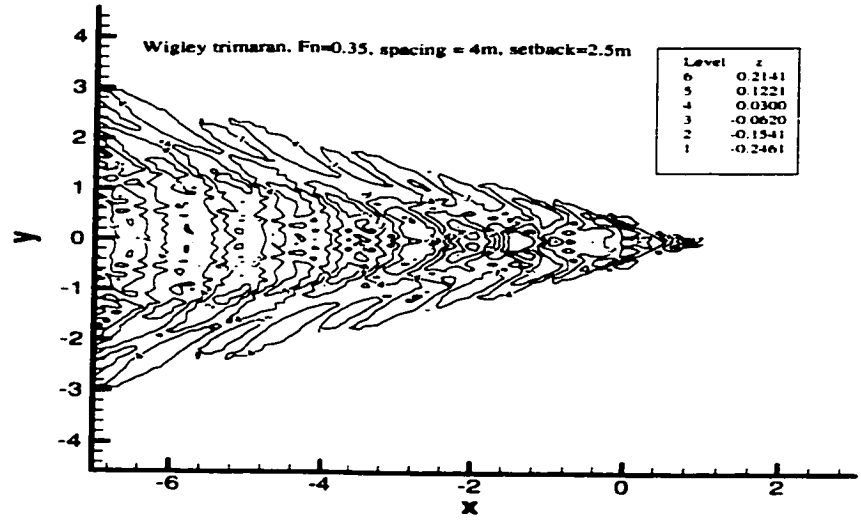

Figure 4.33: Wave contours generated by Wigley trimaran for $F_n = 0.35$, CASE 5

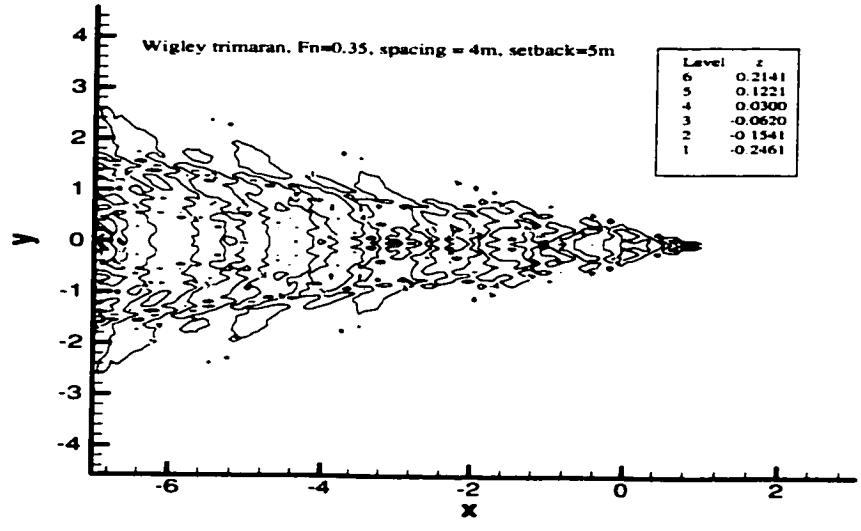

Figure 4.34: Wave contours generated by Wigley trimaran for $F_n = 0.35$, CASE 7

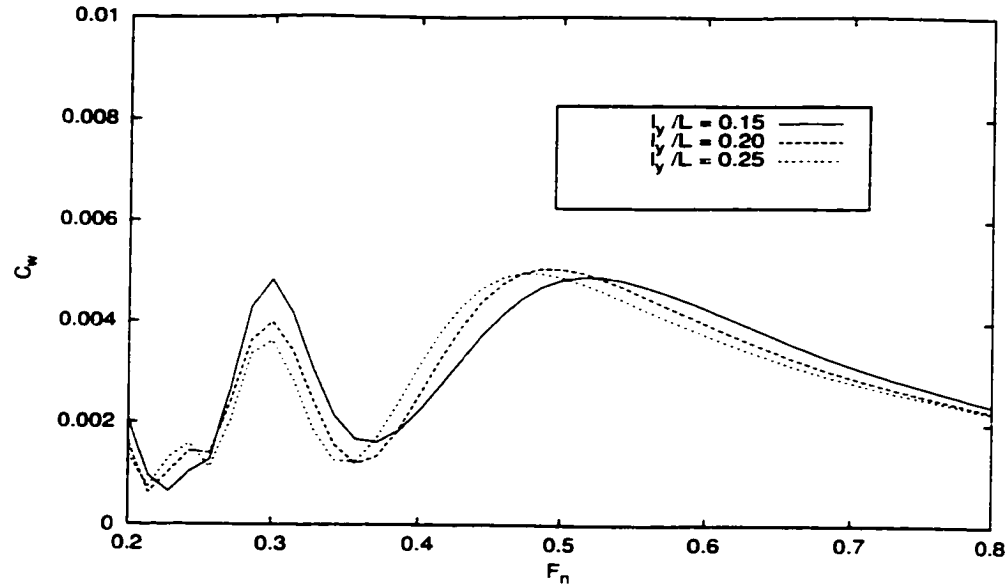

Figure 4.35: Effect of spacing on wave resistance coefficient of the Wigley trimaran ($l_x/L = -0.25$).

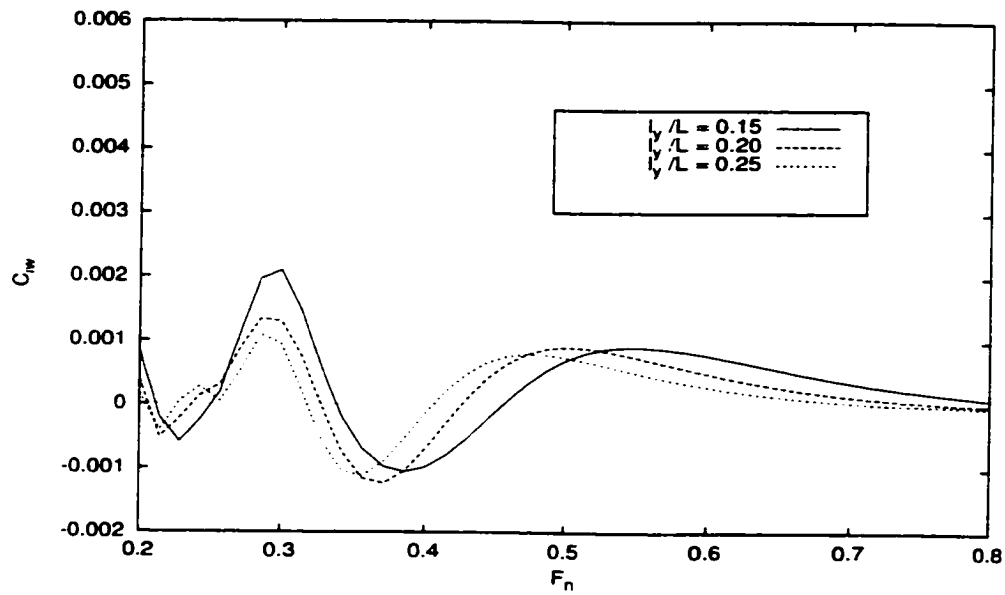

Figure 4.36: Computed wave interaction resistance coefficient of the Wigley trimaran($l_x/L = -0.25$).

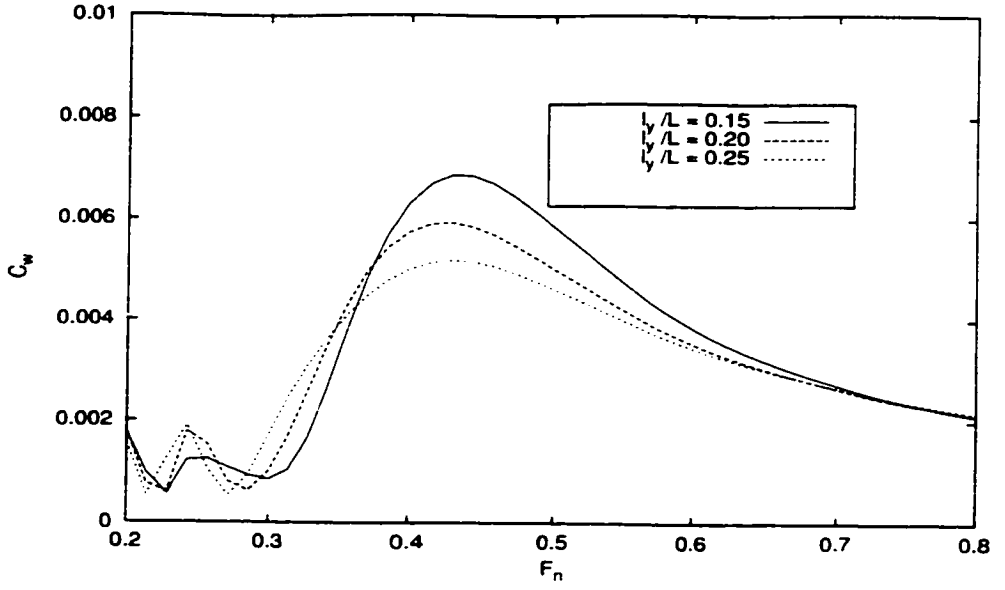

Figure 4.37: Effect of spacing on wave resistance coefficient of the Wigley trimaran($l_x/L = 0.0$)

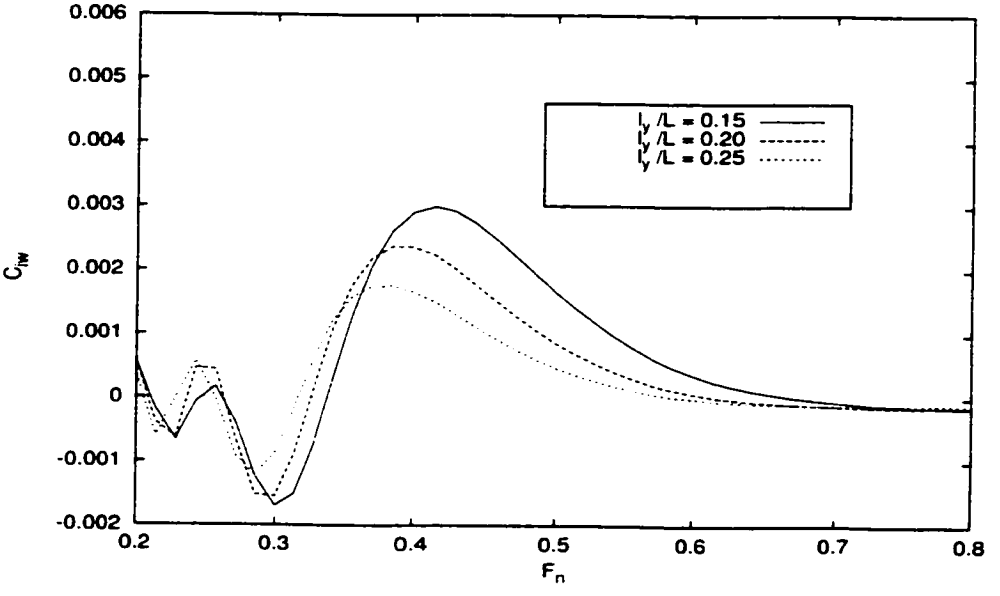

Figure 4.38: Computed wave interaction resistance coefficient of the Wigley trimaran($l_x/L = 0.0$).

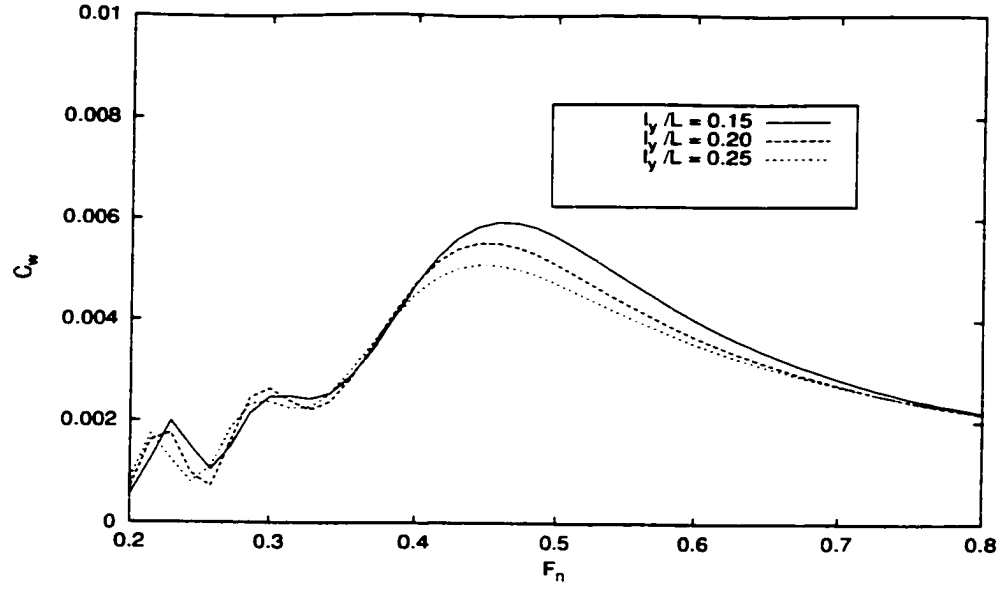

Figure 4.39: Effect of spacing on wave resistance coefficient of the Wigley trimaran($l_x/L = 0.125$).

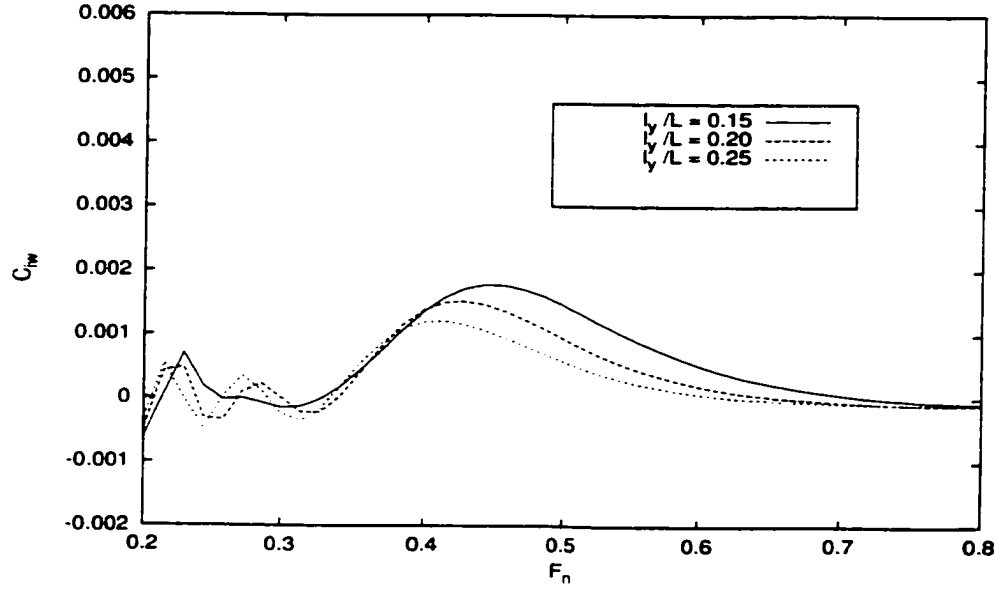

Figure 4.40: Computed wave interaction resistance coefficient of the Wigley trimaran($l_x/L = 0.125$).

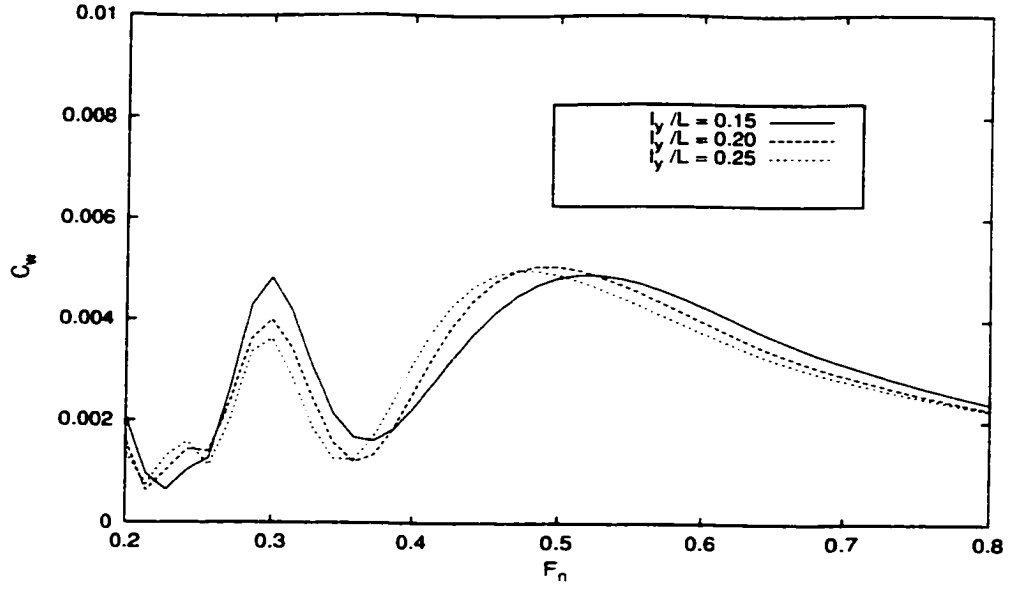

Figure 4.41: Effect of spacing on wave resistance coefficient of the Wigley trimaran($l_x/L = 0.25$).

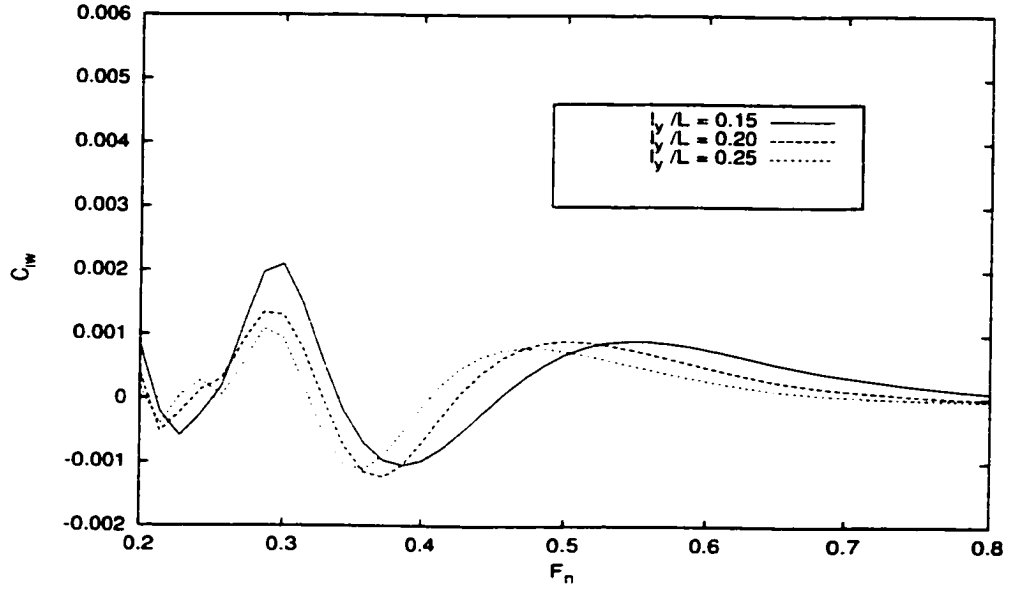

Figure 4.42: Computed wave interaction resistance coefficient of the Wigley trimaran($l_x/L = 0.25$).

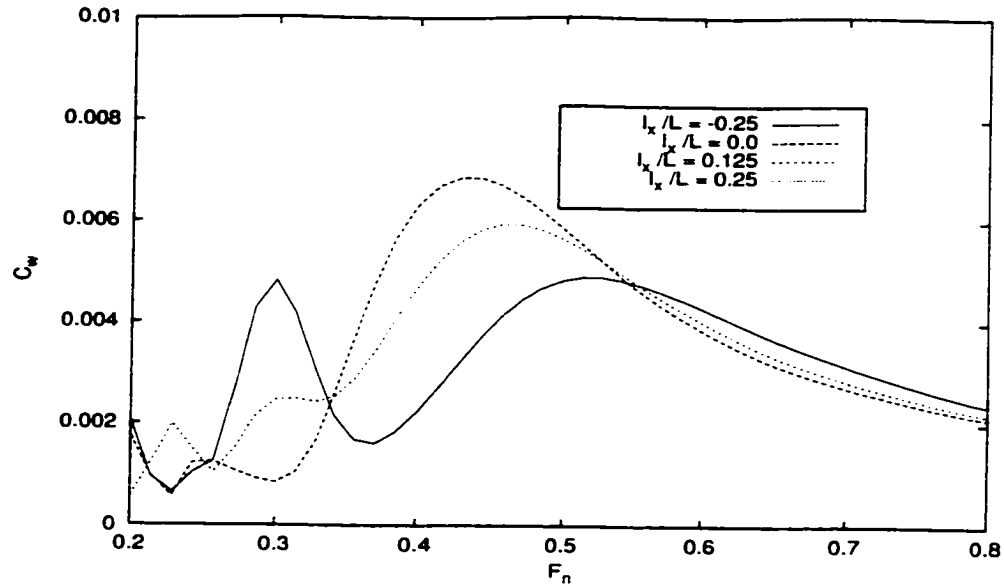

Figure 4.43: Effect of hull setback on wave resistance coefficient of the Wigley trimaran ($l_y/L = 0.15$)

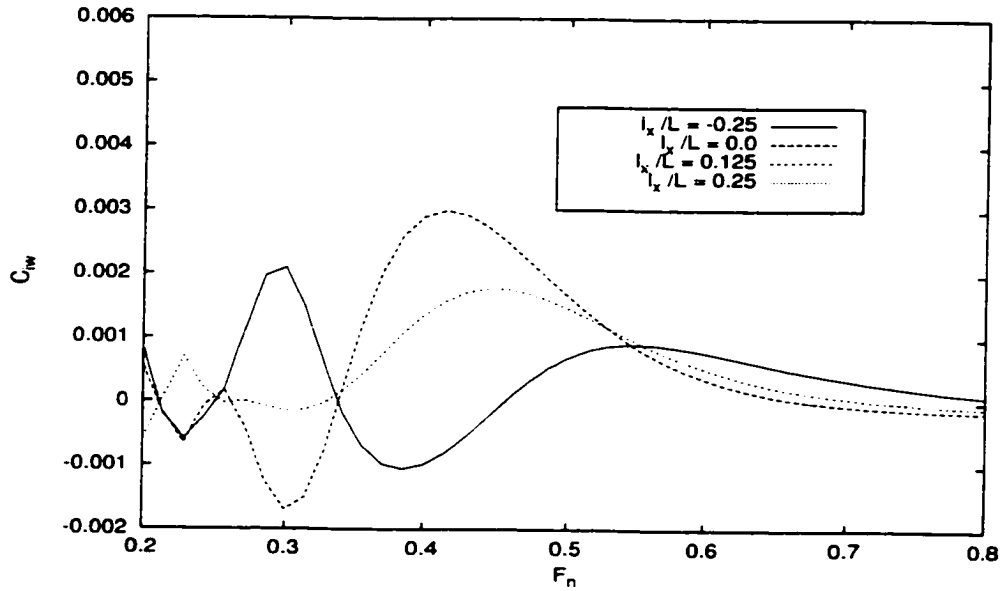

Figure 4.44: Computed wave interaction resistance coefficient of the Wigley trimaran($l_y/L = 0.15$).

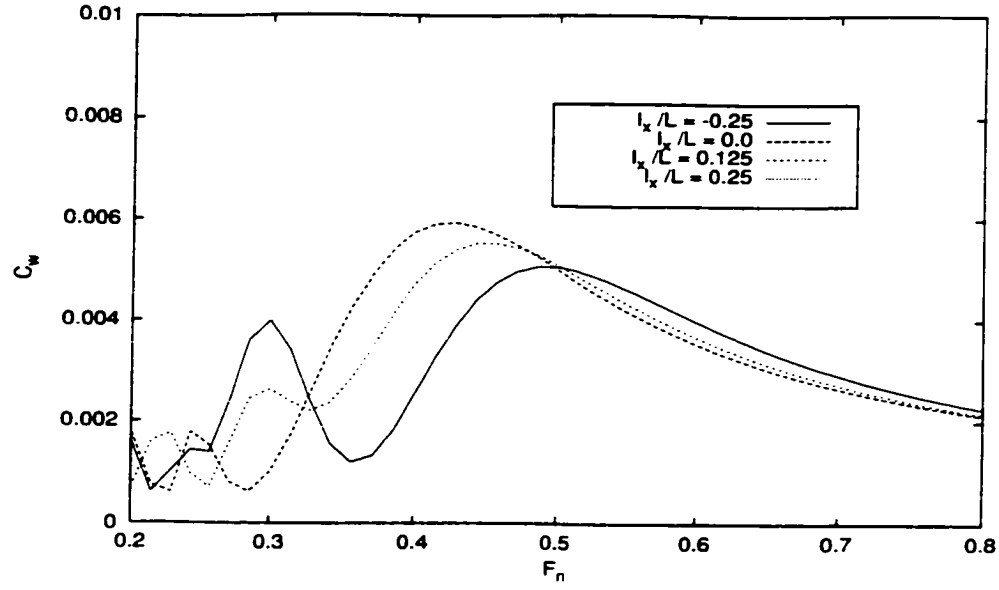

Figure 4.45: Effect of hull setback on wave resistance coefficient of the Wigley trimaran ($l_y/L = 0.20$).

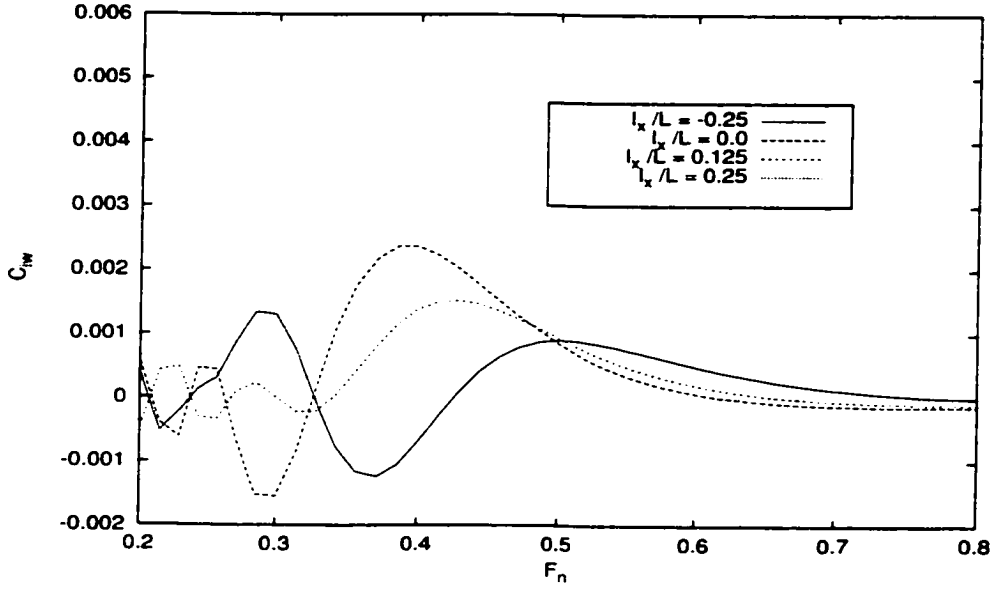

Figure 4.46: Computed wave interaction resistance coefficient of the Wigley trimaran($l_y/L = 0.20$).

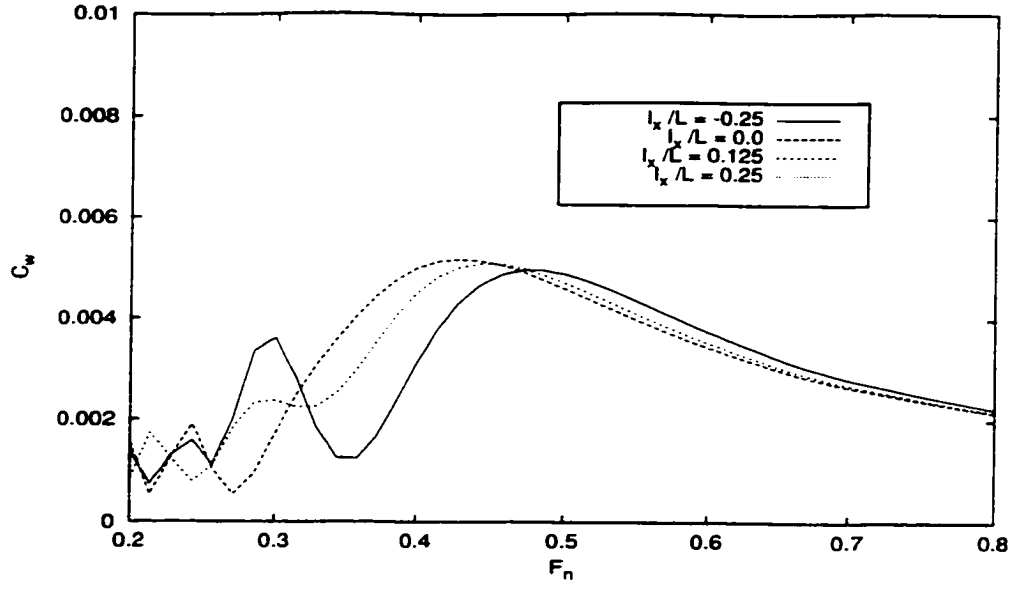

Figure 4.47: Effect of hull setback on wave resistance coefficient of the Wigley trimaran ($l_y/L = 0.25$).

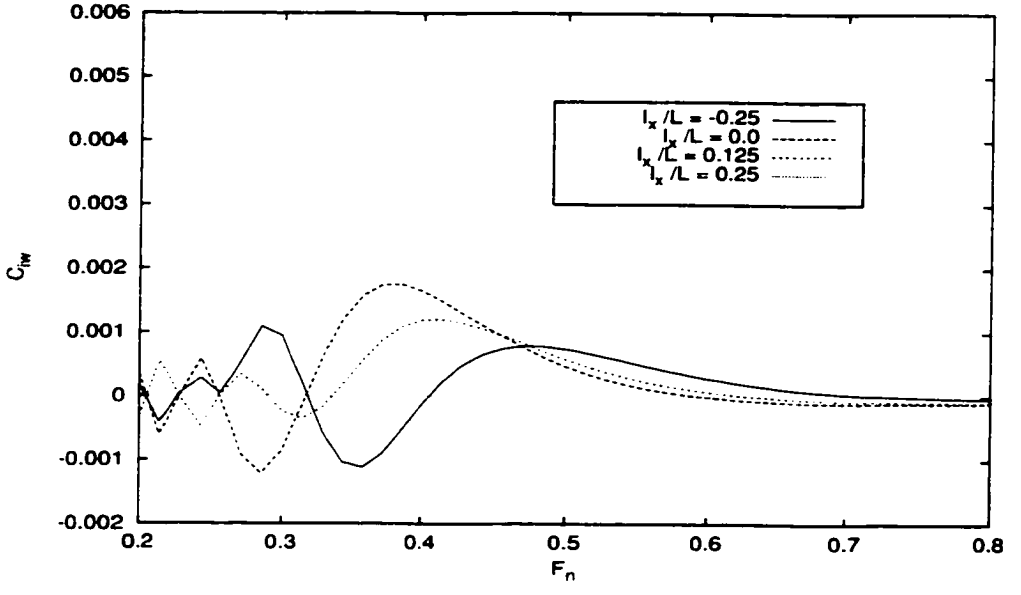

Figure 4.48: Computed wave interaction resistance coefficient of the Wigley trimaran($l_y/L = 0.25$).

The second trimaran model to be presented in this thesis was designed and tested in the Dalhousie towing tank (Peng, *et al.*, 1999). The full-scale principal dimensions are given below. This model is a typical example of a trimaran arrangement of hulls. It had a submerged cylindrical main hull, borrowed from the SWATH concept, to provide the buoyancy required for the vessel, and a narrow strut was used to connect the hull to the deck. Two surface piercing struts were used as the outrigger hulls. Lines drawing is shown in Figure 4.49.

Center main hull Length:	30.0 m
Center main hull Beam:	2.0 m
Center main hull Draft:	3.0m
Outrigger Hull Length:	10.0 m
Outrigger Hull Beam:	0.5 m
Outrigger Hull Draft:	1.0m
Outrigger Hull Spacing:	5.35 m
Outrigger Hull Setback:	1.53m
Total Wet Surface Area:	282.8 m^2
Total Displacement:	105 tonne

Four validation cases were considered as shown in Tables 4.3: In this model, the total resistance coefficients, $C_t = C_w + C_f$ instead of C_w as for the Wigley trimaran, were compared with the experimental data. The form factor correction was not applied here.

Figure 4.50 to Figure 4.53 show the comparison of the computed total resistance coefficients with the experimental results of the Dalhousie trimaran (student report).

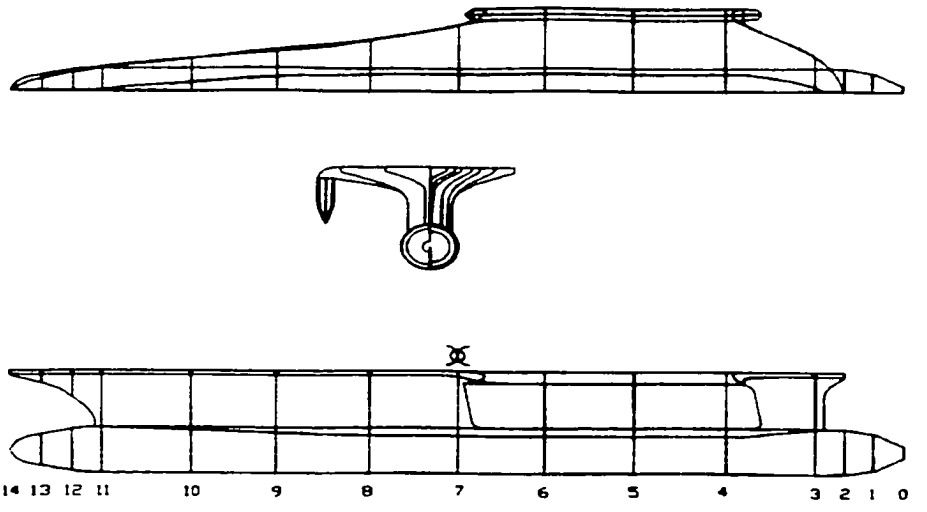

Figure 4.49: Dalhousie trimaran lines drawing

Table 4.3: Validation Conditions for the Dalhousie Trimaran

	$l_x = 1.53m$	$l_x = 5.58$
$l_y = 5.35$	CASE 1	CASE 3
$l_y = 6.65$	CASE 2	CASE 4

At high speeds. the computed resistance coefficients were lower than the model test results. This could be due to the extra water shipping on the deck during the test and the current theory did not include this condition. In general, the computed resistance agree well with the model test data.

In order to investigate the relationship between the wave interaction effect and positions of outriggers, the same conditions were computed for the Dalhousie trimaran as the Wigley trimaran as before. The comparisons of computed results are shown in Figure 4.54 to Figure 4.61 with l_x/L = -0.25, 0.0, 0.125, 0.25, respectively; and in Figure 4.62 to Figure 4.67 for l_y/L=0.15, 0.2, 0.25, respectively.

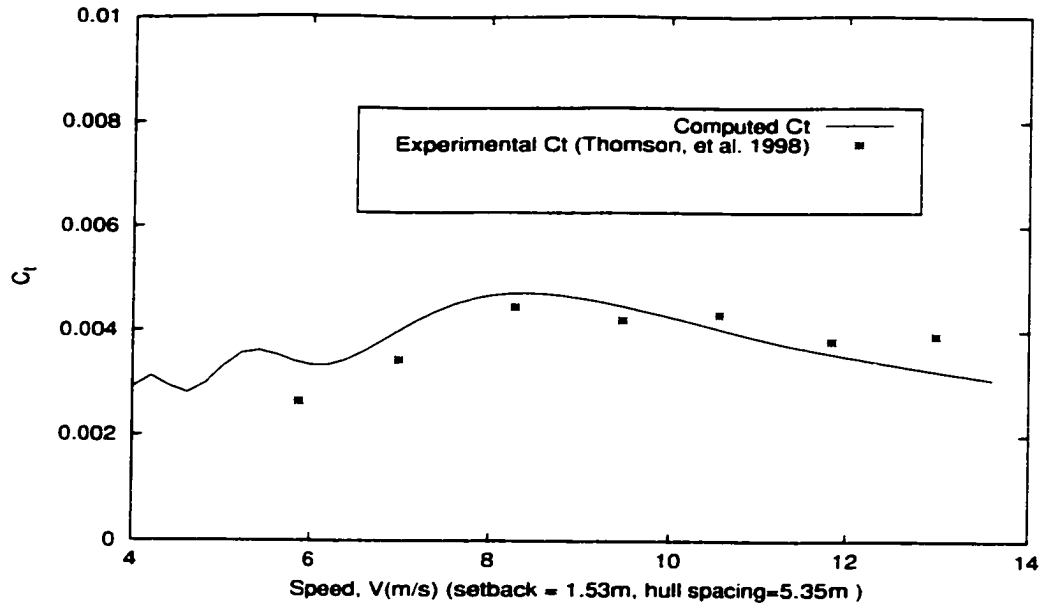

Figure 4.50: Comparison of computed and experimental results for C_t of the Dalhousie trimaran, CASE 1

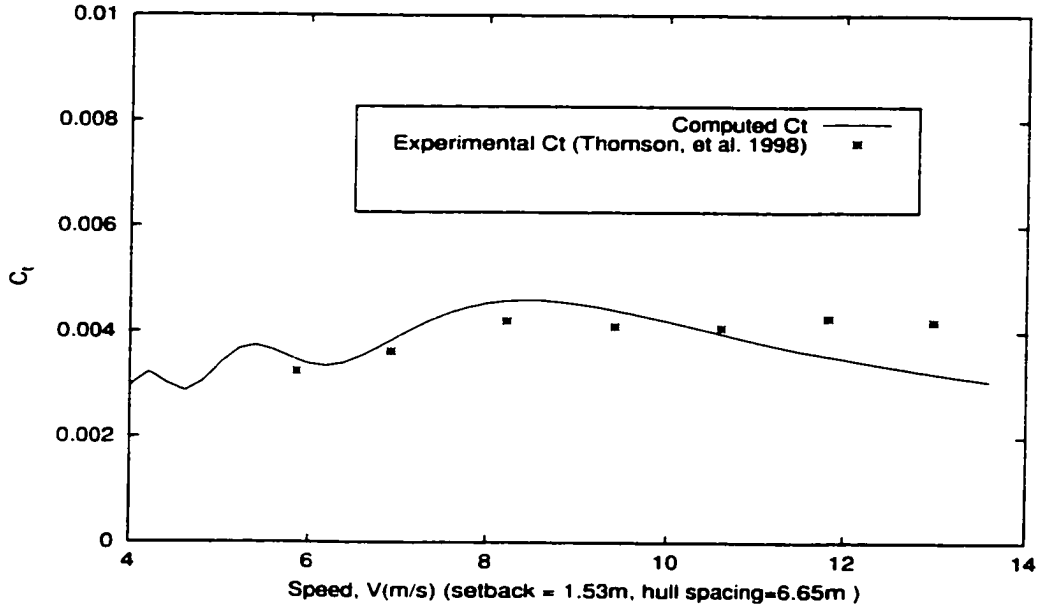

Figure 4.51: Comparison of computed and experimental results for C_t of the Dalhousie trimaran, CASE 2

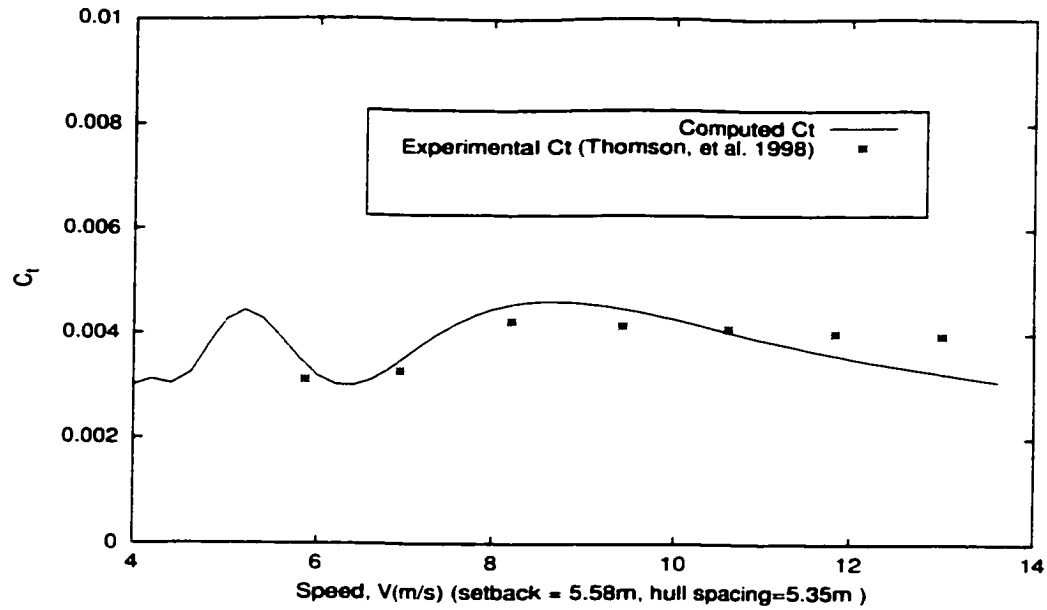

Figure 4.52: Comparison of computed and experimental results for C_t of the Dalhousie trimaran, CASE 3

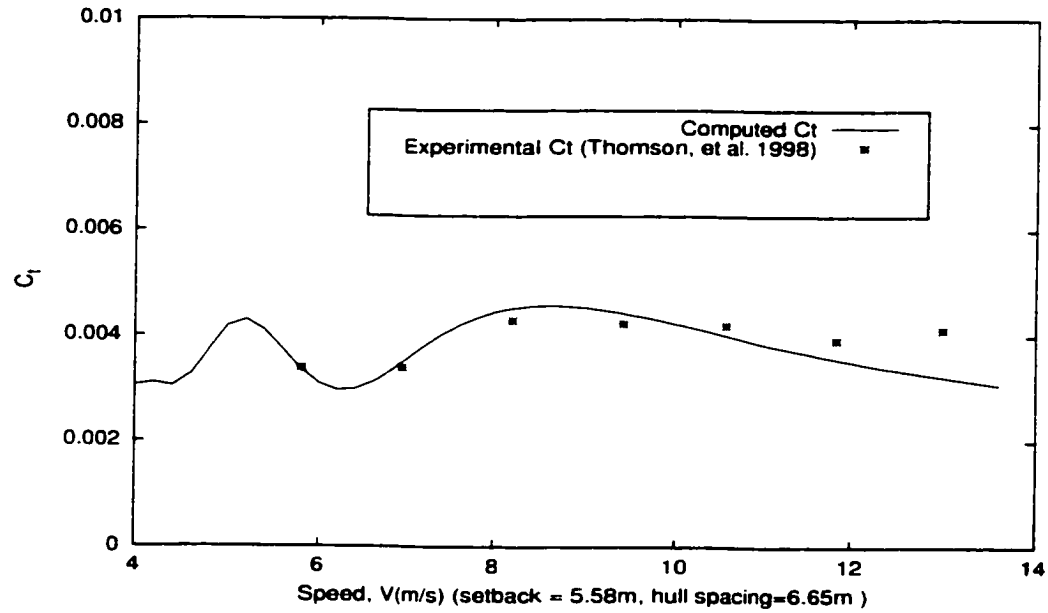

Figure 4.53: Comparison of computed and experimental results for C_t of the Dalhousie trimaran, CASE 4

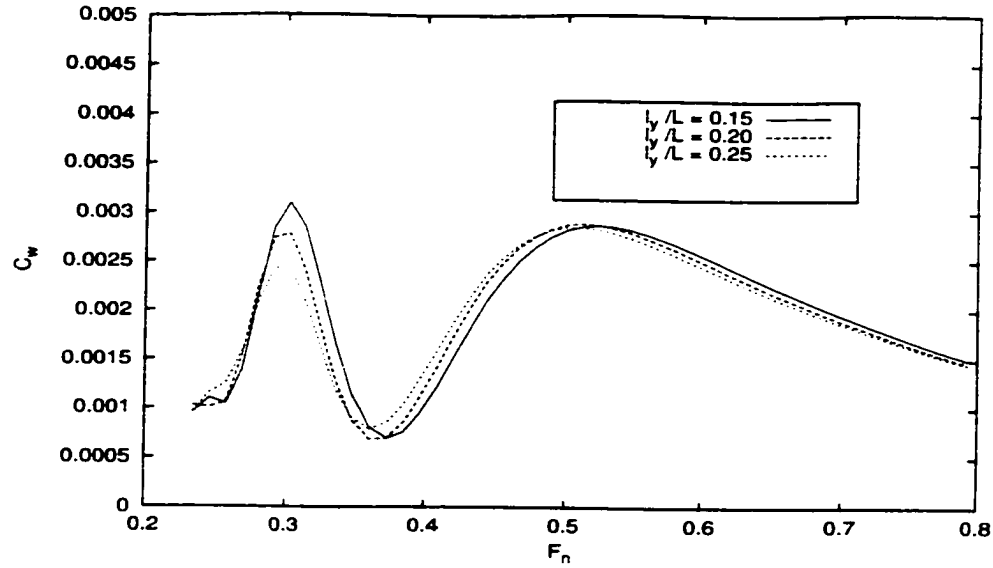

Figure 4.54: Effect of spacing on wave resistance coefficient of the Dalhousie trimaran($l_x/L = -0.25$).

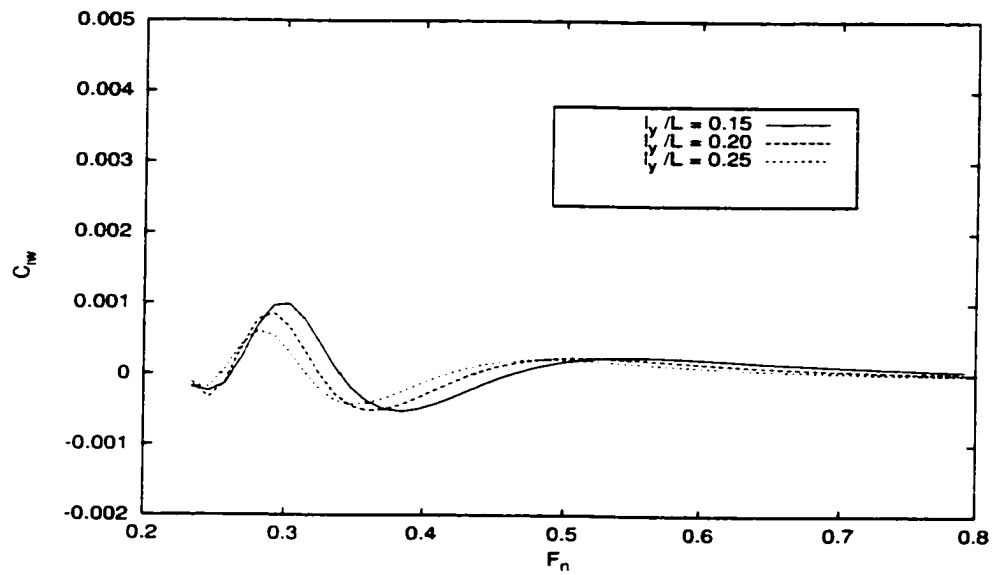

Figure 4.55: Computed wave interaction resistance coefficient of the Dalhousie trimaran($l_x/L = -0.25$).

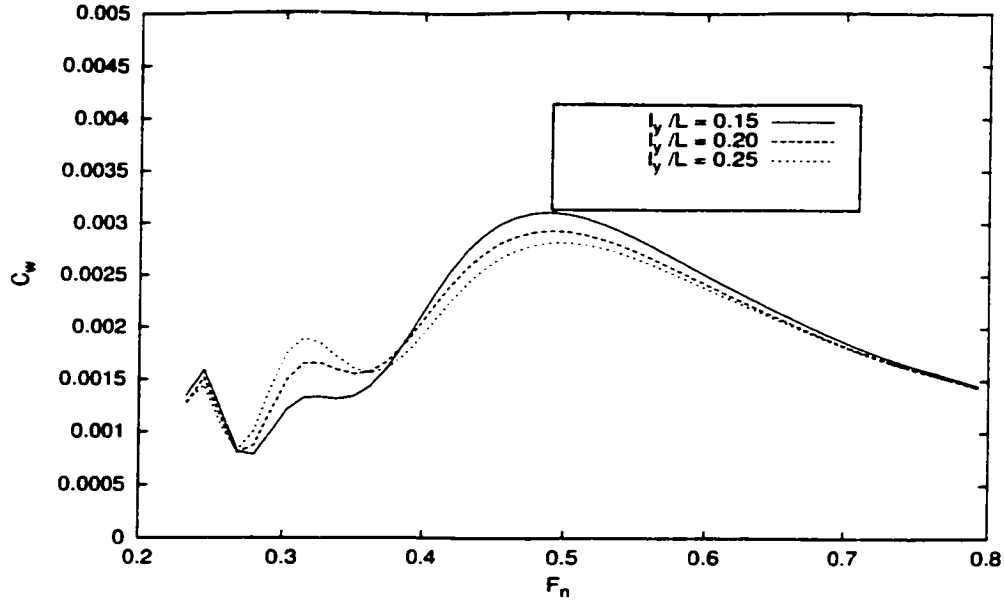

Figure 4.56: Effect of spacing on wave resistance coefficient of the Dalhousie trimaran($l_x/L = 0.0$)

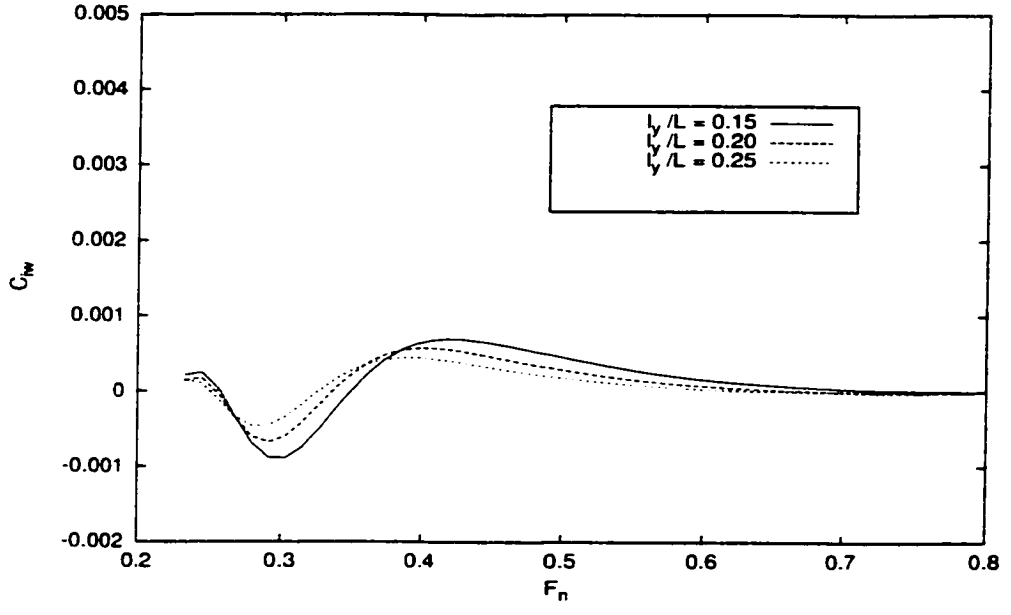

Figure 4.57: Computed wave interaction resistance coefficient of the Dalhousie trimaran($l_x/L = 0.0$).

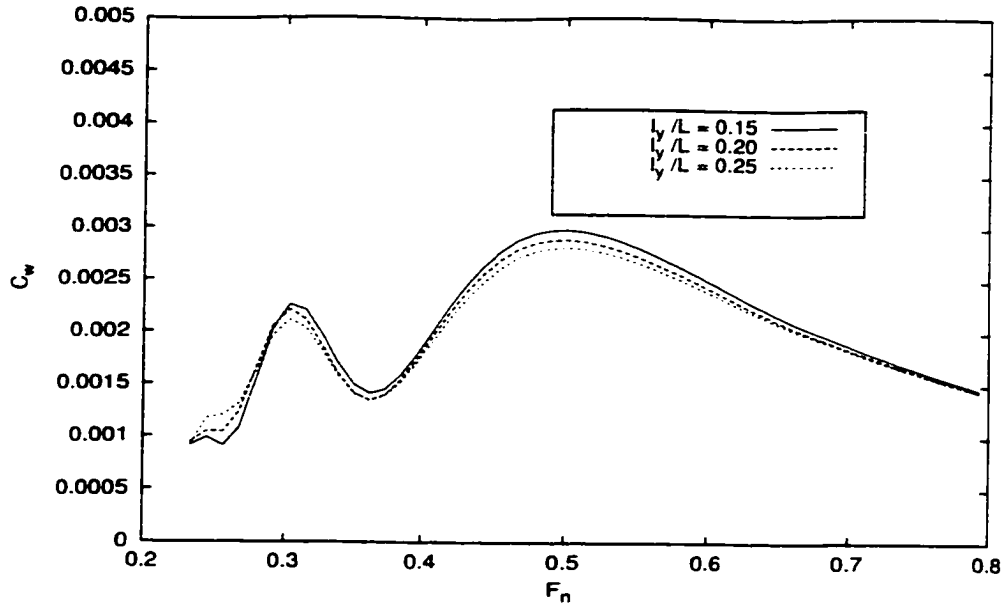

Figure 4.58: Effect of spacing on wave resistance coefficient of the Dalhousie trimaran($l_x/L = 0.125$).

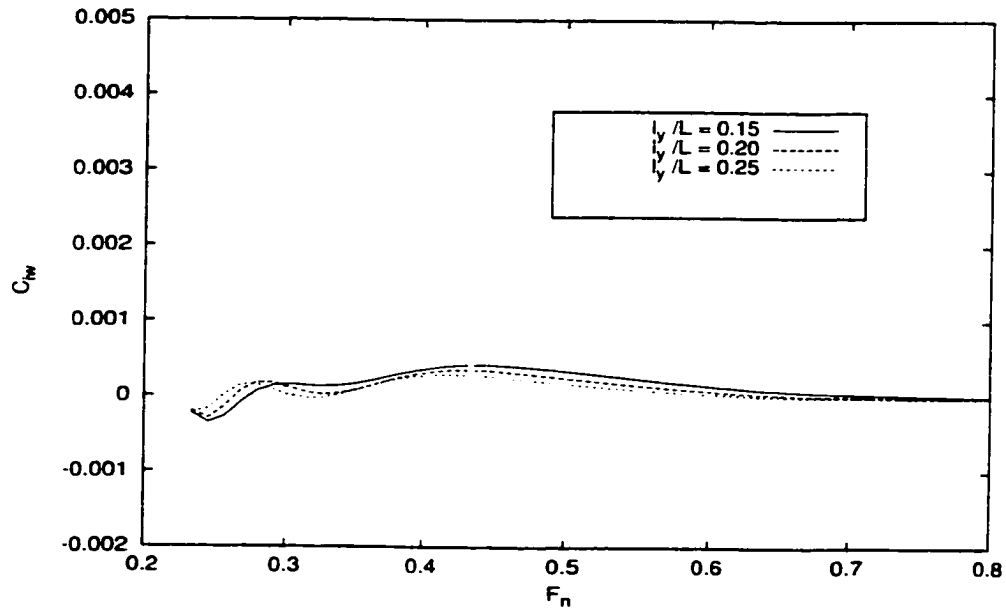

Figure 4.59: Computed wave interaction resistance coefficient of the Dalhousie trimaran($l_x/L = 0.125$).

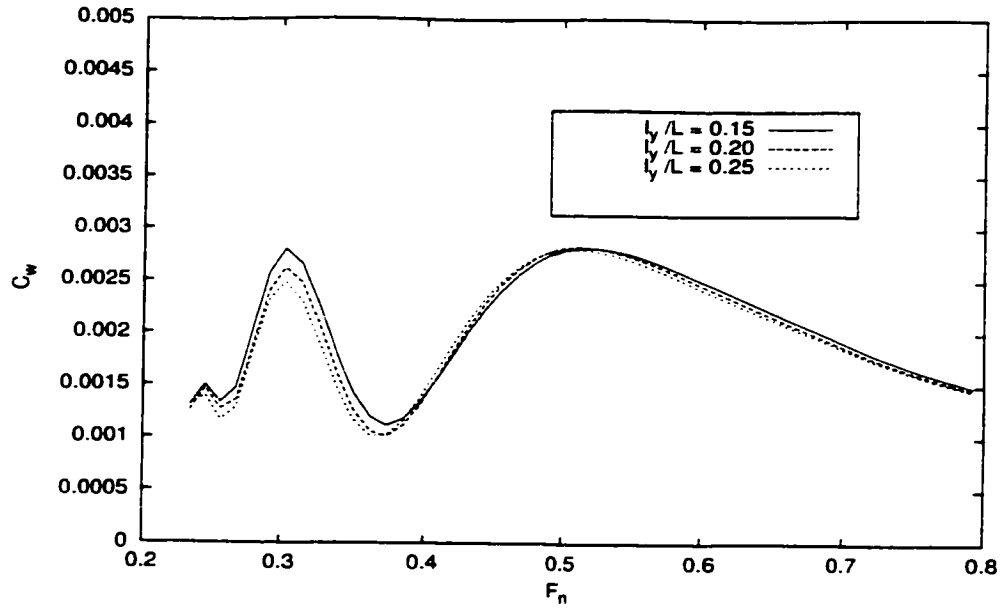

Figure 4.60: Effect of spacing on wave resistance coefficient of the Dalhousie trimaran ($l_x/L = 0.25$).

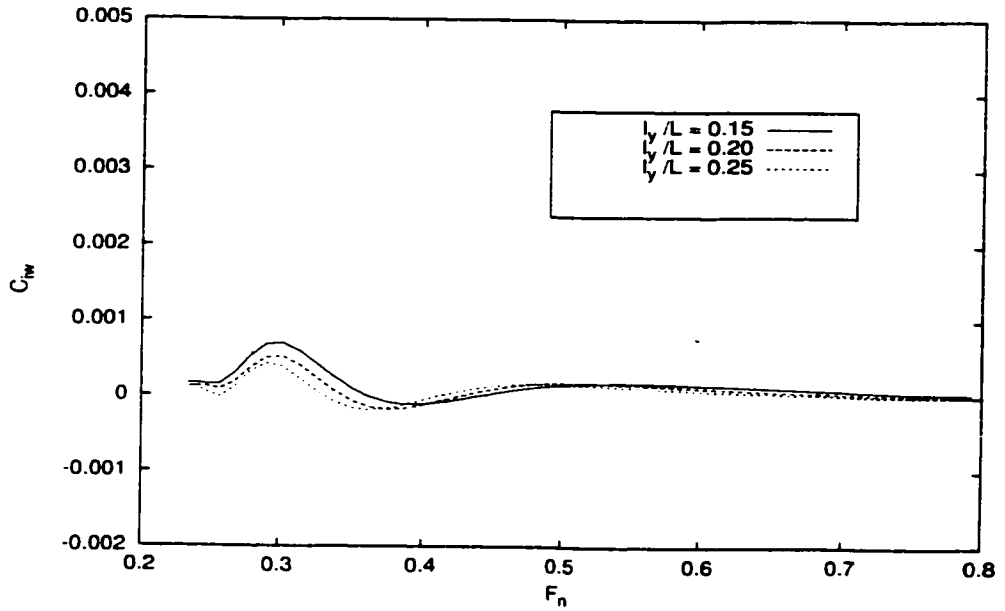

Figure 4.61: Computed wave interaction resistance coefficient of the Dalhousie trimaran($l_x/L = 0.25$).

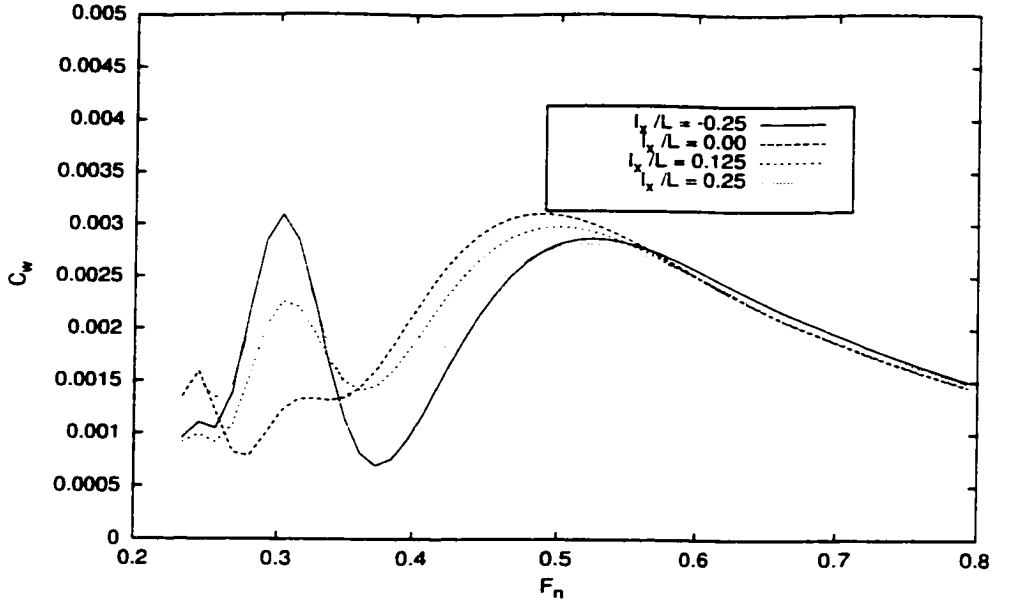

Figure 4.62: Effect of hull setback on wave resistance coefficient of the Dalhousie trimaran($l_y/L = 0.15$)

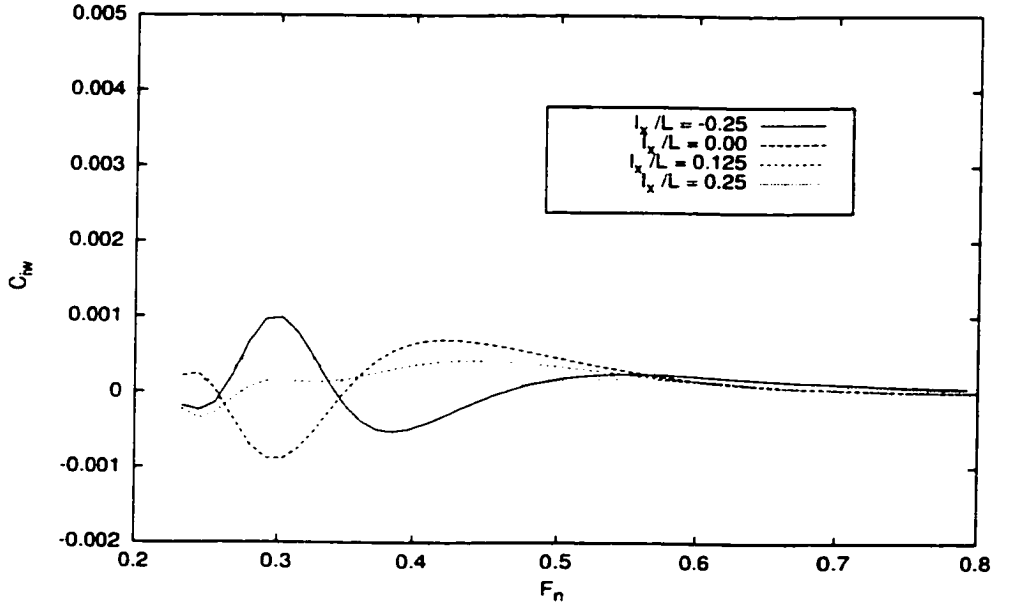

Figure 4.63: Computed wave interaction resistance coefficient of the Dalhousie trimaran($l_y/L = 0.15$).

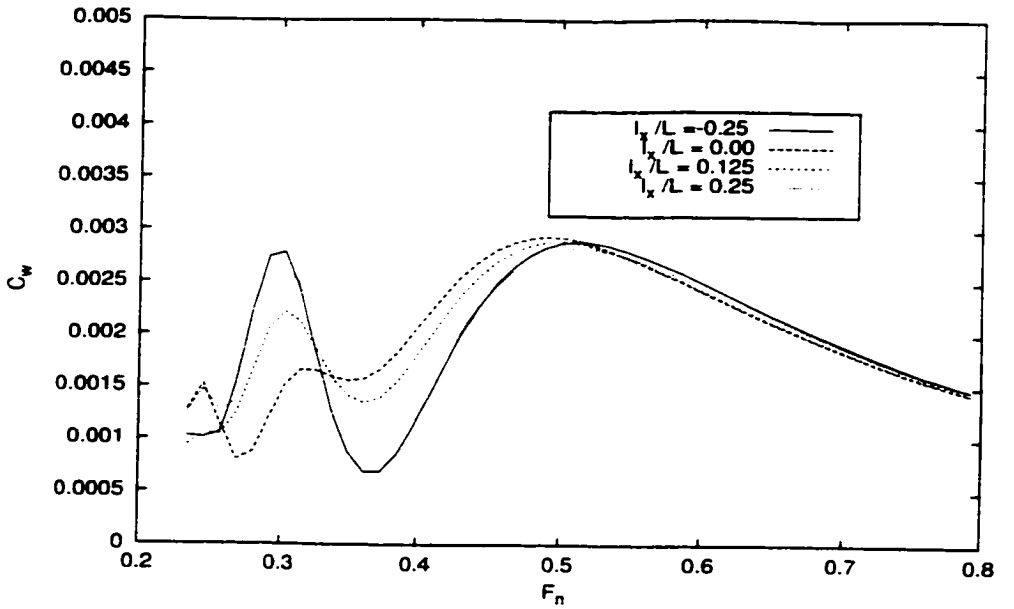

Figure 4.64: Effect of hull setback on wave resistance coefficient of the Dalhousie trimaran($l_y/L = 0.20$).

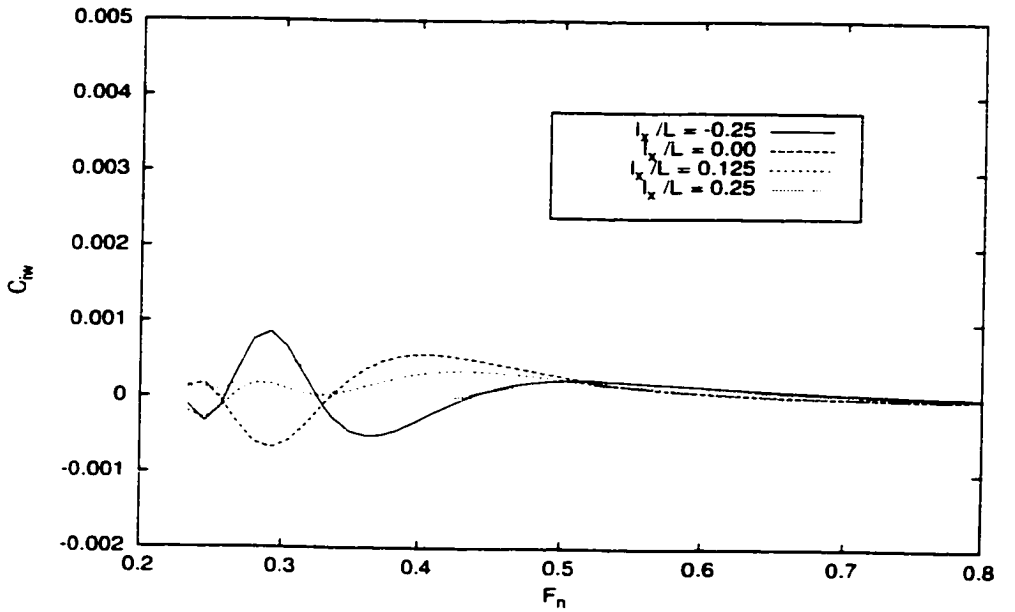

Figure 4.65: Computed wave interaction resistance coefficient of the Dalhousie trimaran($l_y/L = 0.20$).

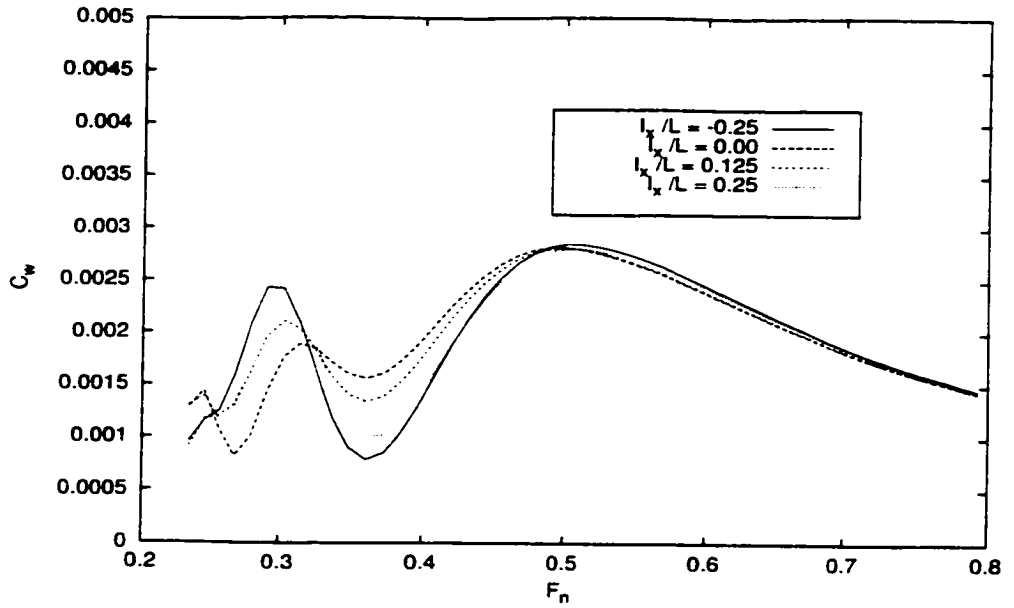

Figure 4.66: Effect of hull setback on wave resistance coefficient of the Dalhousie trimaran($l_y/L = 0.25$).

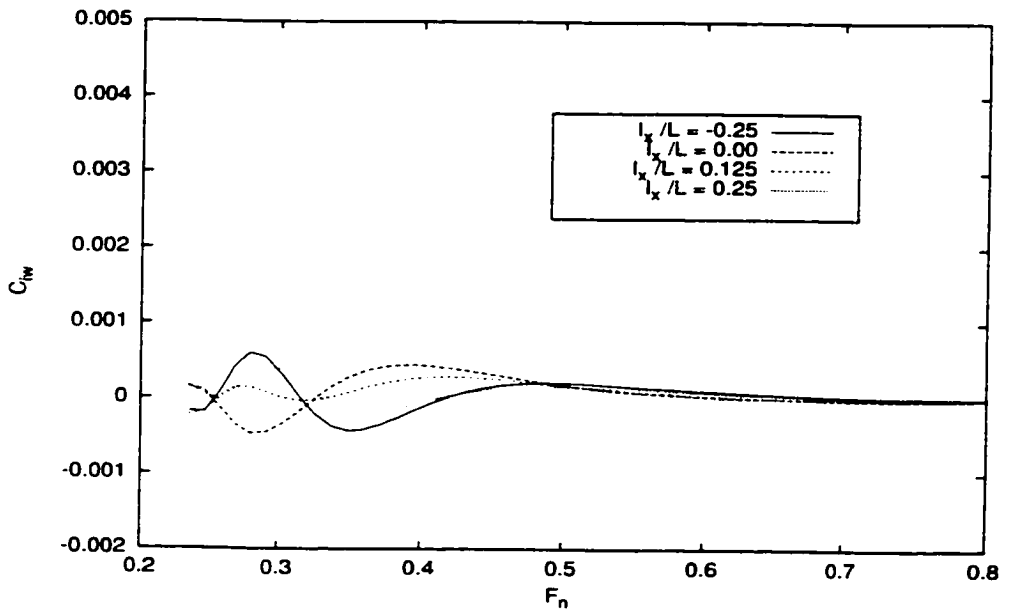

Figure 4.67: Computed wave interaction resistance coefficient of the Dalhousie trimaran($l_y/L = 0.25$).

The third trimaran model selected in this study was Wave Cancellation Multihull (WCM) tested in the David Taylor Model Basin of the U.S. Navy (Wilson, *et al.*, 1993). Principal dimensions of the prototype are summarized as below:

Center Main Hull Length:	118.87 m
Center Main Hull Max Beam:	5.80 m
Center Main Hull Min Beam:	2.64 m
Center Main Hull Draft:	9.14m
Outrigger Hull Length:	57.91 m
Outrigger Hull Beam:	2.01 m
Outrigger Hull Draft:	4.23m
Outrigger Hull Spacing:	32.31 m
Total Wet Surface Area:	3891 m^2
Total Displacement:	4369 tonne

It was a variant of the O'Neill Hullform (OHF) which the center body-center strut combination was replaced by a tapered, strut-like center hull with a trapezoidal cross section, as shown in Figure 4.68.

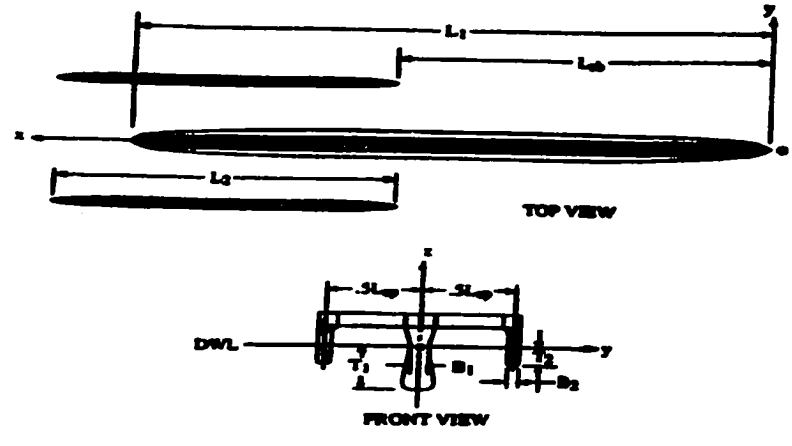

Figure 4.68: WCM trimaran lines drawing

Four validation cases were considered as shown in Tables 4.4:

Table 4.4: Validation Conditions for the WCM Trimaran

	$l_x = 15.20m$	$l_x = 24.50m$	$l_x = 31.15m$	$l_x = 45.50m$
$l_y = 16.0m$	CASE 1	CASE 2	CASE 3	CASE 4

The computed wave resistance coefficients were compared with experimental results by Wilson, *et al.* (1993), as shown in Figure 4.69 to Figure 4.72. Examining these figures, the theoretical and experimental results are in good agreement. The computed curves all show good prediction on the positions of humps and hollows. The wave interaction effect was investigated by changing the positions of the outriggers just the same conditions set up as the Wigley trimarans and the Dalhousie trimarans. The comparisons of computed results are shown in Figure 4.73 to Figure 4.80 with $l_x/L =$ -0.25, 0.0, 0.125, 0.25, respectively; and in Figure 4.81 to Figure 4.86 for l_y/L=0.15, 0.2, 0.25, respectively. Again, the theoretically computed wave resistance coefficients for outriggers at $lx/L = 0.25$ and at $lx/L = -0.25$ are exactly equal, just as the cases of the Wigley trimarans.

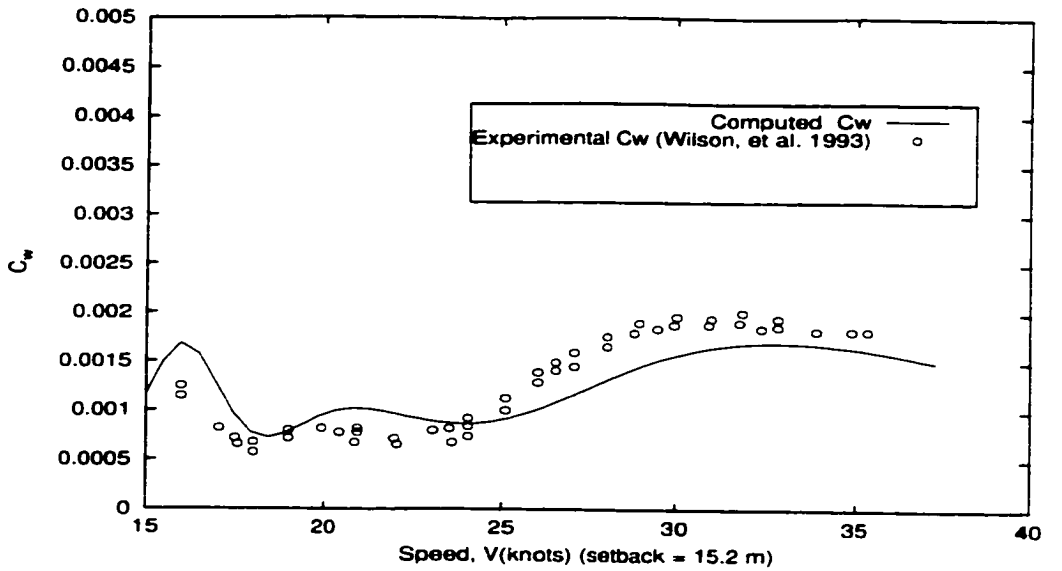

Figure 4.69: Comparison of computed and experimental results for C_w of the WCM trimaran, CASE 1

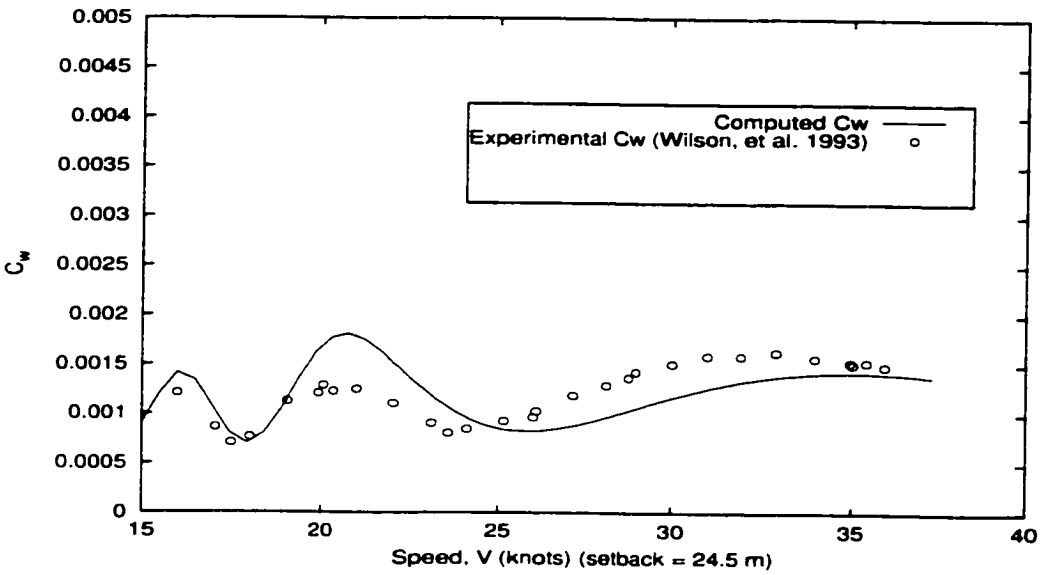

Figure 4.70: Comparison of computed and experimental results for C_w of the WCM trimaran, CASE 2

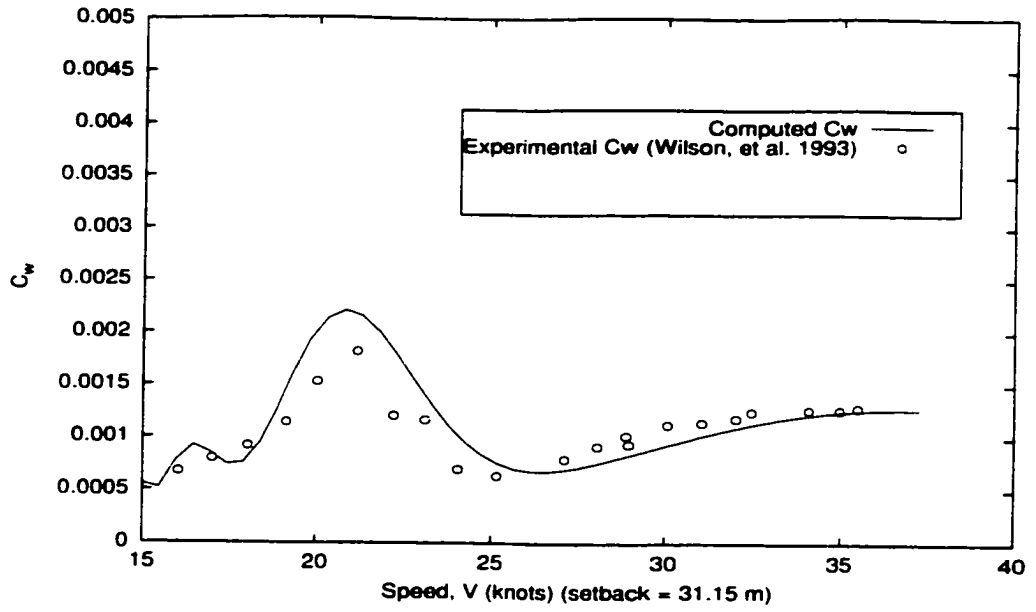

Figure 4.71: Comparison of computed and experimental results for C_w of the WCM trimaran, CASE 3

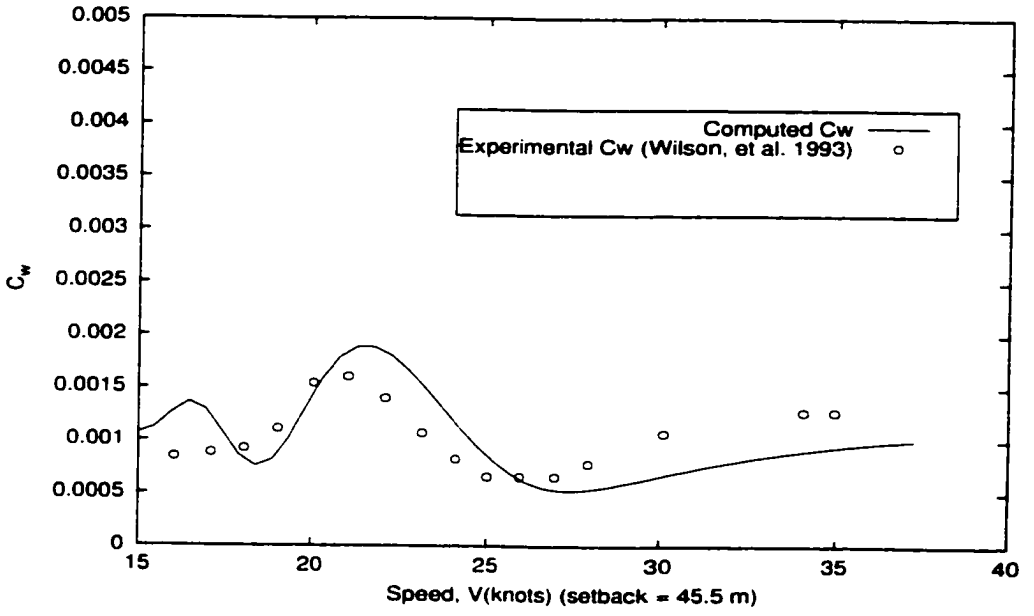

Figure 4.72: Comparison of computed and experimental results for C_w of the WCM trimaran, CASE 4

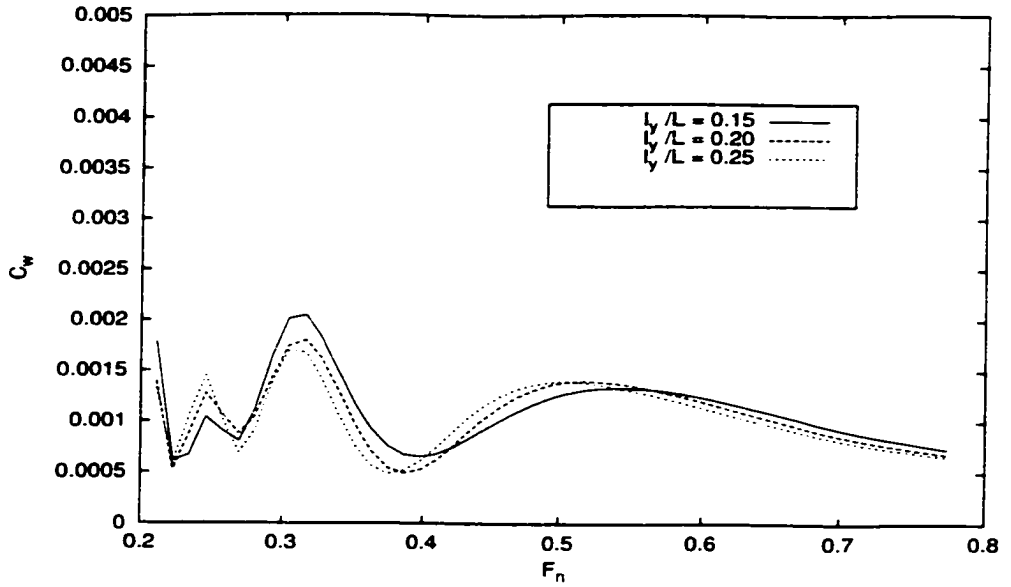

Figure 4.73: Effect of spacing on wave resistance coefficient of the WCM trimaran($l_x/L = -0.25$).

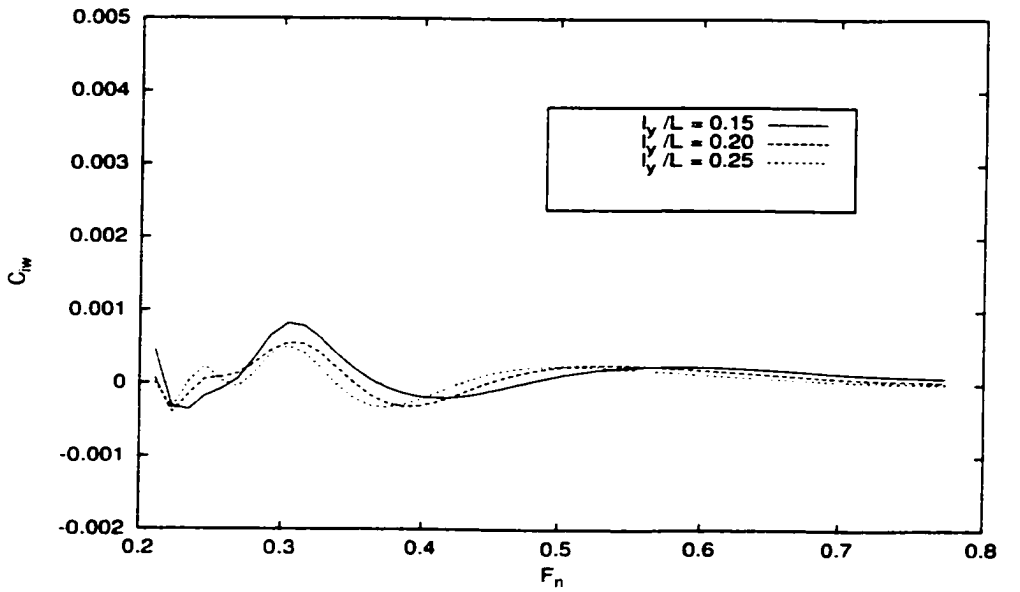

Figure 4.74: Computed wave interaction resistance coefficient of the WCM trimaran($l_x/L = -0.25$).

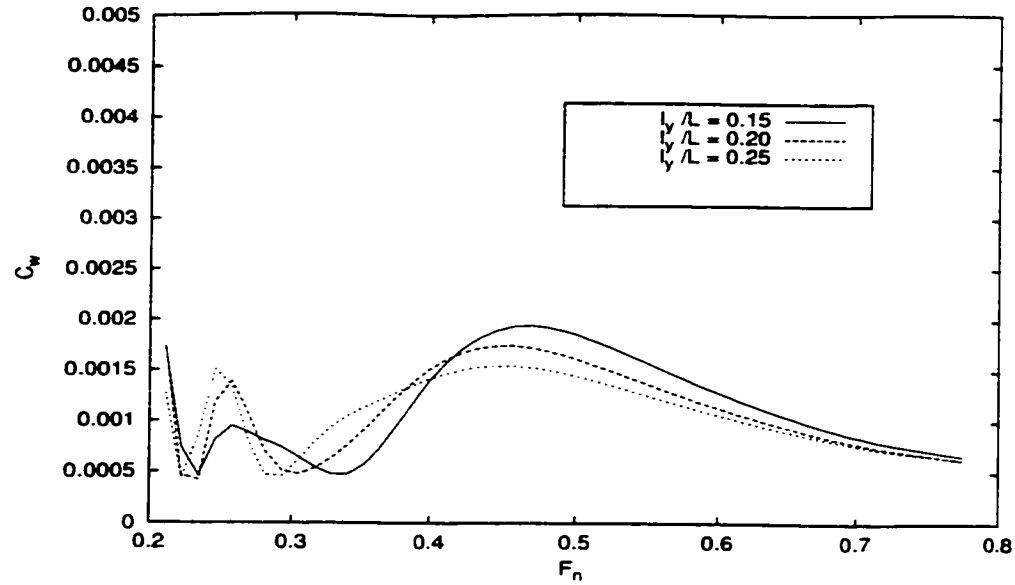

Figure 4.75: Effect of spacing on wave resistance coefficient of the WCM trimaran($l_x/L = 0.0$)

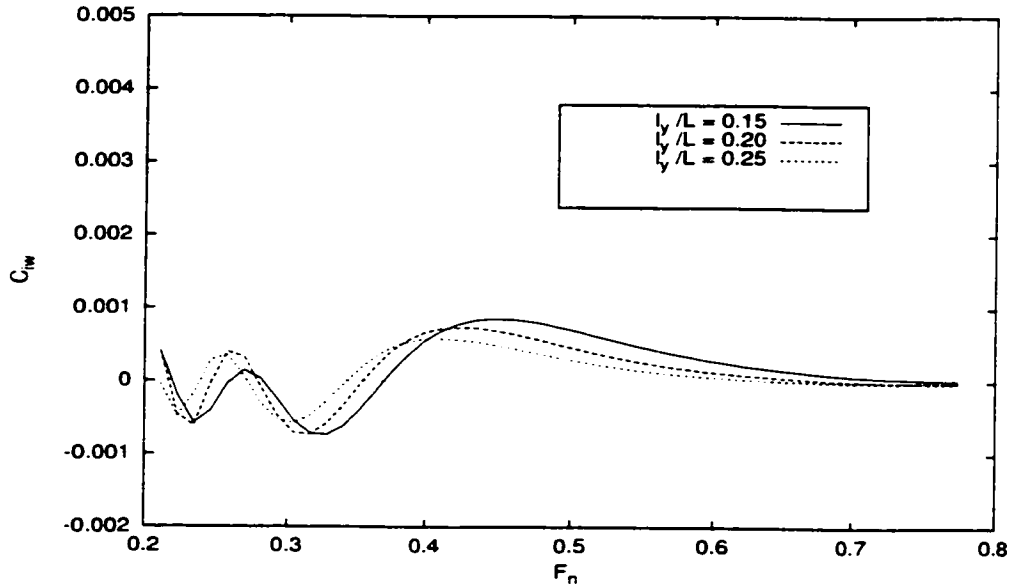

Figure 4.76: Computed wave interaction resistance coefficient of the WCM trimaran($l_x/L = 0.0$).

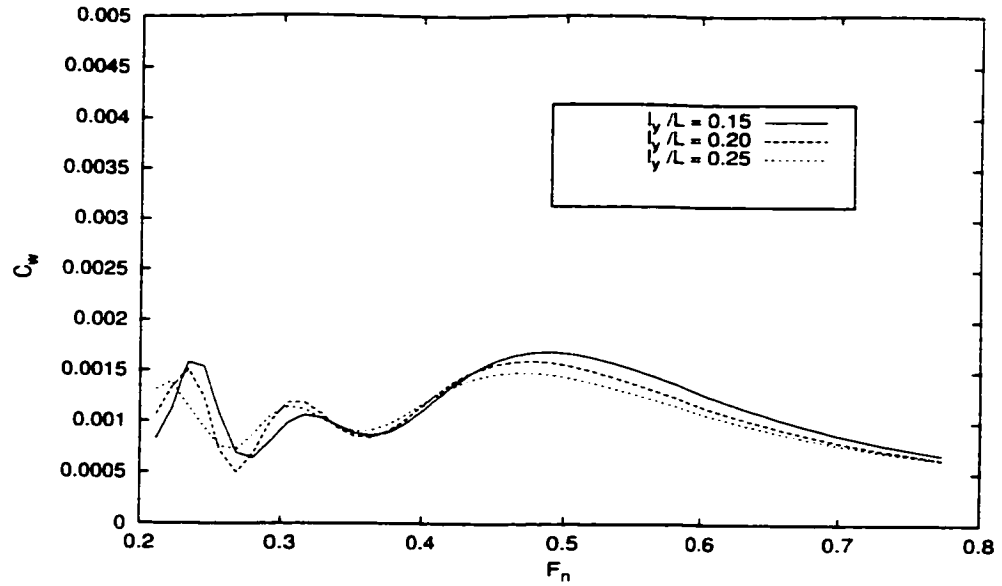

Figure 4.77: Effect of spacing on wave resistance coefficient of the WCM trimaran($l_x/L = 0.125$).

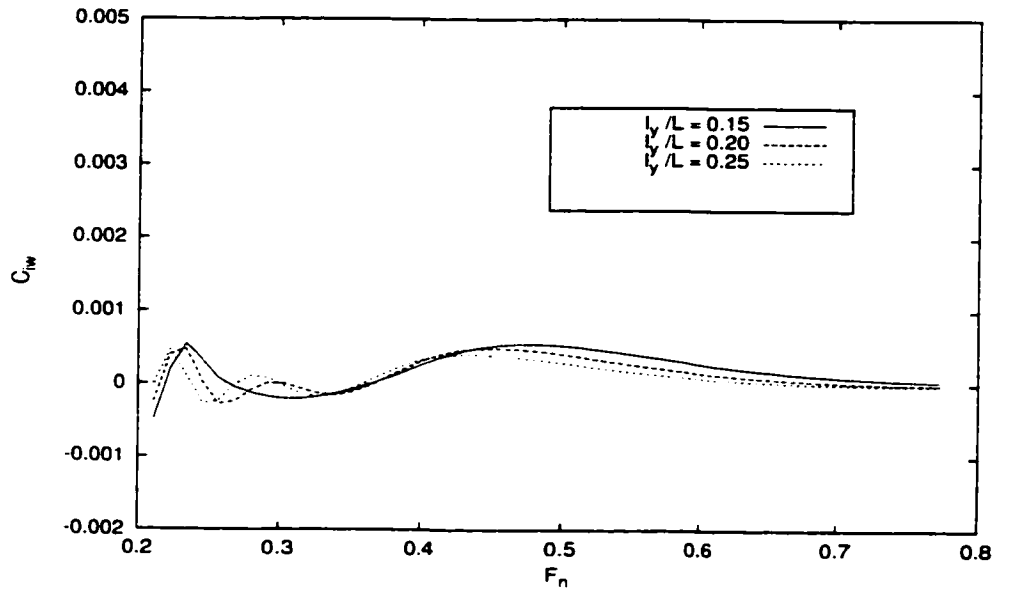

Figure 4.78: Computed wave interaction resistance coefficient of the WCM trimaran($l_x/L = 0.125$).

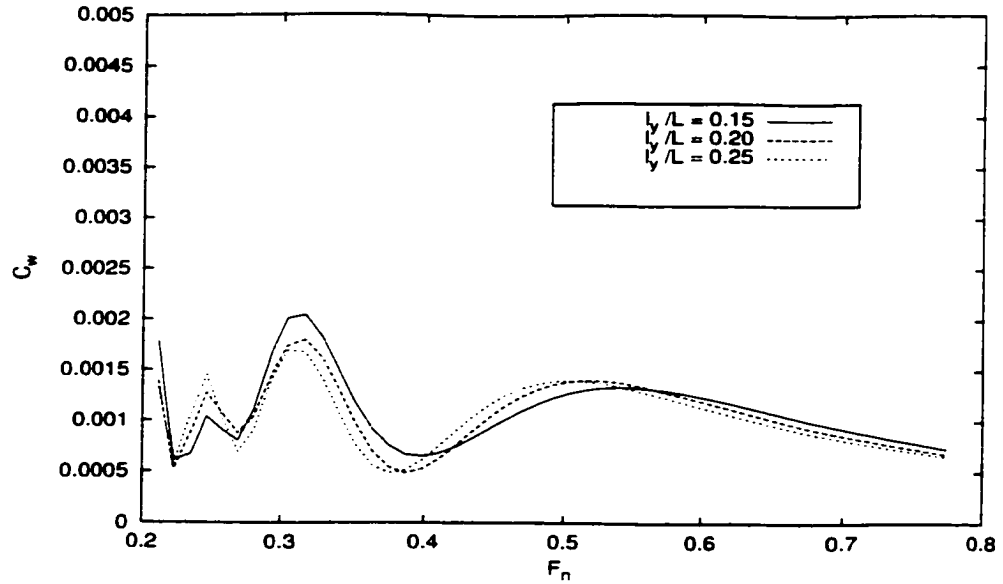

Figure 4.79: Effect of spacing on wave resistance coefficient of the WCM trimaran($l_x/L = 0.25$).

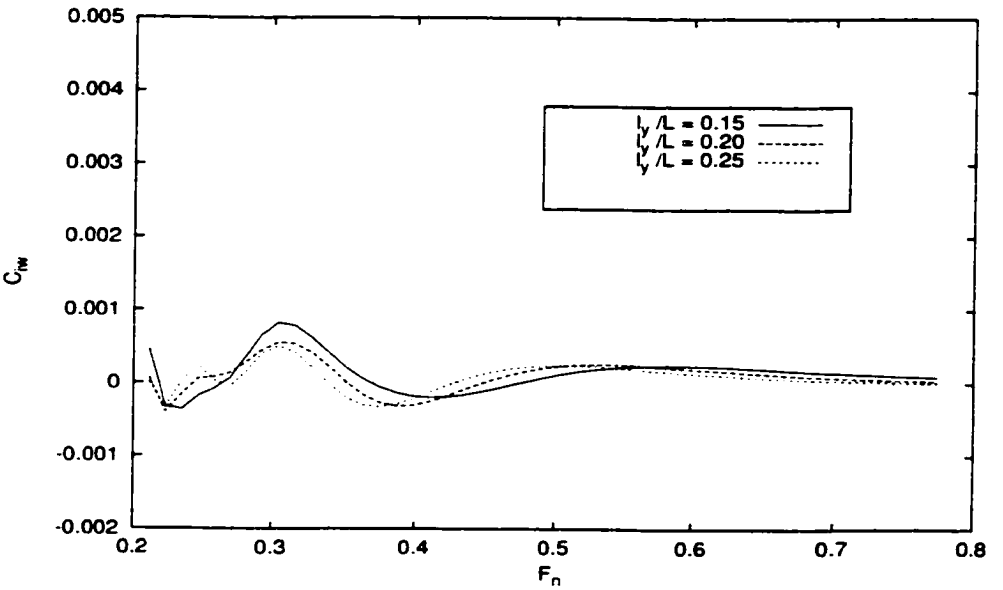

Figure 4.80: Computed wave interaction resistance coefficient of the WCM trimaran($l_x/L = 0.25$).

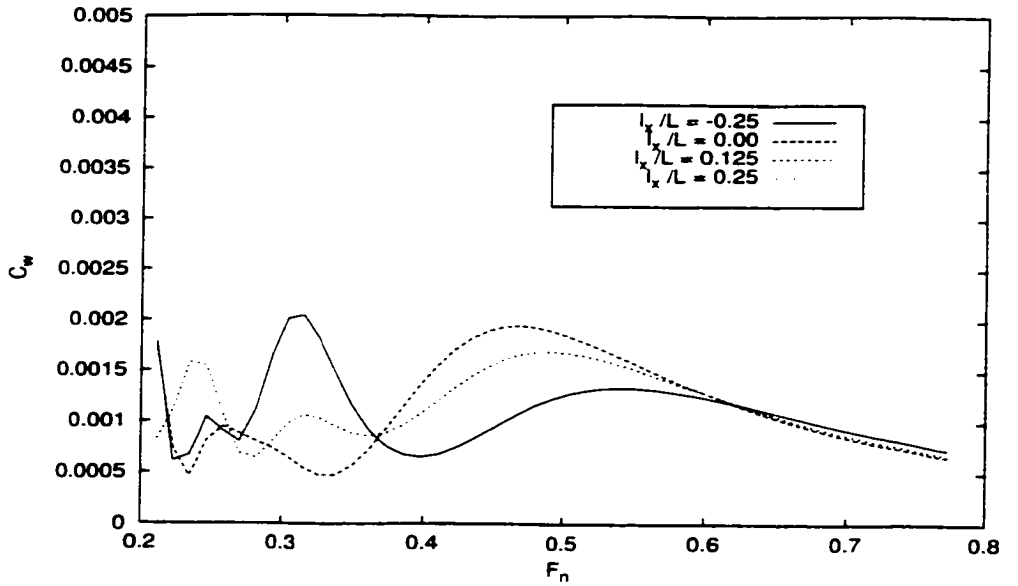

Figure 4.81: Effect of hull setback on wave resistance coefficient of the WCM trimaran($l_y/L = 0.15$)

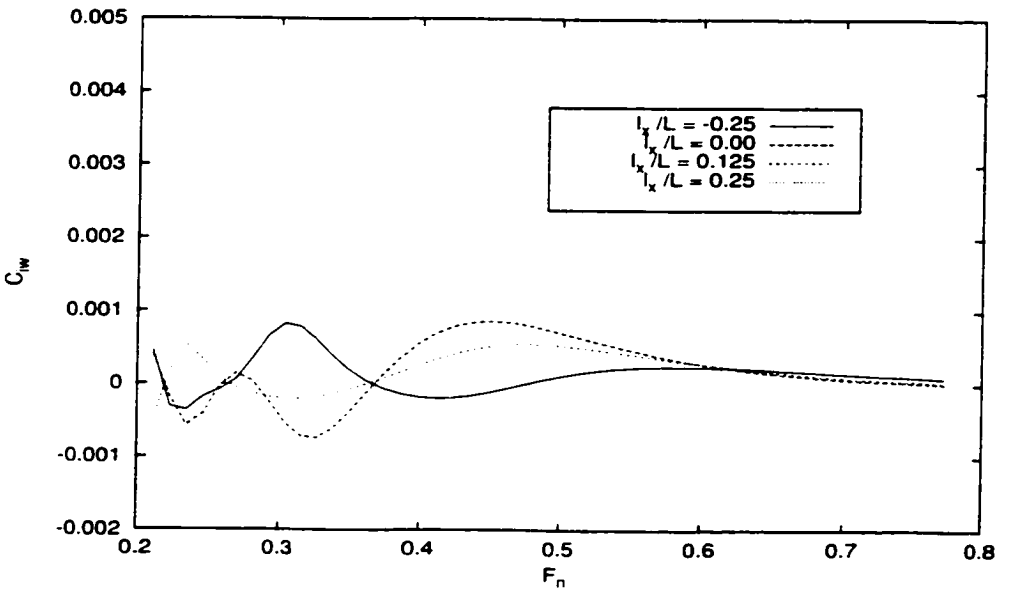

Figure 4.82: Computed wave interaction resistance coefficient of the WCM trimaran($l_y/L = 0.15$).

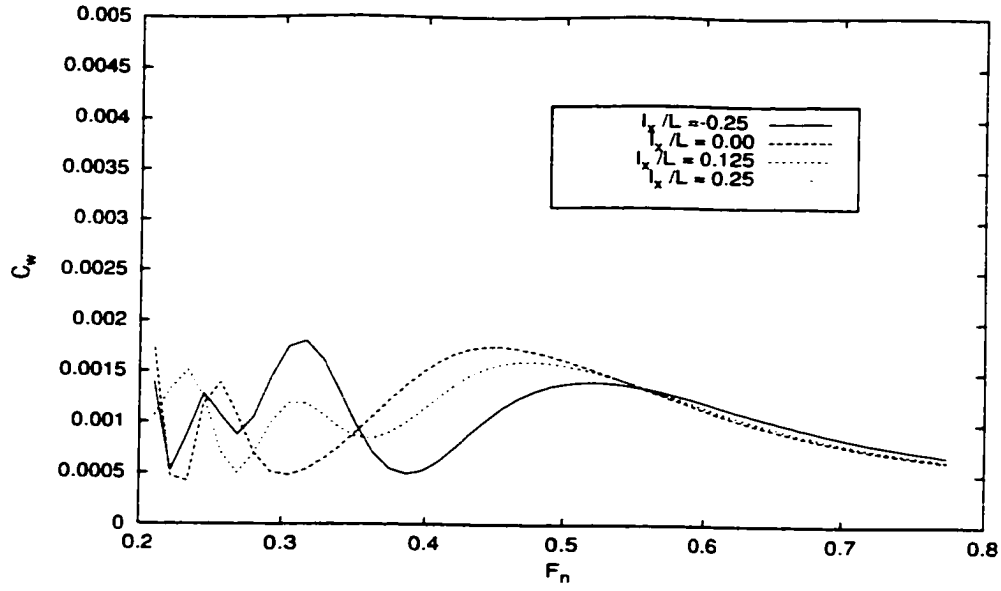

Figure 4.83: Effect of hull setback on wave resistance coefficient of the WCM trimaran($l_y/L = 0.20$).

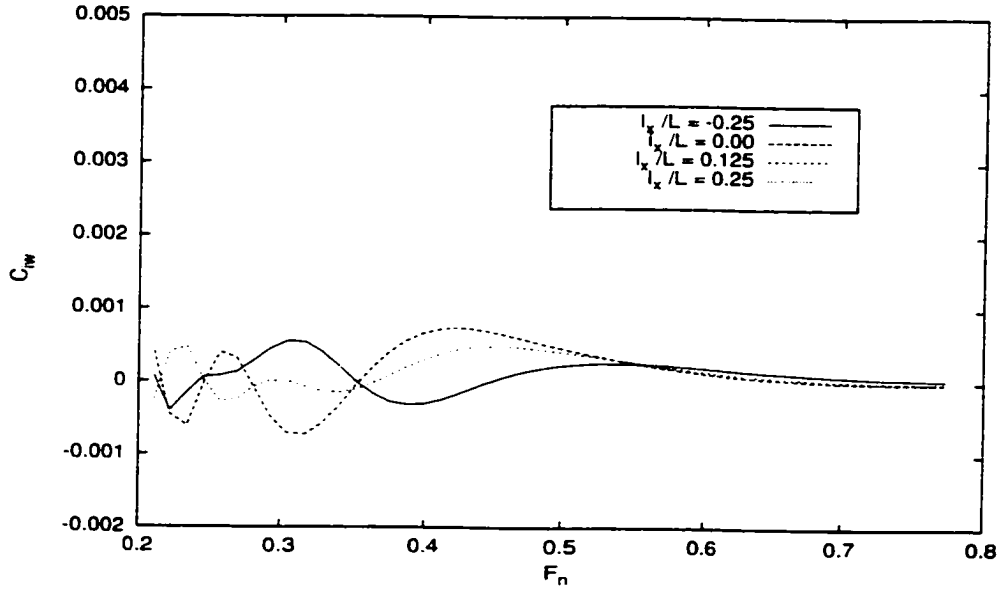

Figure 4.84: Computed wave interaction resistance coefficient of the WCM trimaran($l_y/L = 0.20$).

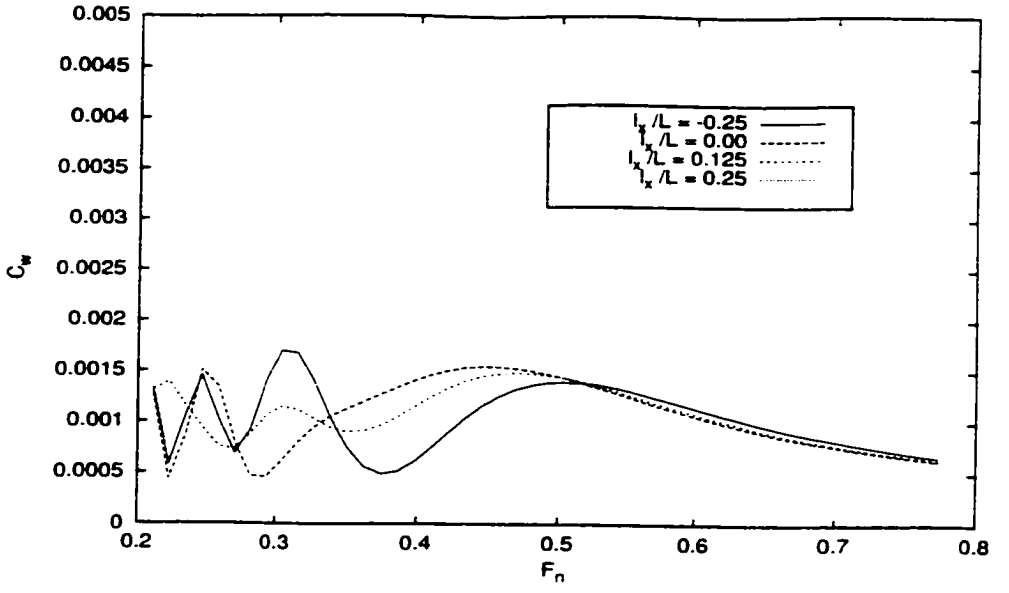

Figure 4.85: Effect of hull setback on wave resistance coefficient of the WCM trimaran($l_y/L = 0.25$).

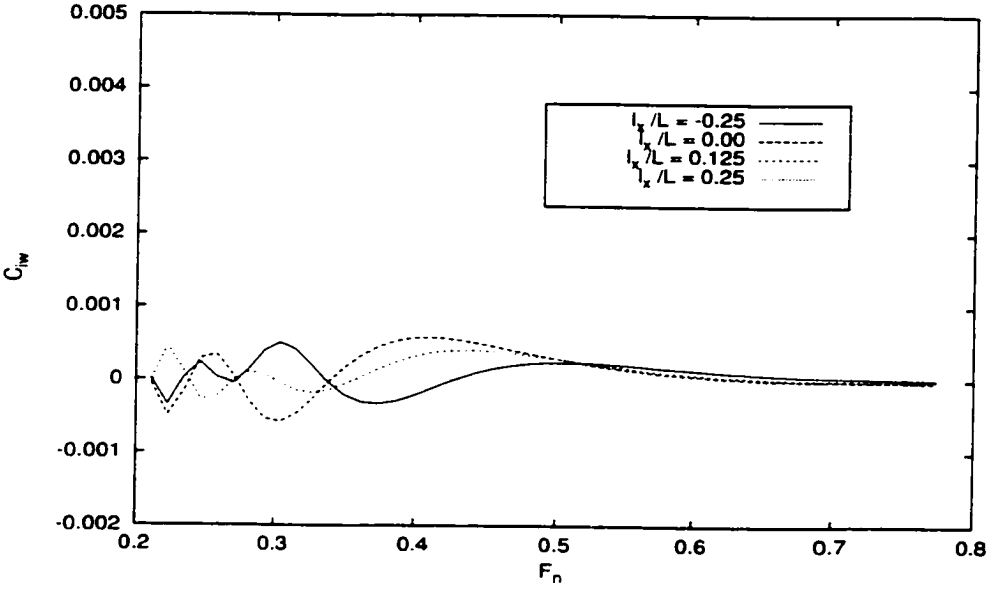

Figure 4.86: Computed wave interaction resistance coefficient of the WCM trimaran($l_y/L = 0.25$).

4.1.5 Quadrimaran Wave Resistance

After the computer program for computing wave resistance of a multihull ship has been fully validated, we have the confidence to study the performance of new types of multihull ships numerically by using our computer program. A right-hand Cartesian coordinated system, moving with the quadrimaran, a four-hull ship, has been assumed. The quadrimaran wave resistance based on thin ship theory with the coordinate system mentioned above is from the basic solution given by equation (2.25):

$$R_w = -16\pi\rho k_0^2 \int_0^{\frac{\pi}{2}} [P^2 + Q^2] \sec^3(\theta) d\theta \tag{4.23}$$

with $i = 1, 2, 3, 4$, for a quadrimaran, where

$$P = \sum_{i=1}^{4} (P_{i\sigma} - P_{i\mu}), \qquad Q = \sum_{i=1}^{4} (Q_{i\sigma} - Q_{i\mu}) \tag{4.24}$$

Three configarations of the quadrimaran of the Wigley form were investigated. All individual hull element had the same dimensions of $L/B = 10$ and $B/T = 1.6$ with $L = 10.0m$, $B = 1.0m$, $T = 0.625m$ again as the trimaran. The setback l_x is defined as the longitudinal distance between midsections of the central main hull and the outriggers, possitive for outriggers towards the stern; and the spacing l_y is defined as the lateral distance between the centerplane of the main hull and that of the outriggers. The three configurations are shown in Figure 4.87 to Figure 4.89. The arrangements for configurations are shown in Table 4.5.

The comparison of the wave resistance coefficients of three quadrimarans are shown

Table 4.5: Arrangements for the Wigley Quadrimaran

	Type A		Type B		Type C	
	$l_x(m)$	$l_y(m)$	$l_x(m)$	$l_y(m)$	$l_x(m)$	$l_y(m)$
*Hull*1	0.0	4.0	0.0	0.0	0.0	2.0
*Hull*2	0.0	-4.0	5.0	4.0	0.0	-2.0
*Hull*3	13.0	4.0	5.0	-4.0	5.0	6.0
*Hull*4	13.0	-4.0	15.0	0.0	5.0	- 6.0

in Figure 4.90. The wave interaction resistance coefficients for three quadrimarans are shown in Figure 4.91. The wave patterns were computed and the wave contours were plotted for three quadrimarans for $F_n = 0.35$ illustrated in Figure 4.92 to Figure 4.97. The maximum wave elevation range is [-0.223, 0.243] for Type A , [-0.354, 0.412] for Type B and [-0.286, 0.283] for Type C. The contour elevtions are $z = -0.2461$ to $z = 0.2144$ with an increments of 0.092.

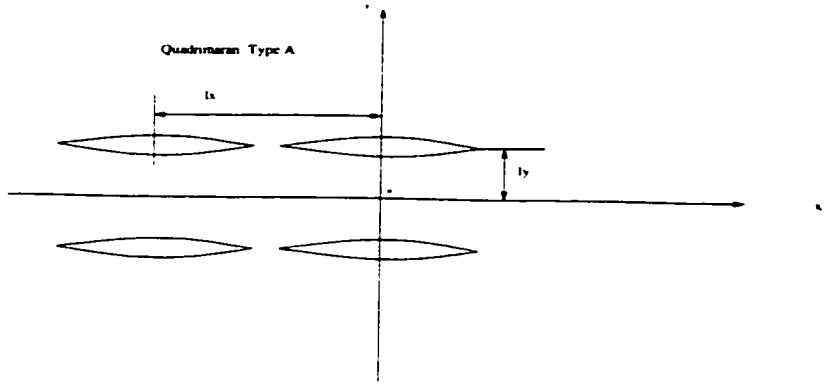

Figure 4.87: Wigley quadrimaran, Type A

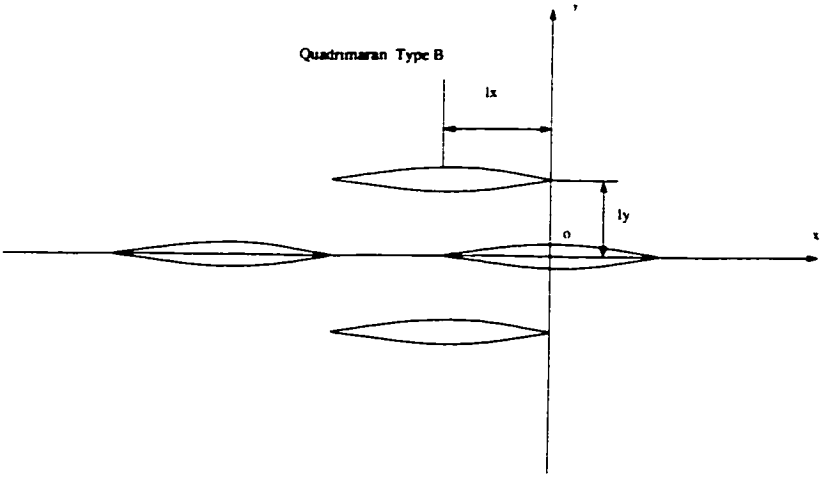

Figure 4.88: Wigley quadrimaran, Type B

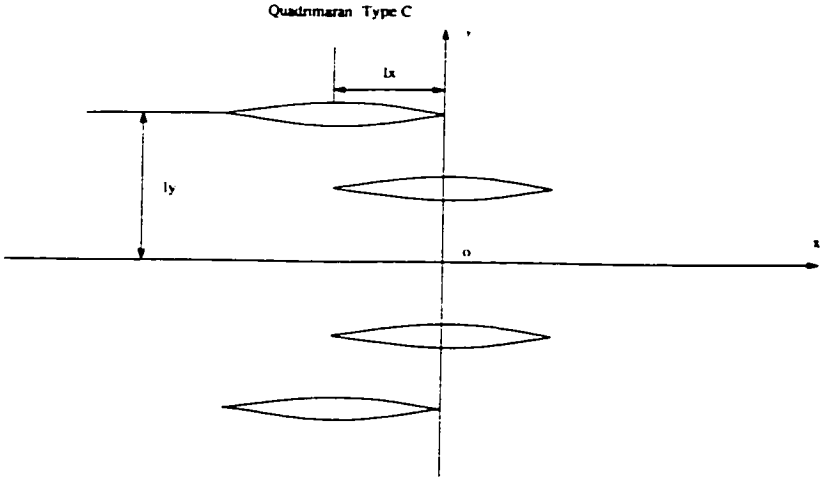

Figure 4.89: Wigley quadrimaran, Type C

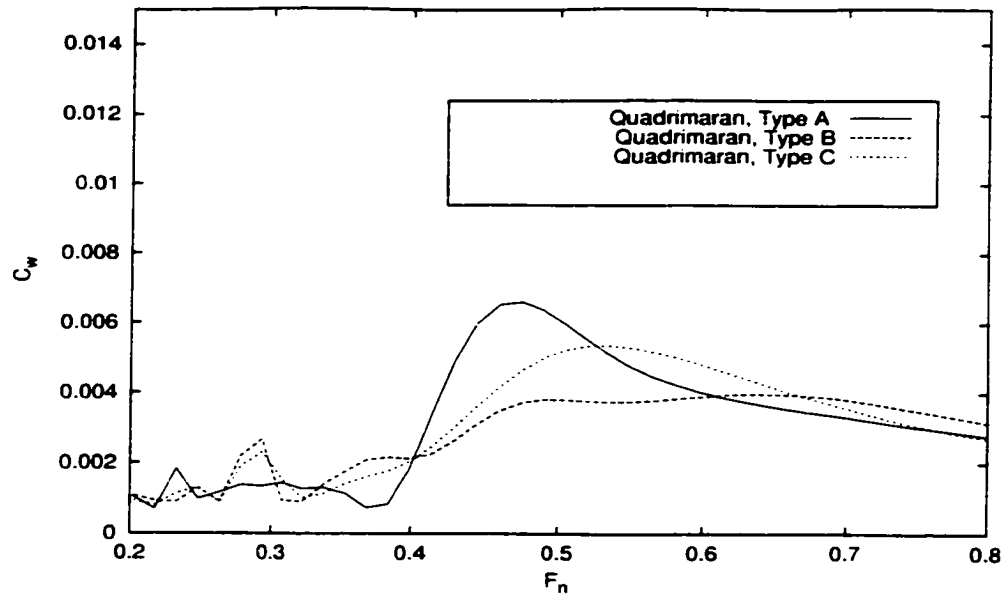

Figure 4.90: Comparison of computed wave resistance coefficients for three quadrimarans

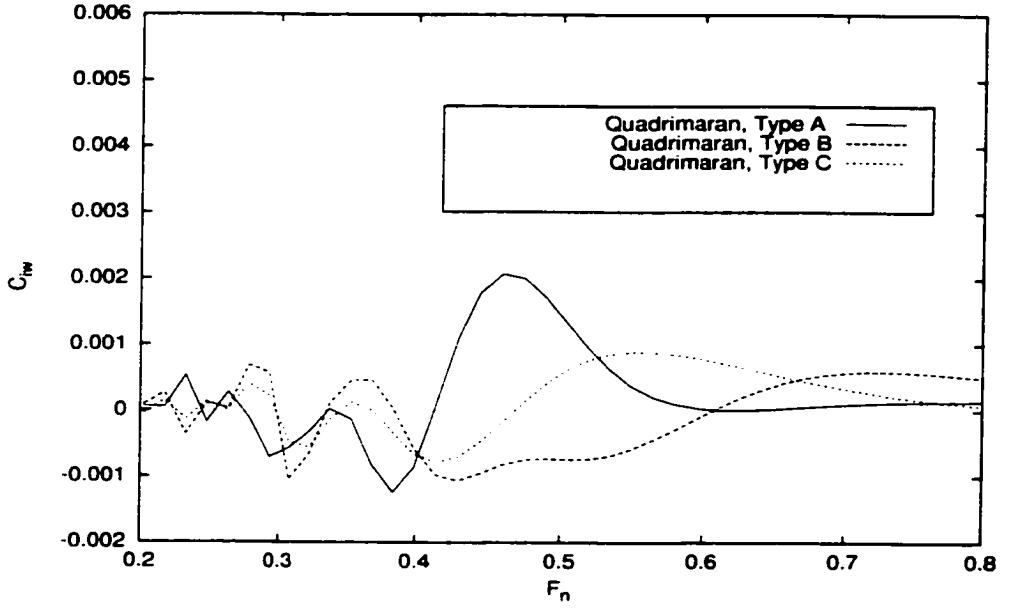

Figure 4.91: Comparison of computed wave interaction coefficients for three quadrimarans

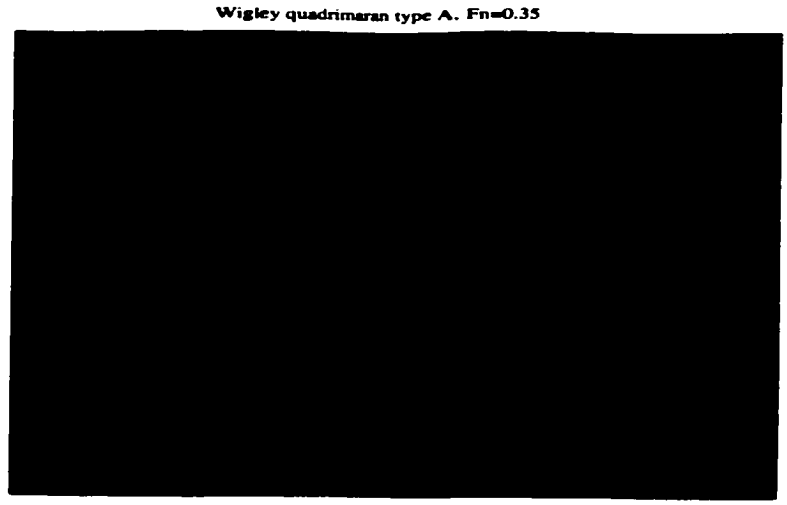

Figure 4.92: Wave pattern generated by the Wigley quadrimaran. Type A

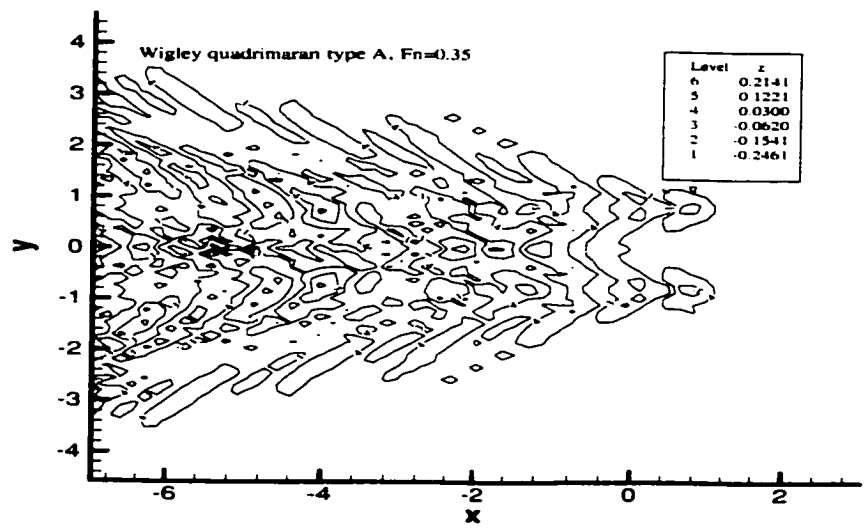

Figure 4.93: Wave contours generated by the Wigley quadrimaran. Type A

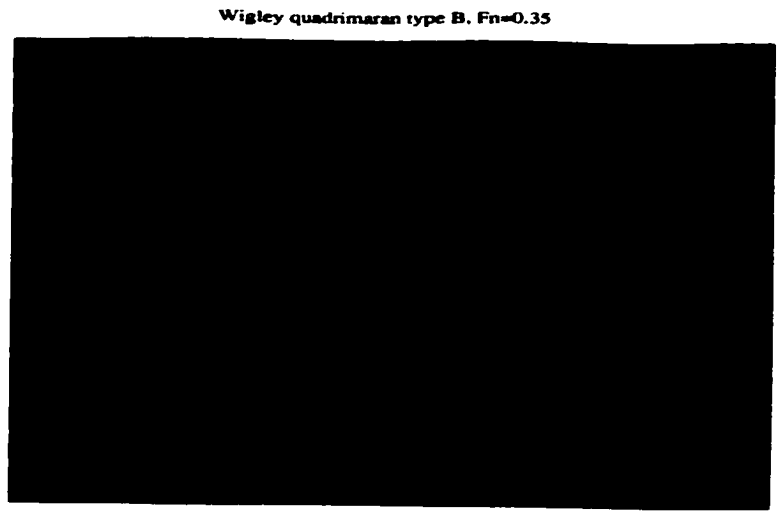

Figure 4.94: Wave pattern generated by the Wigley quadrimaran, Type B

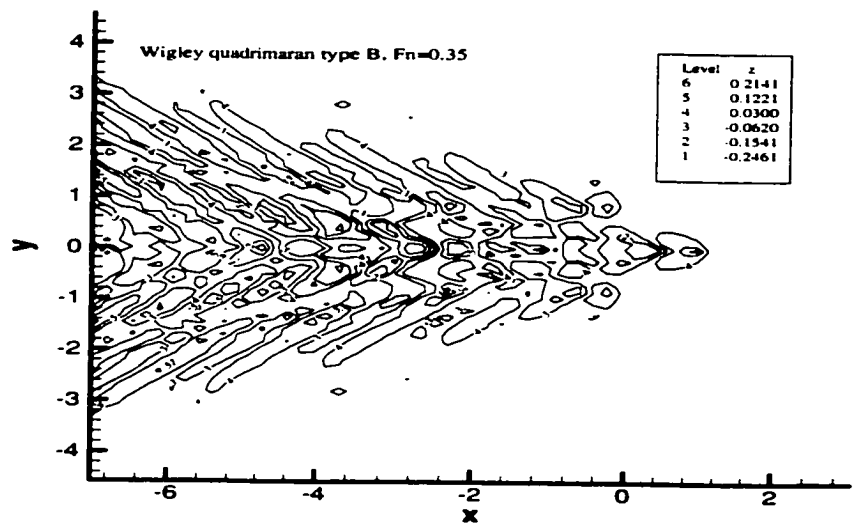

Figure 4.95: Wave contours generated by the Wigley quadrimaran, Type B

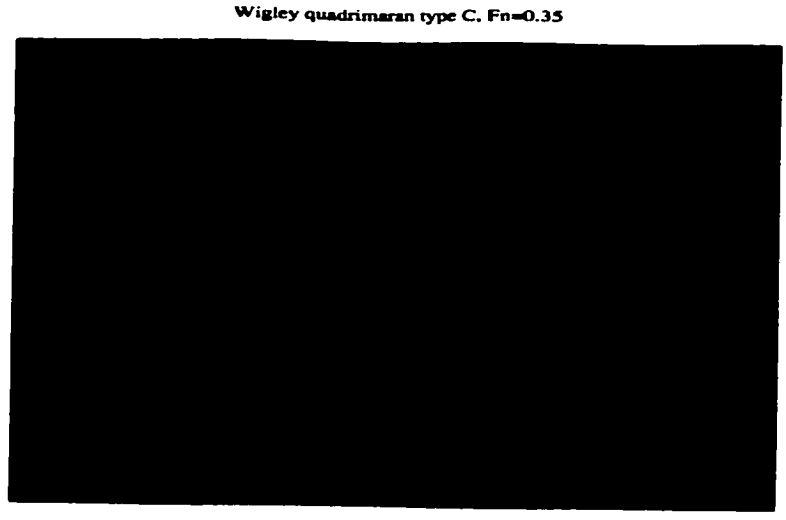

Figure 4.96: Wave pattern generated by the Wigley quadrimaran, Type C

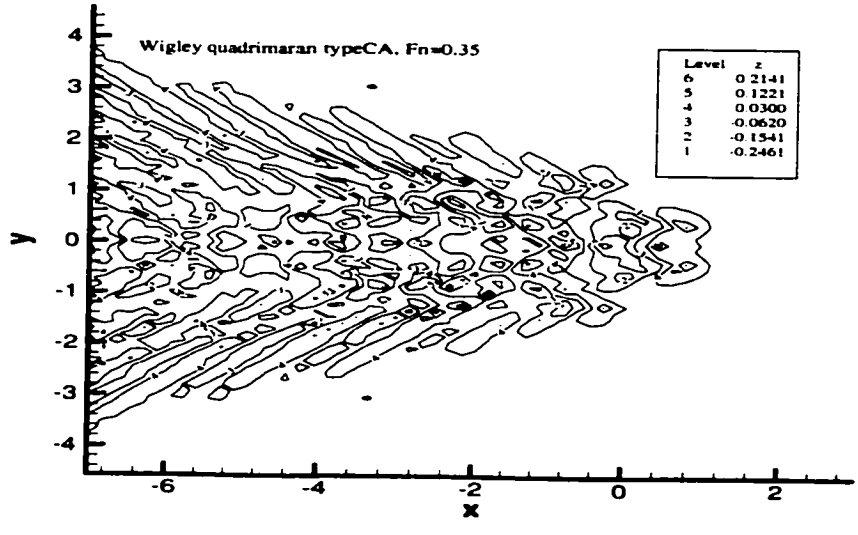

Figure 4.97: Wave contours generated by the Wigley quadrimaran, Type C

4.1.6 Pentamaran Wave Resistance

For further study, the pentamaran, a five-hull ship,was investigated. The same right-hand Cartesian coordinated system moving with the pentamaran has been assumed. The pentamaran wave resistance based on thin ship theory with the coordinate system mentioned above is also from the basic solution given by equation (2.25):

$$R_w = -16\pi\rho k_0^2 \int_0^{\frac{\pi}{2}} [P^2 + Q^2] \sec^3(\theta) d\theta \tag{4.25}$$

with $i = 1, 2, 3, 4, 5$, for a pentamaran,where

$$P = \sum_{i=1}^{5} (P_{i\sigma} - P_{i\mu}), \qquad Q = \sum_{i=1}^{5} (Q_{i\sigma} - Q_{i\mu}) \tag{4.26}$$

Two configarations of pentamarans of the Wigley form were investigated. All hull elements had the same dimensions as the hull elements of quadrimaran. They are shown in Figure 4.98 and Figure 4.99. The arrangements for the pentamaran are shown in Table 4.6.

The comparison of the wave resistance coefficients of two pentamarans are given in Figure 4.100. The wave interaction resistance coefficients of two pentamarans are given in Figure 4.101. The wave patterns and contours were computed for two pentamaran and given in Figure 4.102 to Figure 4.105 for $F_n = 0.35$. The maximum wave elevation range is [-0.323, 0.341] for Type A and [-0.223, 0.271] for Type B. The

Table 4.6: Arrangements for the Wigley Pentamaran

	Type A		Type B	
	$l_x(m)$	$l_y(m)$	$l_x(m)$	$l_y(m)$
$Hull1$	0.0	0.0	0.0	2.0
$Hull2$	5.0	4.0	0.0	-2.0
$Hull3$	5.0	-4.0	5.0	8.0
$Hull4$	5.0	8.0	5.0	-8.0
$Hull5$	5.0	-8.0	5.0	0.0

contour elevations are $z = -0.2461$ to $z = 0.2144$ with an increments of 0.092.

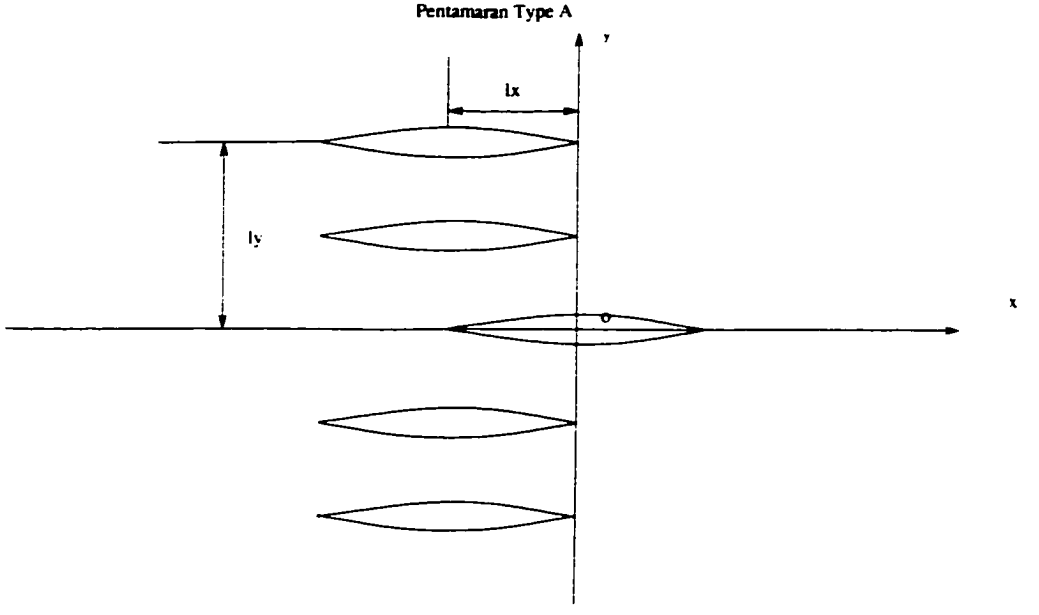

Figure 4.98: Wigley pentamaran, Type A

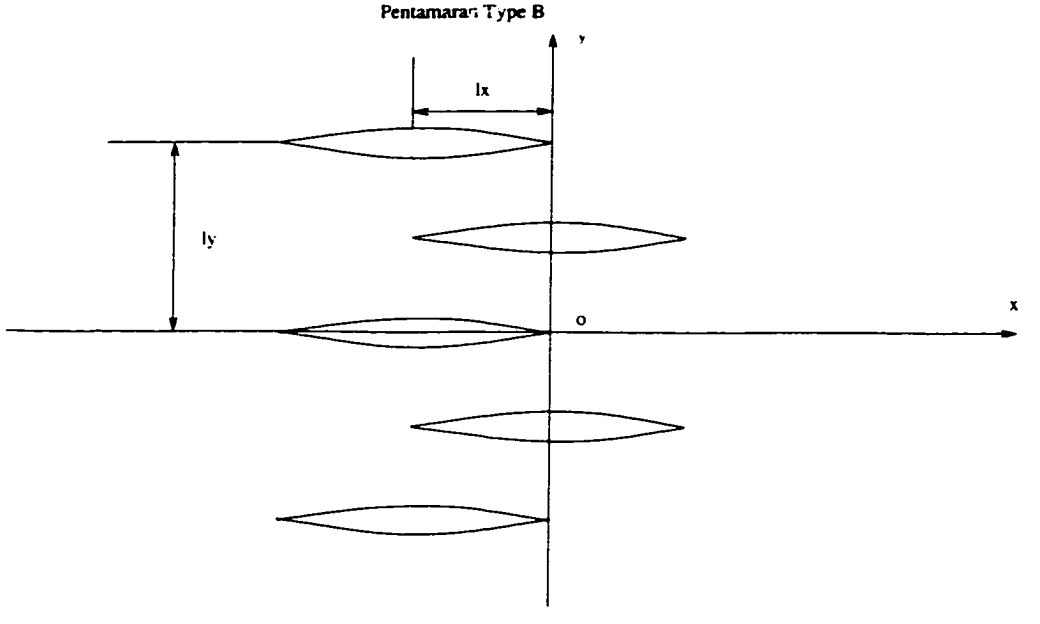

Figure 4.99: Wigley pentamaran, Type B

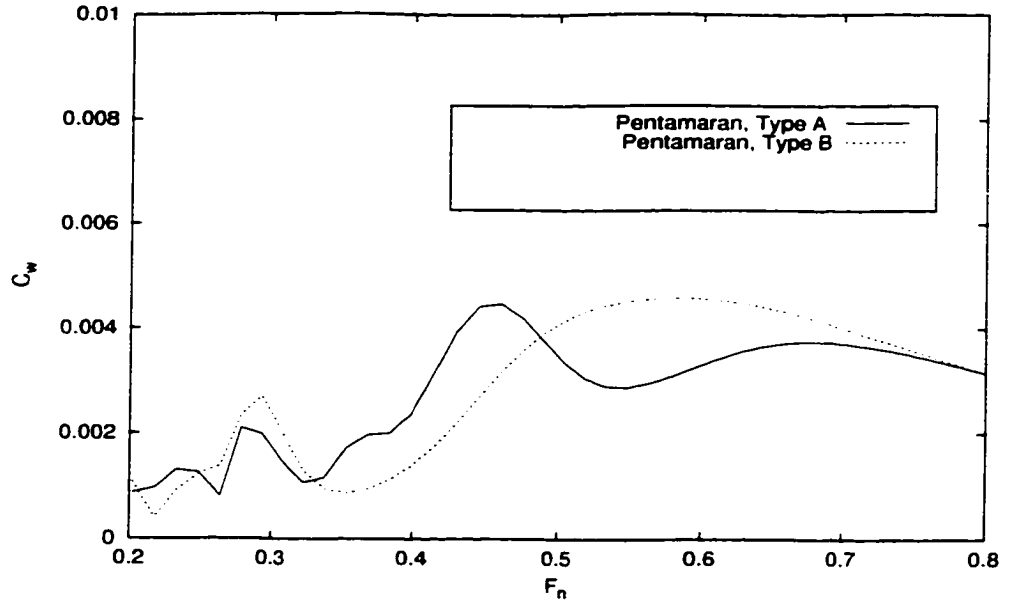

Figure 4.100: Comparison of computed wave resistance coefficients for two pentamarans

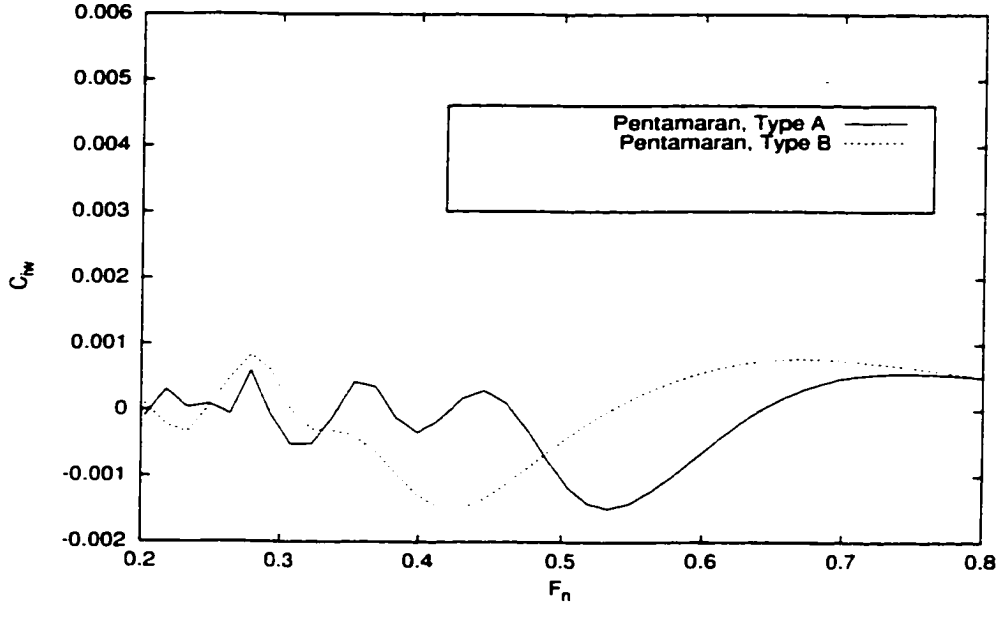

Figure 4.101: Comparison of computed wave interaction coefficients for two pentamarans

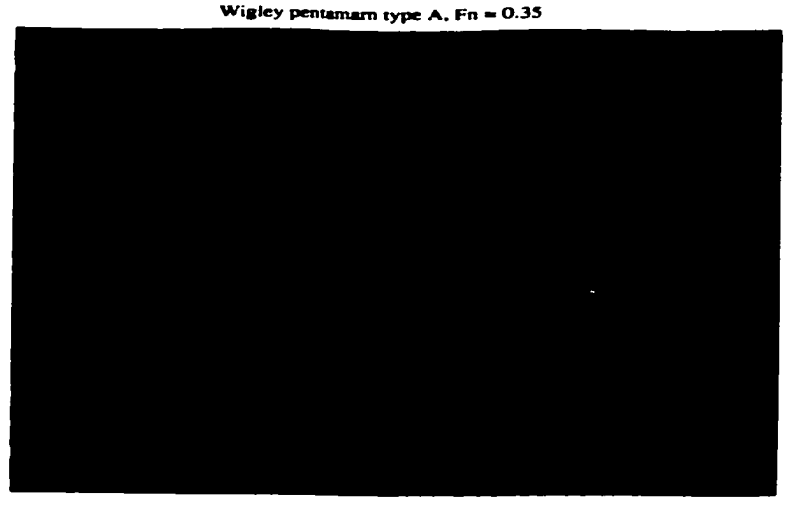

Figure 4.102: Wave pattern generated by the Wigley pentamaran, Type A

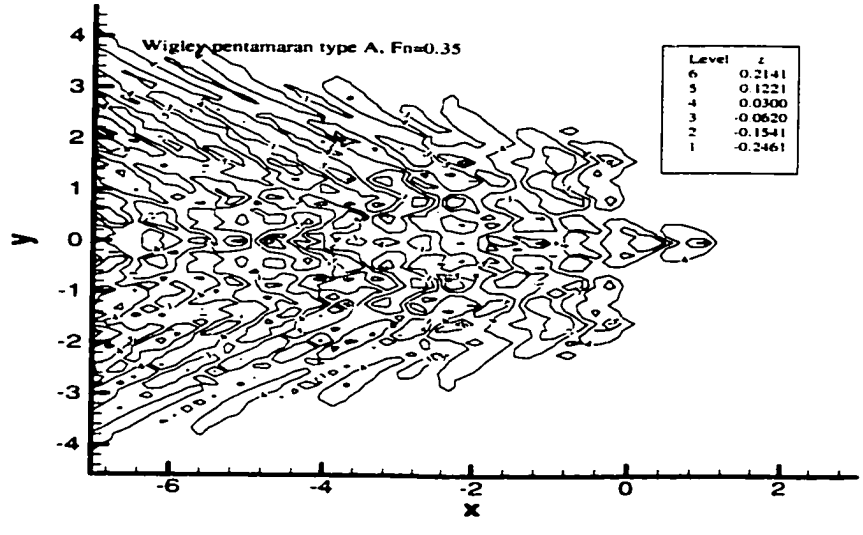

Figure 4.103: Wave contours generated by the Wigley pentamaran, Type A

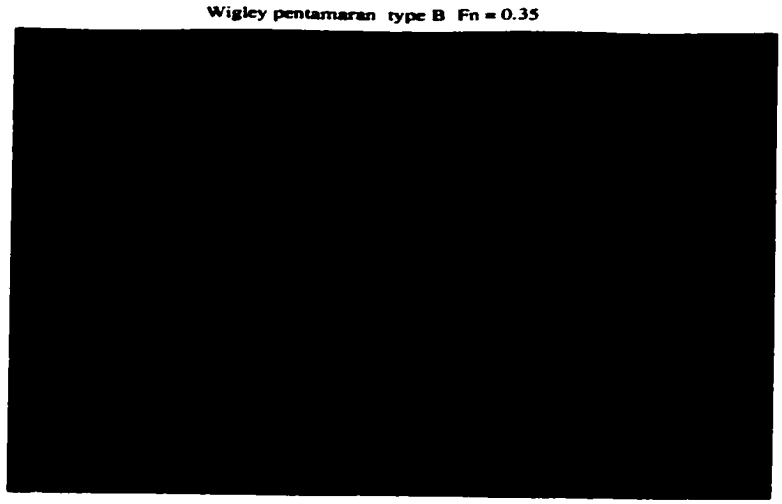

Figure 4.104: Wave pattern generated by the Wigley pentamaran, Type B

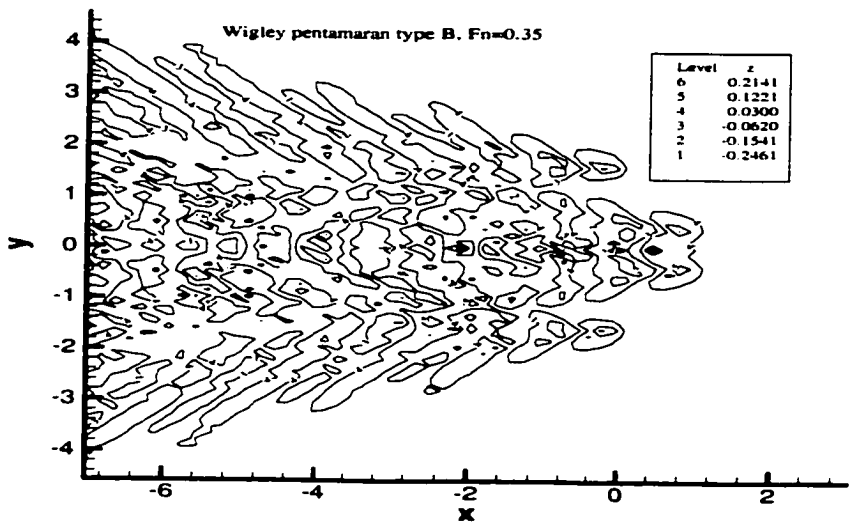

Figure 4.105: Wave contours generated by the Wigley pentamaran, Type B

4.2 Computation of Catamaran Motion in the Time Domain

Based on the theory discussed in Chapter 3, a computer program using the three-dimensional panel methods (see Figure 4.106) was developed (Peng, et al., 2000) for computing catamaran motion in waves in time domain. In order to validate the program, an effort was made to compare the computed motions of a Wigley catamaran with the experimental results from Siregar, (1995) and van't Veer and Siregar, (1995).

The coordinate systems were shown in Figure 3.1 in Chapter 3. The Wigley hull for motion computations is described by the following mathematical form:

$$y = \frac{B}{2}(1-\xi^2)(1-\zeta^2)(1+\frac{1}{5}\eta^2) + \xi^2(1-\xi^8)(1-\zeta^2)^4 \tag{4.27}$$

where

$$\xi = \frac{x}{L/2} \in [-1, 1] \tag{4.28}$$

$$\zeta = \frac{z}{T} \in [-1, 0] \tag{4.29}$$

The principal dimensions of the Wigley model are listed below:

Length, L(m)	2.5 m
Beam, B(m)	0.357 m
Draught, T(m)	0.139m

Volume, $\nabla(m^3)$	0.06953 m^3

Three hull spacing ratios were considered with $2l_y/B = 1.04$. 2.10 and 3.14. The hull spacing $2l_y$ is defined as the lateral distance between the center-planes of demihulls at the design waterline. For three hull spacings, computations were carried out for the model at three forward speeds, $F_n = 0.15$, 0.30, and 0.45, in head seas. The wave frequencies were determined from experimental data (Siregar, 1995).

The computed heave, x_3, and pitch, x_5, were plotted in Figure 4.107 and Figure 4.112, respectively. The heave and pitch are nondimensionalized as $x_3' = x_3/\xi_a$ and $x_5' = x_5/(k\xi_a)$, respectively, where ξ_a is the amplitude of incident wave and k is the wave number. The computed motions were compared with experimental data by van't Veer and Siregar (1995).

Typical motion curves and response functions can be found in Figure 4.113 through Figure 4.118. The formulation of response function can be found in Qiu, et al. 2001.

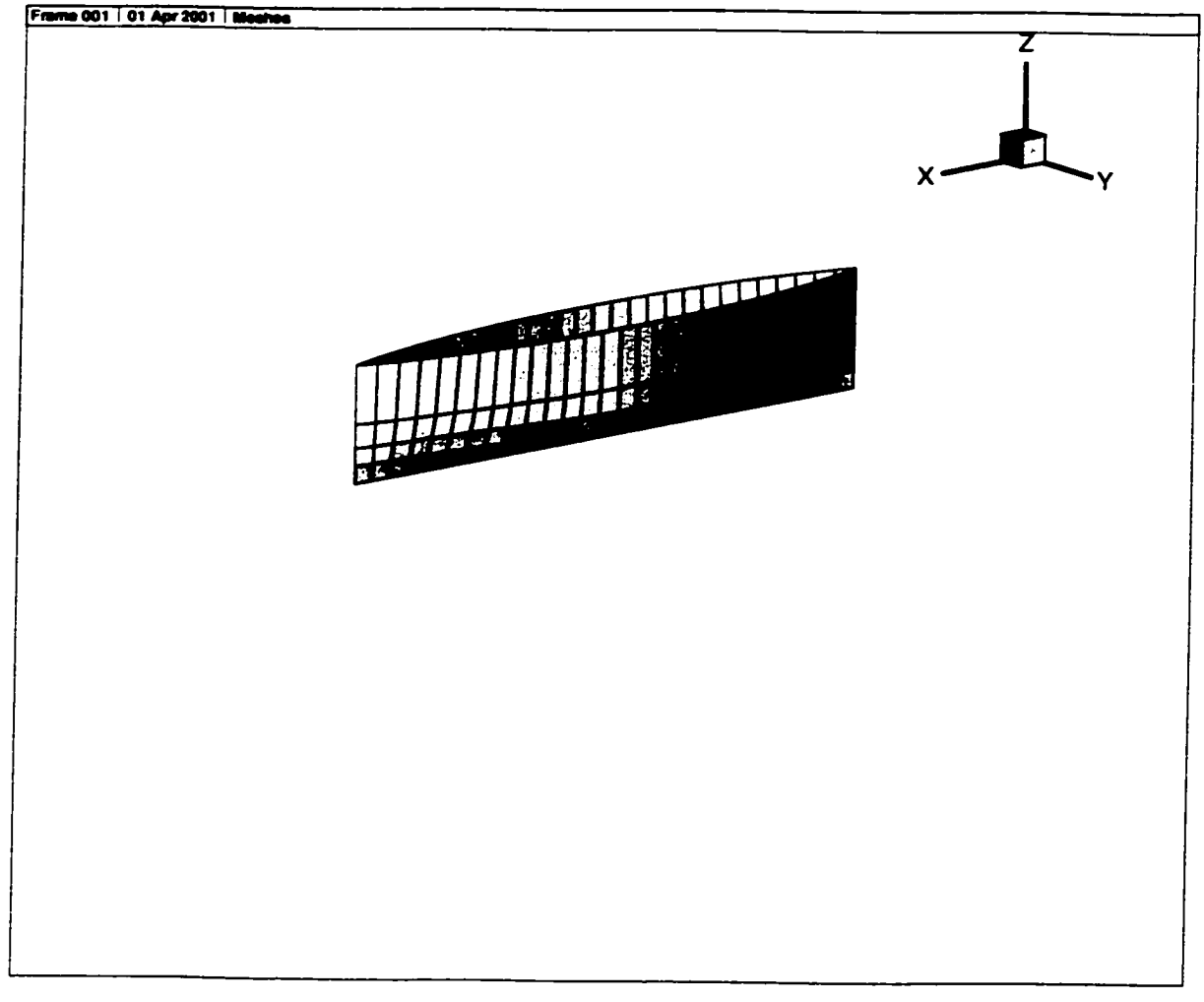

Figure 4.106: Panelization of Wigley Catamaran

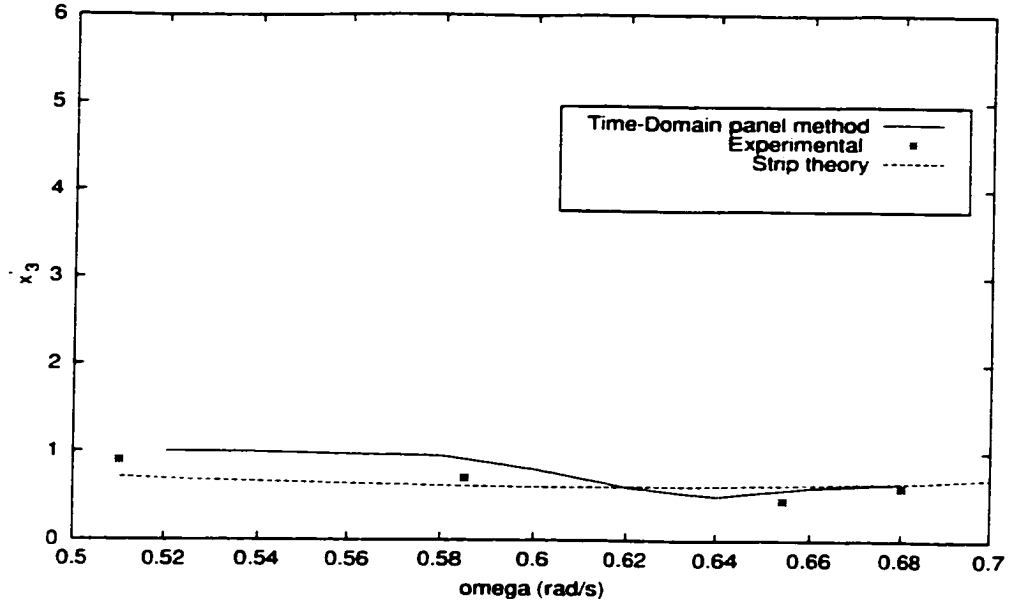

Figure 4.107: Computed heave for $F_n = 0.15, 2l_y/B = 1.04$

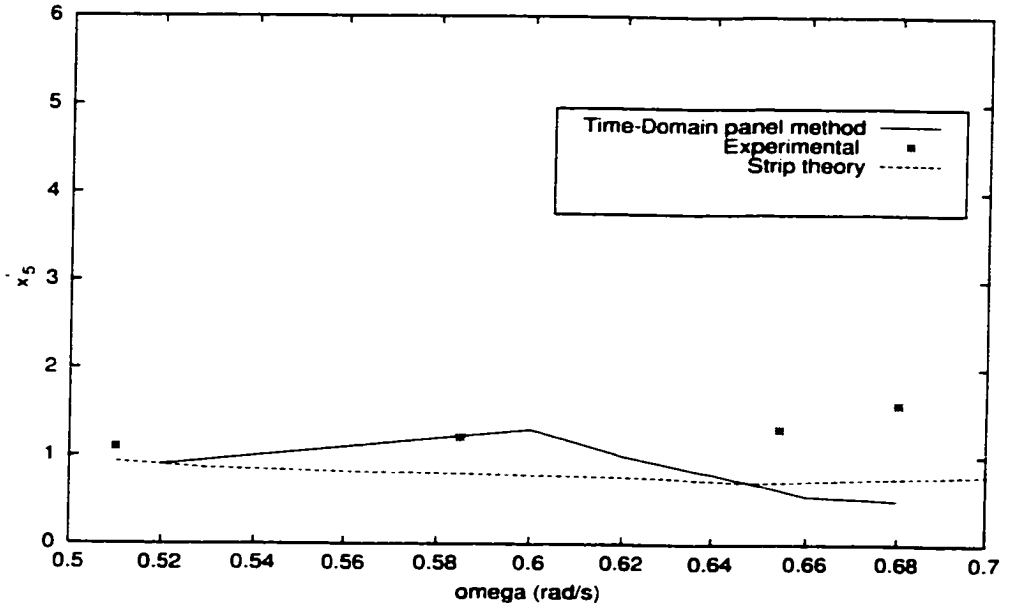

Figure 4.108: Computed pitch for $F_n = 0.15, 2l_y/B = 1.04$

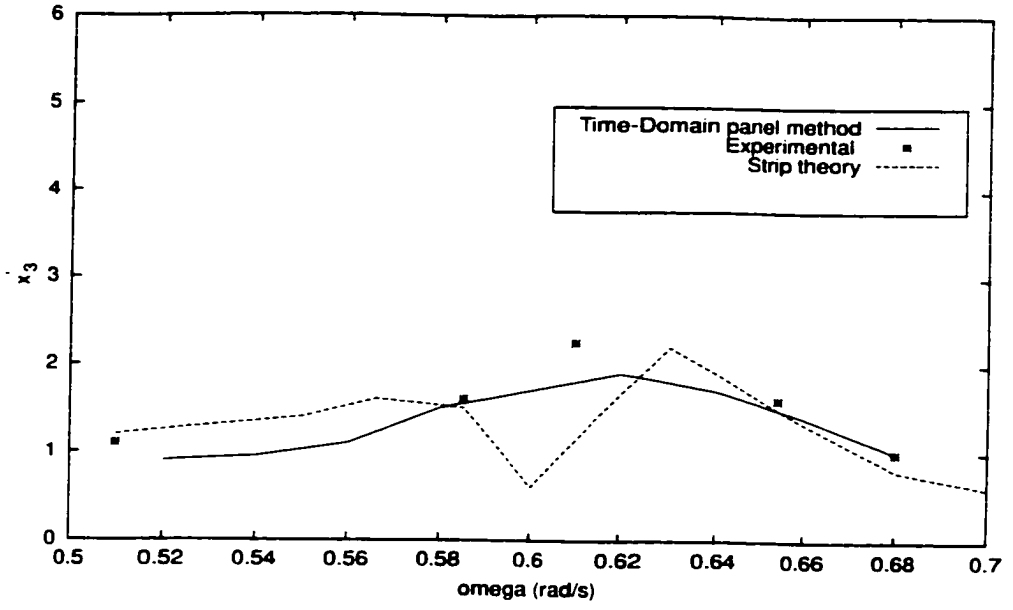

Figure 4.109: Computed heave for $F_n = 0.30, 2l_y/B = 2.10$

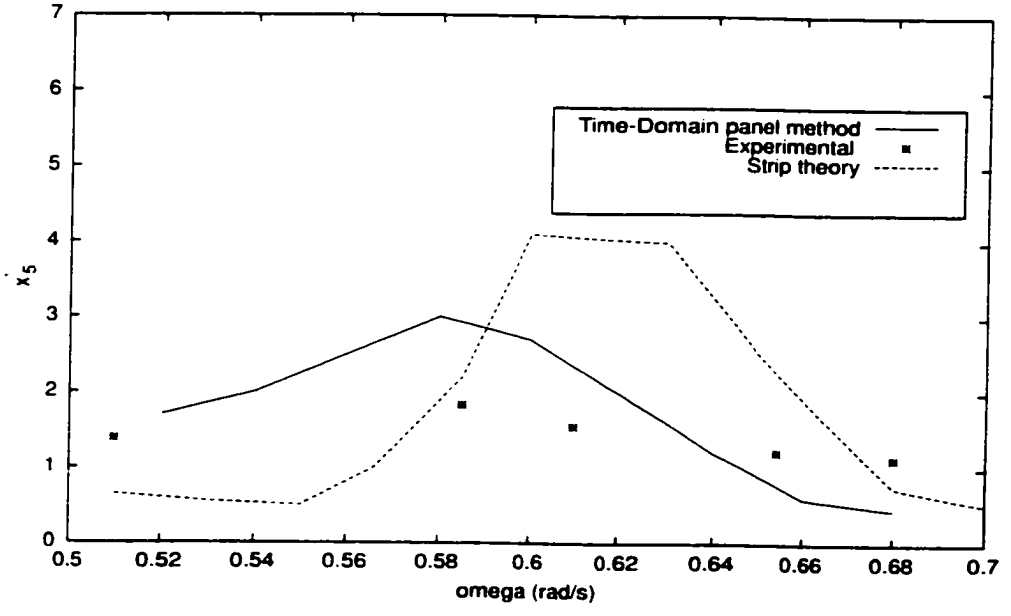

Figure 4.110: Computed pitch for $F_n = 0.30, 2l_y/B = 2.10$

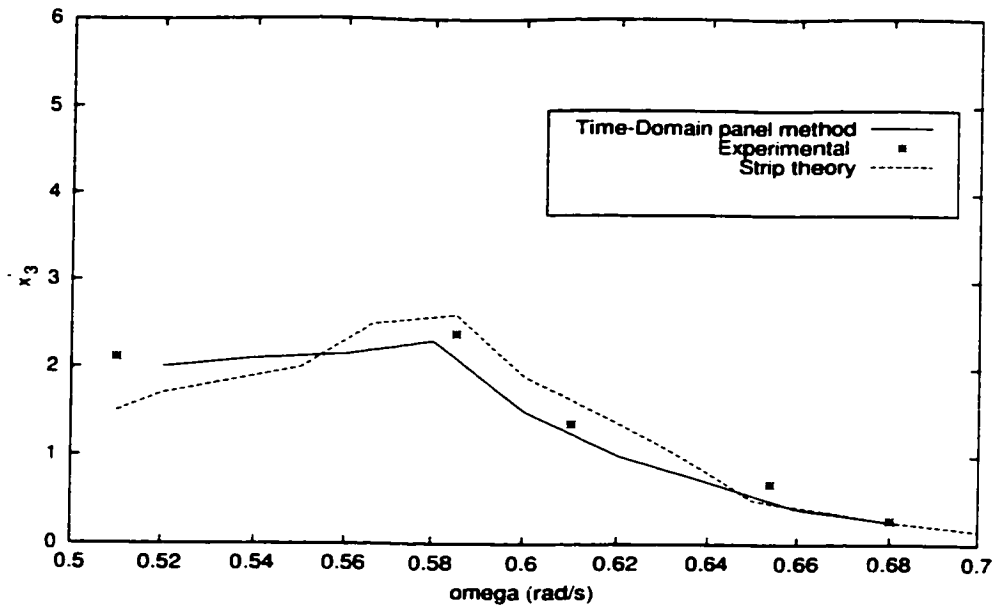

Figure 4.111: Computed heave for $F_n = 0.45, 2l_y/B = 3.14$

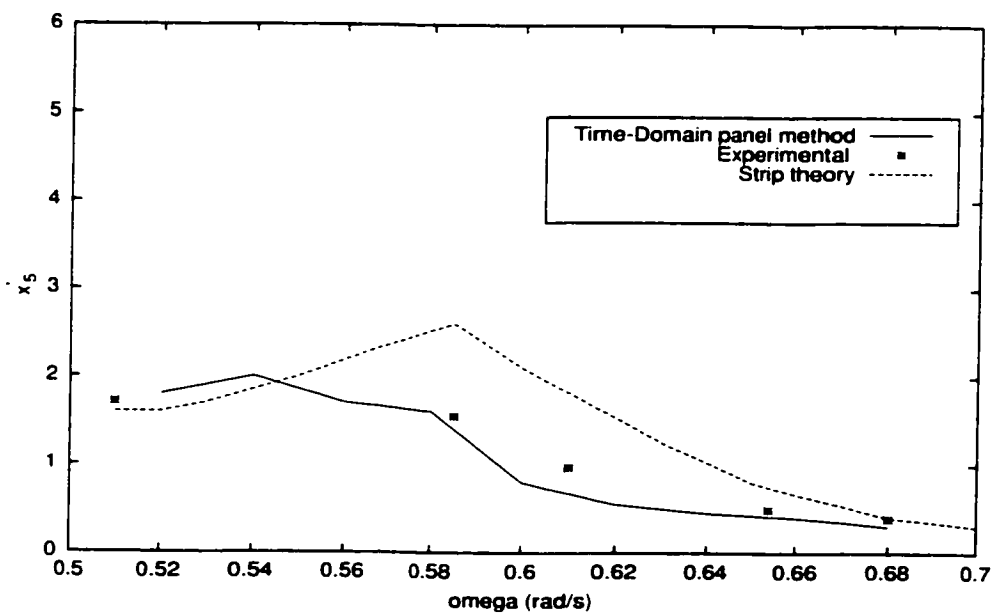

Figure 4.112: Computed pitch for $F_n = 0.45, 2l_y/B = 3.14$

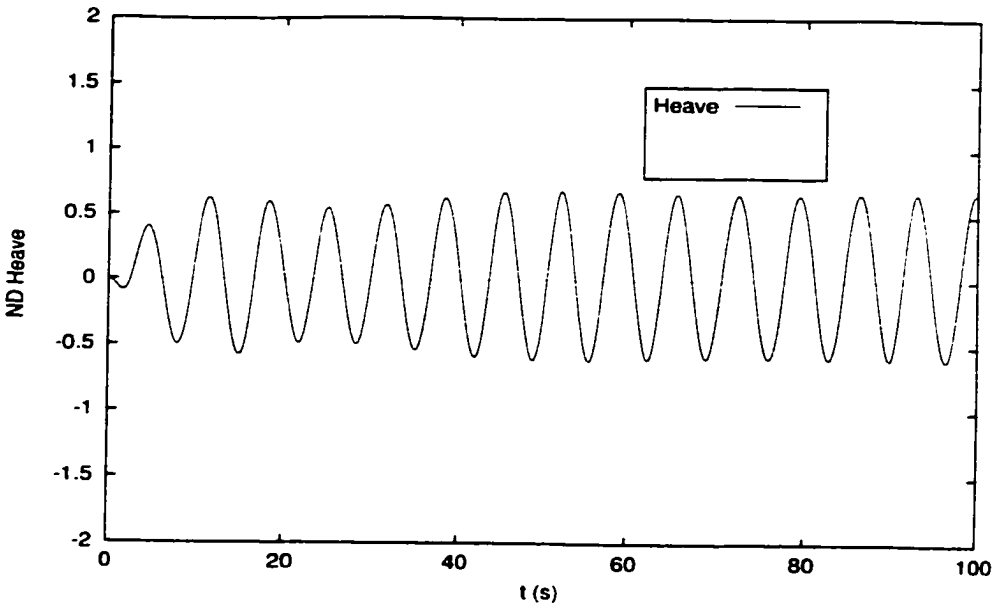

Figure 4.113: Computed heave history for $F_n = 0.15, 2l_y/B = 1.04$

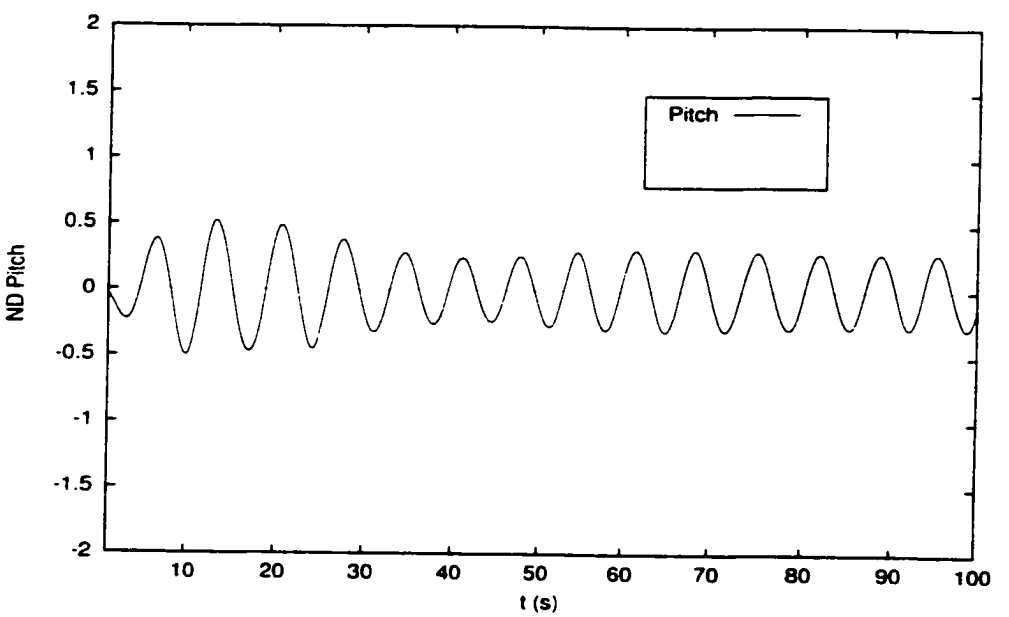

Figure 4.114: Computed pitch history for $F_n = 0.15, 2l_y/B = 1.04$

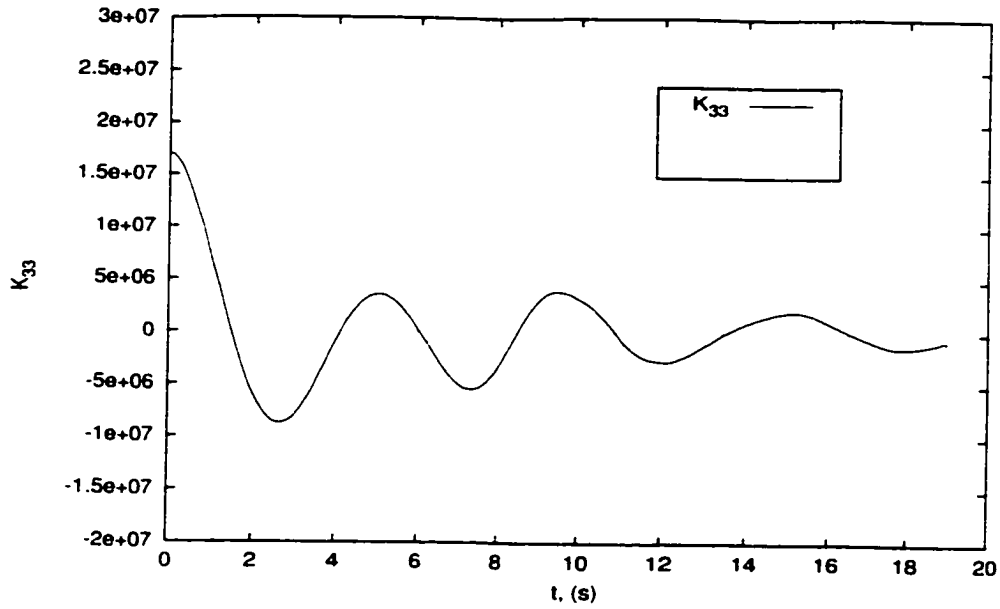

Figure 4.115: Response function of K33, $F_n = 0.15. 2l_y/B = 1.04$

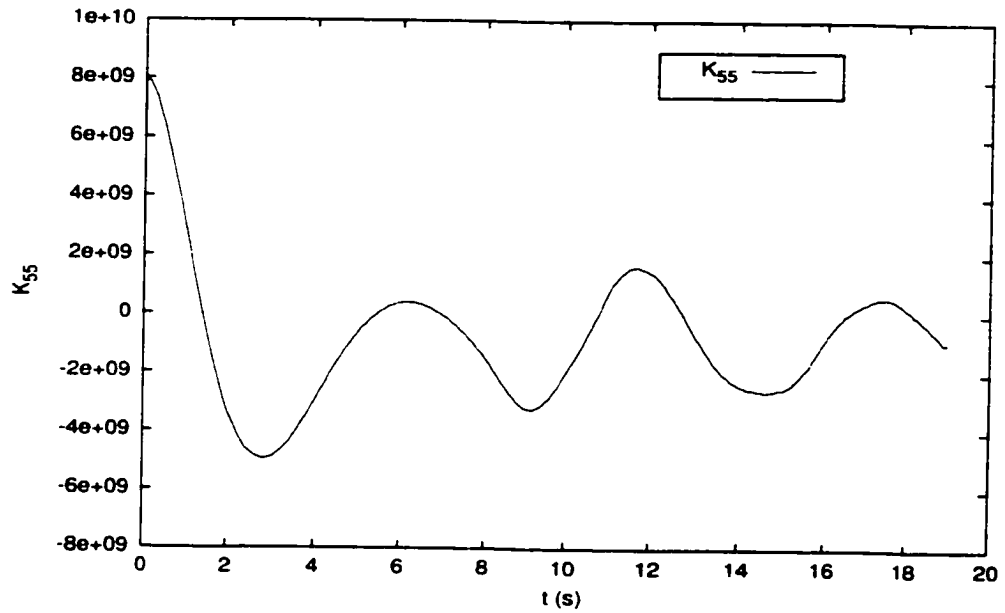

Figure 4.116: Response function of K55, $F_n = 0.15, 2l_y/B = 1.04$

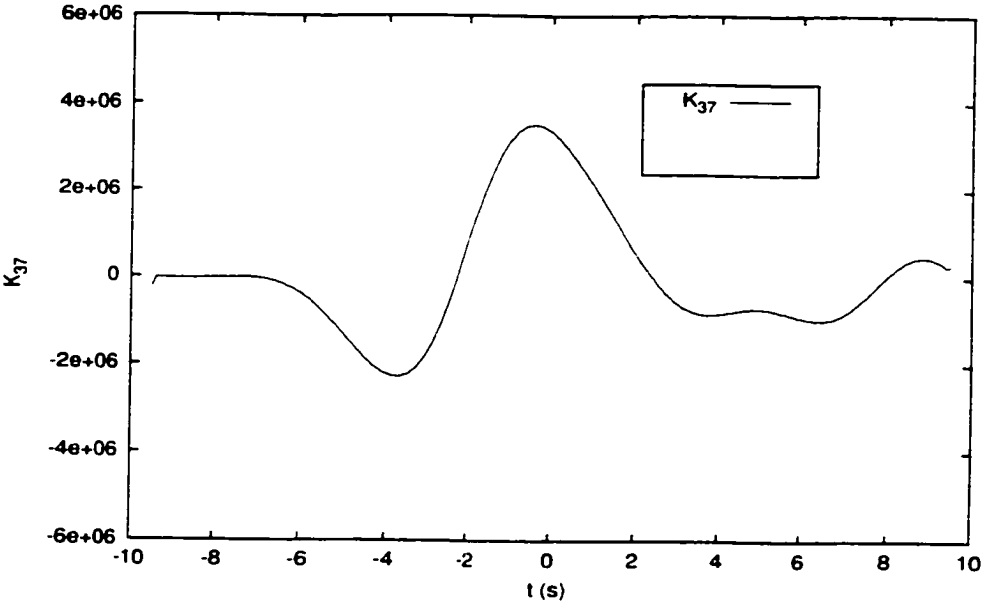

Figure 4.117: Response function of K37, $F_n = 0.15, 2l_y/B = 1.04$

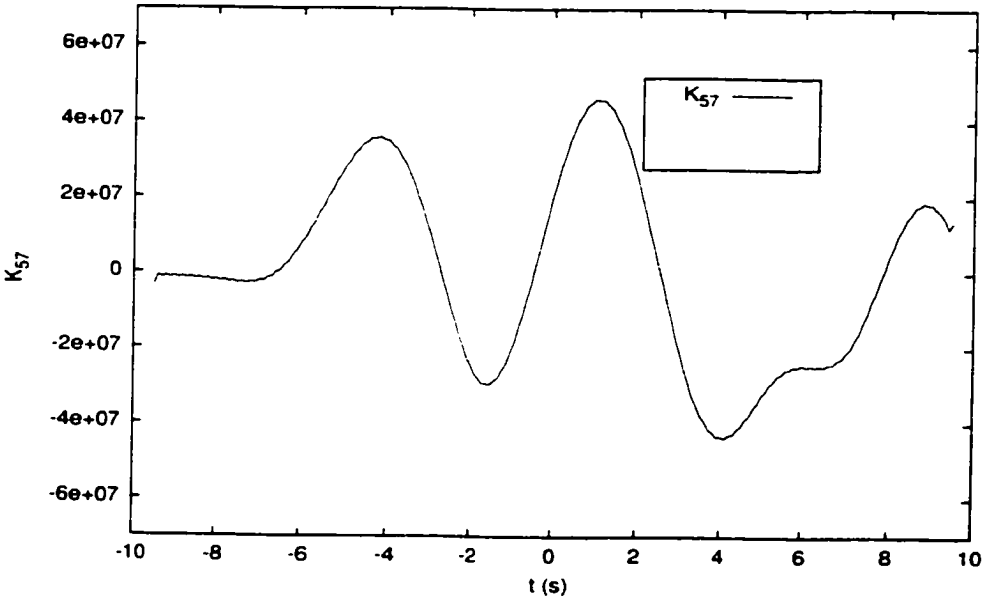

Figure 4.118: Response function of K57, $F_n = 0.15, 2l_y/B = 1.04$

Chapter 5

Concluding Remarks and Recommendations

This thesis investigates two aspects of the hydrodynamics of multi-hull ships, namely wave resistance and motion in waves. Conclusions and recommendations for the current work are presented in separated sections below.

5.1 Wave Resistance and Wave Pattern of Multi-Hull Ships

Numerical investigations have been carried out to explore the multi-hull ship wave resistance and the effect of wave interference between the hulls. Based on the linear theory of wave resistance and the thin ship assumption, a computer program has

been developed for these investigations. The hulls assumed to be of arbitrary forms with various arrangement configurations and the corresponding wave patterns were computed and respective wave contours were plotted. The hull numbers can be arbitrary. By using the tent function, the hull form can be easily expressed by the hull offset. Two types of catamaran and three types of trimaran were chosen for the validation work involving comparisons with available published information and experimental data. The computed wave resistance coefficients were observed in good agreement with the experimental data, especially in high speed range. It is interesting that second hump matches experimental results for most trimaran cases, but it is well-known that in a monohull case this hump produced by the thin-ship theory doesn't match experimental results. It shows that the thin ship theory is applicable for multihulls for wave resistance computation and also demonstrating the effectiveness of the tent function implementation. The properties of wave-making resistance of high-speed multi-hull ships can be studied by the present program if the hull element has sufficiently small beam/length ratio.

As noted earlier, two groups of wave systems are created by a moving ship: the diverging waves spreading out from the ship's centerline and the transverse waves perpendicular to the ship's centerline. Since the energy is expended in the formation of these waves as a ship advances through the calm water, these waves account for the wave resistance portion of the total resistance. Comparison of computed wave patterns with experimental ones offers a qualitative method of assessing accuracy of wave resistance computation. A program was developed to enable these computation to be performed. The numerical results and experimental data were observed to be in reasonably good agreement except for the area near the bow and the stern where

the linear theory may not be applied. Following validation of the computer program, the wave pattern could be used to study the wave interaction effect of hull elements.

The validated software tool for wave resistance computation and wave pattern visualization were the approach to study the wave interference phenomenon of multi-hull ships. One of the main objectives of this study was to identify how multihull ship configuration details influence ship wave resistance. Configuration details include variations of hull camber, spacing and setback. From the analysis it is concluded that:

1. Although one catamaran was studied, it was found the spacing effect was greater than the camber effect.

2. It could be concluded that the trimaran performance strongly depended on the outriggers longitudinal position, but was not sensitive to the spacing. It is possible to reduce significantly the wave-making resistance by realizing favorable wave interference of hull wave systems. Optimum trimaran configurations are able to achieve a reduction of almost 50% wave resistance with respect to the worst condition of outrigger position for certain speeds. At very high F_n, for more than 0.6, the wave interaction starts to reduce to zero. Thus the resistance reduction of multihull ships depends very much on the hull element arrangement. Normally, the trimaran with outriggers aligned with the stern would produce smaller wave resistance coefficient than that with the outrigger aligned with the middle of the hull, for F_n= 0.35 to 0.55. For F_n= 0.25 to 0.35, the optimum outrigger position is aligned with the middle of the main hull. For trimarans, the negative interaction wave resistance occurred only in the range

of $F_n = 0.25$ to 0.45.

3. The ship hull-form effect on wave resistance was investigated in this thesis. In Figure 5.1, the wave resistance coefficients of different ship forms are illustrated. We found that the WCM trimaran was the best ship form. Comparing the Wigley trimaran, Wigley quadrimaran and Wigley pentamaran, we found that at $F_n = 0.5$ to 0.6, the pentamaran A is the best. If F_n was greater than 0.6, Wigley trimaran is the best. Generally speaking, the Wigley quadrimaran is the best form. However, if F_n is greater than 0.6, trimaran becomes the best.

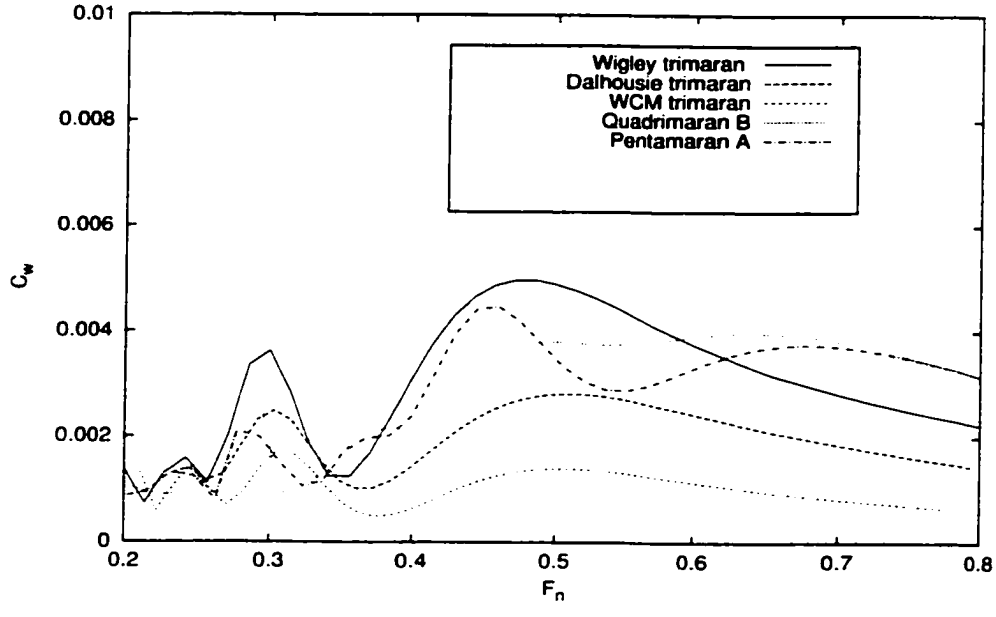

Figure 5.1: Comparison of computed wave resistance coefficient for different type multihull

4. For quadrimarans and pentamarans, the negative wave interaction resistance range would be increased to $F_n = 0.6$ and above (see Figure 4.91 and Figure 4.101). This would provide more choices for the multihull ship design.

The wave patterns and wave contours are useful tools for analysis. Further work should include the investigation of the rate of decay of the waves generated by high-speed multihull ships. Based on the program developed in this thesis, some fundamental parameters affect the wave decay, such as length of the vessel and the choice between the monohull and multihull or the type of the multihull, will be studied. At present, the wave resistance and wave patterns were computed based on the linear theory. Large and breaking bow and stern waves should be other topics to be studied in the future.

5.2 Multi-hull Ship Motion in Waves

A panel method has been developed for computing multihull motions in wave in the time domain . With the non-impulse response functions, the integral differential equations of motions were solved in terms of the time-domain Green function to compute multihull motions with forward speed. This method is not limited for catamaran motion computation. By this method, the numerical difficulties from the Fourier transform method could be avoided and the wave interaction between each hull was automatically considered. Nonlinear effects of the catamaran motions in large amplitude waves are considered in the Froude-Krylov forces. The linear assumption is applied to the forces due to the radiated and diffracted waves.

The computed heave and pitch motions were compared with experimental data and results from a strip-theory program (van't Veer and Siregar, 1995). In the case of $F_n = 0.30$ and $2l_y/B = 2.10$, the computed heave and pitch are presented in Figure

4.107 and Figure 4.108. The predicted heave values show a reasonable agreement with the experimental results. However, it seemed that it was more difficult to predict pitch than heave for the cases of low speeds and narrow spacings. In this case the spacing is very small.

In the case of $F_n = 0.30$ and $2l_y/B = 2.10$, the computed heave and pitch are presented in Figure 4.109 and Figure 4.110. The computed values show better agreement with experimental data for the case of $F_n = 0.15$ and $l_y/B = 1.04$. For the high-speed case, $F_n = 0.45$ and $2l_y/B = 3.14$, the computed heave and pitch show a good agreement with test data. It also can be observed in Figure 4.111 and Figure 4.112 that at high speed the computed results were better than those from strip theory. It is shown that the present method is especially useful to analyze catamaran motions with forward speed.

In this thesis, only pitch and heave motions have been computed in regular waves. The computation of motions for six degrees of freedom can be developed in the future. Further validation should be carried out for different wave conditions and other types of multi-hull ships. The prediction of pressure distribution and seaload computation on multi-hull ships could be developed. Unsteady wave washes generated by a multihull ship using time-domain panel method should be conducted as well. Above all, the numerical methods and computer programs developed in this thesis should be a contribution to Canada for the advanced high-speed vessel development in the future.

References

1. Akers, R., "SLICE", Professional Boatbuilder, June/July, 2000.

2. Andrews, D. and Zhang, J.W., "Considerations in the Design of a Trimaran Frigate", RINA Symposium on High Speed Vessels for Transport and Defence, London, 1995.

3. Andrew, R.N., Barr, J.J.M. and Price, W.G., " Predicton of Ship Wavemaking Resistance and Other Steady Flow Parameters Using Neumann-Kelvin Theory", Proceedings of the Royal Institution of Naval Architects, 1987.

4. Battistin, D. "Analytical, Numerical and Experimental Investigation on the Wave Resistance Interfernece Phenomenon of Trimaran Configurations", NAV 2000.

5. Brizzolara, S., Bruzzone, D., Cassella, P., Scamardella, A. and Zotti, I., "Wave Resistance and Wave patterns for High-Speed Crafts; Validation of Numerical Results by Model Test." 22th Symposium on Naval Hydrodyamics, Washington, 1998.

6. Beck, R.F. and Magee, A., "Time-Domain Analysis for predicting Ship Motions", Proceedings of IUTAM Symposium, Dynamics of Marine Vehicles and

Structures in Waves, London, 1990.

7. Beck, R.F. and King, B., "Time-Domain Analysis of Wave Exciting Forces on Floating Bodies at Zero Forward Speed", Applied Ocean Research, Vol. 11, 1989.

8. Beck, R.F. and Liapis, S.J., "Transient Motion of Floating Bodies at Zero Forward Speed", Journal of Ship Research, Vol. 31, 1987.

9. Cummins, W.E., "The Impulse Response Function and Ship Motions", Schiffstechnik, Vol. 9, 1962, pp. 101-109.

10. Cong, L., and Hsiung, C.C., "Computing Wave Resistance, Wave Profile, and Sinkage and Trim of Transom Stern Ships", Proceedings of the Third International Conference on Computer Aided Design, Manufacture and Operation in the Marine and Offshore Industries, Key Biscayne, Florida, USA, January 1991, pp. 99-112.

11. Cong, L.Z., Huang, Z.J., Ando, S. and Hsiung, C.C. "Time-Domain Analysis of Ship Motions and Hydrodynamic Pressures on a Ship Hull in Waves". 2nd International Conference on Hydroelasticity in Marine Technology, Fukuoka, Japan 1998.

12. Chang, M.S., "Computation of three-dimensional Ship Motion with Forward Speed", Second International Conference on Numerical Ship Hydrodynamics, University of California, Berkeley, 1977, pp. 124-135.

13. Dawson, C.W., "A Practical Computer Method for Solving Ship-Wave Problems", Proceedings of the Second International Conference on Numerical Ship Hydrodynamics, University of California, Berkeley, 1977, pp. 30-38.

14. Doctors, L.J. and Beck, R.F., "Convergence Properties of the Neumann-Kelvin Problem for a Submerged Body", Journal of Ship Research, Vol. 31, No. 4, 1987, pp. 227-234.

15. Finkelstein, A., "The Initial Value Problem for Transient Water Waves", Communications on Pure and Applied Mathematics, Vol. 10, 1957, pp. 511-522.

16. Froude, W., "The Fundamental Principles of the Resistance of Ships", The Papers of William Froude, The Institution of Naval Architects, London, 1955.

17. Gadd, G.E., "A Method of Computing the Flow and Surface Wave Pattern Around Hull Forms", Transactions of the Royal Institute of Naval Architects, Vol. 118, 1976, pp. 207-215.

18. Guevel, P., Delhommeau, G. and Cordonnier, J.P., " Numerical Solution of the Neumann-Kelvin Problem by the Method of Singularities", Proceedings of Second International Conference of Numerical Ship Hydrodynamics, Berkley, September 1977, pp. 107-123.

19. Guevel, P. and Bougis, J., "Ship -motion with Forward Speed in Infinite Depth", International Ship Building Progress, No. 29, 1982.

20. Havelock, T., "The Wave-Making Resistance of Ships: A Theoretical and Practical Analysis", The Collected Papers of Sir Thomas Havelock on Hydrodynamics, Office of Naval Research Department of the U.S. Navy, ONR/ACR, 1965.

21. Hsiung, C.C., "Optimal Ship Forms for Minimum Wave Resistance", Journal of Ship Research, Vol. 25, No. 2, 1981.

22. Hsiung, C.C. and Xu, H., "Determining Optimal Forms of a Catamaran for Minimum Resistance by the Mathematical Programming Method", Schiffstechnik Bd.35, 1988.

23. Hsiung, C.C. and Webster, W.C., "A Simple Numerical Method for Computing Michell Integral", College of Engineering, University of California, Berkeley, 1971.

24. Huang, Z.J. and Hsiung, C.C., "Nonlinear Shallow Water Flow on Deck Coupled with Ship Motion". The 21st Symposium on Naval Hydrodynamics, Trondheim, Norway, 1996.

25. Inglis, R.B. and Price, W.G., "A three-dimensional Ship Motion theory- Comparison between theoretical and experimental data of the hydrodynamic coefficient with forward speed". Transaction of the Royal Institution of Naval Architecture, vol. 124, 1981.

26. Kashiwagi, M., "Interaction Forces between Twin Hulls of a Catamaran Advancing in Waves (Part 1: Radiation Problem)". Journal of the Naval Architecture of Japan, Vol. 173, 1993.

27. Kashiwagi, M., "Interaction Forces between Twin Hulls of a Catamaran Advancing in Waves (Part 2: Wave Exciting Forces and Motions in Waves)", Journal of the Naval Architecture of Japan, Vol. 174, 1993.

28. Kofoed-Hansen, H., and Mikkelsen, A.C., "Wake Wash from Fast Ferries in Denmark", Proc. Fourth International Conference on Fast Sea Transportation (FAST' 97), Sydney, Australia, Vol. 1, 1997, pp. 471-478.

29. Larsson, L., Janson, C. and Brun, P., "A Numerical Investigation of Trimaran Configurations", FAST'97.

30. Larsson, L., Kim, K.J. and Zhang, D.H. " New Viscous and Inviscid CFD-technique for Ship Flows". 5th Int. Conf. Numerical Ship Hydrodynamics, Hiroshima, Japan. 1998.

31. Liapis, S. and Beck, R.F., "Seakeeping Computations Using Time Domain Analysis", Proceedings of 4th International Conference on Numerical Ship Hydrodynamics, Washington, D.C. 1985.

32. Lin, W.C., "The Force and Moment on a Twin Hull Ship in a steady Potential Flow", 10th Symposium on Naval Hydrodynamics, 1974.

33. Lin, W.M. and Yue, D.K., "Numerical Simulations for Large Amplitude Ship Motions in the Time Domain". Proceedings of the 18th Symposium on Naval Hydrodynamics, Ann Abor, Michigan, 1990.

34. Lin, W.M. and Yue, D.K., "Large Amplitude Motions and Wave Loads for Ship Design". Proceedings of the 20th Synposium on Naval Hydrodynamics, Santa Barbara, California, 1994.

35. Lord Kelvin, "Deep Sea Ship Waves", Proceedings of Royal Society Edinburgh, No. 25, June 1905, pp. 1060-1084.

36. Michell, J.H., "The Wave-Resistance of a Ship", Philosophical Magazine, Series 5, Vol. 45, No. 272, London, January 1898, pp. 105-123.

37. Morino, L., Chen, L.T. and Suciu, E.O., "Steady and Oscillatory Subsonic

and Supersonic Aerodynamics around Complex Configurations". AIAA Journal, Vol. 13, No. 3, March 1975, pp.368-374.

38. Newman, J.N., "The Theory of Ship Motion", Advances in Applied Mechanics, Vol. 18, pp.222-283, 1978.

39. Newman, J.N., "Evaluation of the Wave-Resistance of the Green Function: Part 1- the Double Integral", Journal of Ship Research, Vol. 31, No. 2, 1987, pp. 79-90.

40. Newman, J.N., "Evaluation of the Wave-Resistance of the Green Function: Part 2- the Single Integral", Journal of Ship Research, Vol. 31, No. 3, 1987, pp. 145-150.

41. Noblesse, F., "A Slender-Ship Theory of Wave Resistance", Journal of Ship Research, Vol. 27, 1983, pp. 13-33.

42. Ogilvie, T.F., "Recent Progress toward the Understanding and Prediction of Ship Motions", Proceedings 5th Symposium on Naval Hydrodynamics, ONR, Washington, D.C., 1964.

43. Papanikolaou, A., Kaklis, P., Koskinas, C. and Spanos, D., "Hydrodynamic Optimization of Fast-Displacement Catamarans", Proceeding of 21th Symposium of Naval Hydrodynamics, 1996.

44. Peng, H., Qiu, W. and Hsiung, C.C., "Computing Resistance for a High Speed Trimaran with Tent Function", CFD99, Halifax, 1999.

45. Peng, H., Qiu, W. and Hsiung, C.C., "Time-Domain Prediction of a Catamaran in Head Seas", 2nd International Conference on Oceanic Enginering, Valdivia,

Chile, 2000.

46. Peng, H., Lacy, G., Huang, Z.J. and Hsiung, C.C., "Nonlinear Roll Damping of Nava Scotia Inshore Fishing Boats", Proceedings of the Twenty-Fourth American Towing Tank Conference, Texas, 1995.

47. Qiu, W., Peng, H. and Hsiung, C.C. "Validation of Time-Domain Predictions of Motion, Sea Load, and Hull Pressure of a Frigate in Regular Waves", 23nd Symposium on Naval Hydrodynamics, Val de Reuil, France, 2000.

48. Qiu, W., Peng, H. and Hsiung, C.C., "Theoretical Manual for SEALOADS Version 1.1 - a Computer Program for Prediction of Nonlinear Ship Motion, Hydrodynamic Pressure and Sealoads in the Time Domain", Technical Report, Martec Limited, Halifax, N.S., 2001.

49. Salvesen, N., Tuck, E.O. and Faltinsen, O., "Ship Motions and Sea Loads," Transactions SNAME, vol 78, 1970.

50. Shearer, J.R., "A preliminary Investigation of the Discrepancies between the Calculated and Measured Wave-making of Hull Forms," North-East Coast Inst. Eng. Shipbld. Trans. 67, 1951.

51. Suzuki, K. and Ikehata, M., "Fundamental Study on Optimum Position of Outriggers of Trimaran from View Point of Wave Making Resistance", Proceedings of 2nd FAST'93 Conference, Yokohama, 1993.

52. Stoker, J.J., Water Wave. International Science Publishers, Inc., New York, 1957.

53. Stumbo, S., Fox, K., Dvorak, F., and Elliot, L., "The Prediction, Measurement, and Analysis of Wake Wash from Marine Vessels", Marine Technology, Vol. 36, No. 4, 1999, pp. 248-260.

54. Thomson, M., Peach, S., Albert, I., MacIntosh, M., Oakley, G., "Design and Development of the Trimaran", Dalhousie, 1998.

55. van't Veer, A.P. and Siregar, F.R.T., "The Interaction Effects on a Catamaran Travelling with Forward Speed in Waves", FAST'95, 1995.

56. van't Veer, R., "Analysis of Motions and Loads on a Catamaran Vessels in Waves", FAST'97, 1997.

57. Wehausen, J.V. and Laitone, E.V., "Surface Wave", Handbuch der Physik, Springer-Verlag, Berlin, Vol. 9, 1960, pp. 446-778.

58. Wehausen, J.V., "Initial Value Problem for the Motion in an Undulating Sea of a Body with Fixed Equilibrium Position", Journal of Engineering Mathematics, Vol. 1, 1967.

59. Wehausen, J.V., "The Motion of Floating Bodies", Annual Review of Fluid Mechanics, Vol. 3, 1971.

60. Wu, G.X. and Eatock Taylor, R., "A Green function form for Ship Motion at Forward Speed", International Shipbuilding Progress, Vol. 34, No. 398, 1987.

61. Yang, C. and Loehner, R., "Fully Nonlinear Ship Wave Calculation Using Unstructured Grid and Parallel Computing", 3rd Osaka Colloquium, Advanced CFD Applications to Ship Flow and Hull Form Design, Osaka, 1998.

62. Ye, H.K. and Hsiung, C.C., "Time-Domain Motion Computations of Twin- and Mono-Hull Ships in Head Seas", International Ship Building Progress, Vol. 46, No. 445, 1999.

63. Zhang, Z., Lao, G. and Peng, H., "Performance and Pressure Distribution on Blades of Highly Skewed Propellers by Using Unsteady Lifting Surface Theory" (In Chinese), Journal of Dalian University of Thechnology, Vol. 34, No. 6, 1994.